

The University of Maine

DigitalCommons@UMaine

---

Electronic Theses and Dissertations

Fogler Library

---

Summer 8-22-2019

## Reaction Kinetics Analysis of C-O Hydrogenolysis in Phenol and 5-Hydroxymethylfurfural

Daniela Ignacia Stuck Valenzuela  
*University of Maine*, [daniela.stuck@maine.edu](mailto:daniela.stuck@maine.edu)

Follow this and additional works at: <https://digitalcommons.library.umaine.edu/etd>

---

### Recommended Citation

Stuck Valenzuela, Daniela Ignacia, "Reaction Kinetics Analysis of C-O Hydrogenolysis in Phenol and 5-Hydroxymethylfurfural" (2019). *Electronic Theses and Dissertations*. 3110.  
<https://digitalcommons.library.umaine.edu/etd/3110>

This Open-Access Thesis is brought to you for free and open access by DigitalCommons@UMaine. It has been accepted for inclusion in Electronic Theses and Dissertations by an authorized administrator of DigitalCommons@UMaine. For more information, please contact [um.library.technical.services@maine.edu](mailto:um.library.technical.services@maine.edu).

**REACTION KINETICS ANALYSIS OF C-O HYDROGENOLYSIS IN PHENOL AND  
5-HYDROXYMETHYLFURFURAL**

By

Daniela Ignacia Stück Valenzuela

B.S. University of Concepcion, 2016

A THESIS

Submitted in Partial Fulfillment of the

Requirements for the Degree of

Master of Science

(in Chemical Engineering)

The Graduate School

The University of Maine

August 2019

Advisory Committee:

Thomas J. Schwartz, Assistant Professor of Chemical Engineering, Advisor

Brian G. Frederick, Associate Professor of Chemistry, Co-advisor

William J. DeSisto, Professor of Chemical Engineering

© 2019 Daniela Stück

All Rights Reserved

# REACTION KINETICS ANALYSIS OF C-O HYDROGENOLYSIS IN PHENOL AND 5-HYDROXYMETHYLFURFURAL

By Daniela Ignacia Stück Valenzuela

Thesis Advisors: Dr. Thomas J. Schwartz, Dr. Brian G. Frederick

An Abstract of the Thesis Presented  
in Partial Fulfillment of the Requirements for the  
Degree of Master of Science  
in Chemical Engineering  
August 2019

Converting biomass to alternative fuels has attracted significant interest in recent decades. Lignin, a principal component of biomass, is composed of phenolic monomers, which can be depolymerized using fast pyrolysis to yield a “bio-oil”. However, bio-oil is not immediately suitable as a biofuel because of its high oxygen content, and it is necessary to efficiently remove these oxygen atoms by hydrodeoxygenation (HDO). This project is focused on the elucidation of the reaction kinetics associated with carbon-oxygen hydrogenolysis in phenolic molecules, which is a significant reaction for the production of hydrocarbon fuels from biomass pyrolysis oils. The studied molecules are 5-hydroxymethylfurfural (HMF) and phenol, both used as model compounds.

For phenol hydrodeoxygenation (HDO) the optimal pathway is direct deoxygenation (DDO), but at relevant temperatures, C-C double bond saturation is a significant side reaction, following the hydrogenation pathway (HYD). The importance of metal-TiO<sub>2</sub> sites has been shown for a variety of reactions. Previous research in our group has shown that Ru/TiO<sub>2</sub> is highly active for the conversion of phenol to benzene and that water could act as a co-catalyst. In this work, we clarify

the role of water in C-O hydrogenolysis catalyzed by this material. Here, we designed and carried out a series of reaction kinetics experiments that illustrate the complex effect water has on the DDO mechanism. We measured reaction orders for phenol hydrogenolysis with respect to water and phenol over Ru supported on TiO<sub>2</sub> rutile and anatase using a high-pressure liquid phase flow reactor operated in a kinetically-controlled regime.

Our most interesting results show that the reaction is positive-order with respect to water for Ru/rutile and negative-order for Ru/anatase. These observations correlate with heats of water adsorption measurements on TiO<sub>2</sub> indicating that anatase is more hydrophilic than rutile<sup>1</sup> and suggest that under particular circumstances, water molecules at the interfacial sites could become the most abundant surface intermediate (MASI). Also, the reaction is zero order with respect to phenol in the absence of water for Ru/anatase and it shifts from positive to negative order at higher phenol concentrations for Ru/rutile. Those differences with catalytic support identity suggest that the reaction mechanisms are different for each catalyst. For rutile, we believe that phenol is a MASI at two different sites: the interfacial site and the metal site that leads to the HYD pathway. For anatase, it is expected that phenol is only a MASI at one of those sites.

HMF can also undergo hydrodeoxygenation in a series of intermediate reactions until it becomes 2,5-dimethylfuran. We perform a comparison between different Ni and Ru catalysts supported on Co<sub>3</sub>O<sub>4</sub> with respect to literature performance. Our results were consistent with the literature, but we have obtained a different reaction intermediate, product distribution, and site time yields. We believe that those differences are due to difficulties in reproducing the catalysts by the co-precipitation method.

## DEDICATION

This thesis is dedicated to my family. They have always supported me in my decisions and were on my side to choose the path that is best for me, even if this decision includes leave them alone for many years. They raised me to look always for success and I feel they did an amazing job in that.

I thank to the Carrasco-Ruiz Family for their unconditional help along this process. Pamela was there for all the important moments and decisions related to move and settle to Maine, in an academic and personal way. She was the first person in advising me about the pros and cons of moving to Maine, telling me what to expect. She spends so much time with me looking for apartments, cars, and helping me to settle in even when she had a thesis to finish and a kid to take care. I will never forget the good times spent at their place in NH that I consider my home here, having a familiar Chilean vibe and enjoying time with kids, pets, amazing food and a good conversation.

Also I thank my friends that I made in Maine, it feels like I know them my whole life. Thank you for your unconditional emotional support on thoughts moments and for the amazing memories that I will keep forever. Just remember: “Who needs money if you have friends and schemes?”

## ACKNOWLEDGEMENTS

This project was founded by the National Science Foundation under Grant Nr. CHE-1565843. Any opinions, findings, and conclusions or recommendations expressed in this material are those of the authors and do not necessarily reflect the views of the National Science Foundation.

I thank Javiera Navarro from University of Concepcion for all of her work in the HMF project during her REU at University of Maine. Most of the batch reaction experiments and analysis of results were done by her, and she provided significant evidence to determine that catalytic performance was different than expected according to literature.

Also, from University of Concepcion, I thank Dr. Teresita Marzioletti for providing me academic support for the theory behind the HMF project, even after completing my undergraduate degree with her.

I thank several UMaine Faculty that provide me academic advice for different parts of this project. To Dr. Clay Wheeler and Dr. Peter van Walsum for helping me understanding the non-ideal behavior of the flow reactor, and for their help with Aspen Plus software to set up a proper working model. Also, I thank Dr. Adriaan van Heiningen for advising me with his expertise in reaction kinetics, that help me understand why the reaction must happen in the liquid phase.

I thank my colleagues Pamela Ruiz, Jose Luis Carrasco and Akbar Mahdavi for their advises and keeping track with my project, providing their expertise in the area when I needed.

Lastly but not least important, I thank all my co-workers at UMaine Catalysis Lab for all of their support along these years. To Hussein Abdulrazzaq for tons of help in troubleshooting with flow reactor equipment. To Matthew Kline, Meredith Allen, Chris Albert and Jalal Tavana for general help in lab related issues and to Elnaz Jamalzade for her help in catalysis characterization and analysis by chromatography.

## TABLE OF CONTENT

DEDICATION .....	iii
ACKNOWLEDGEMENTS .....	iv
TABLE OF CONTENT .....	vi
LIST OF TABLES .....	iii
LIST OF FIGURES .....	v
CHAPTER 1: C-O HYDROGENOLYSIS.....	1
CHAPTER 2: PHENOL HYDRODEOXYGENATION.....	13
2.1. Introduction .....	13
2.2. Objectives .....	17
2.2.1 General Objective .....	17
2.2.2 Specific Objectives .....	17
2.3. Methodology.....	17
2.3.1 Materials .....	17
2.3.2 Catalyst Preparation.....	18
2.3.3 High Pressure Flow Reactor Experiments .....	18
2.4. Determination of Reaction Conditions .....	22
2.4.1 Pretreatment.....	23
2.4.2 Non-Ideality.....	24
2.4.3 Mass Transfer Limitations .....	26
2.4.4 Thermodynamic equilibria analysis .....	28

2.4.5	Benzene and Cyclohexane interconversion .....	28
2.4.6	Kinetic isotope effect (KIE).....	29
2.5.	Results .....	29
2.5.1	Data Treatment .....	29
2.5.2	Differential Conditions .....	32
2.5.3	Mass Transfer Limitations .....	34
2.5.4	Benzene and cyclohexane interconversion .....	36
2.5.5	Thermodynamics equilibria analysis .....	36
2.5.6	Effect of water on DDO kinetics .....	38
2.5.7	Effect of phenol for rutile and anatase .....	42
2.5.8	Kinetic isotope effect (KIE).....	43
2.6.	Discussion.....	44
2.6.1	Effect of water and crystal structure of the support .....	44
2.6.1	Effect of phenol .....	47
2.6.2	Derivation of the rate expression .....	48
2.7.	Conclusions .....	57
CHAPTER 3: FUTURE WORK .....		59
REFERENCES .....		61
APPENDIX A: 5-HYDROXYMETHYLFURFURAL HYDROGENOLYSIS .....		68
APPENDIX B: CATALYTIC STABILITY, SOLVENT SELECTION, AND OTHER PRELIMINARY WORK .....		92
APPENDIX C: TROUBLESHOOTING GUIDE.....		108
BIOGRAPHY OF THE AUTHOR.....		120

## LIST OF TABLES

<i>Table 2.1 Intermediate parameter calculated for mass and heat transfer limitation parameters, for phenol, hydrogen and water in both liquid and gas phase. ....</i>	35
<i>Table 2.2 Results for calculation of mass and heat transfer parameters for phenol, hydrogen and water in both liquid and gas phase. All of the parameters meet the criteria but it is also noticeable that water in the liquid phase presents a significant value of the Weiss-Prater number that needs to be considered. ....</i>	35
<i>Table 2.3 Benzene and cyclohexane flowrates, out of a reactor fed by a solution of 0.1 M of benzene or cyclohexane in decalin. Reaction conditions: 573K and 4482kPa Ru/TiO<sub>2</sub>-Rutile. WHSV of 19530 h<sup>-1</sup> for benzene and 12620 h<sup>-1</sup> for cyclohexane respectively, GHSV of 970 h<sup>-1</sup> hydrogen. Conversion &lt; 15%. ....</i>	36
<i>Table 2. 4 Results of energy analysis estimates with Aspen Plus™. Conversion and selectivity from a Gibbs reactor estimated for just benzene, just cyclohexane and both DDO and HYD pathway. Reaction conditions: 573K and 4482kPa. WHSV of 235h<sup>-1</sup> of phenol 0.5M in decalin, GHSV of 970 h<sup>-1</sup> hydrogen. ....</i>	37
<i>Table 2. 5 Results of energy analysis estimates with Aspen Plus™. Product distribution from a Gibbs reactor estimated for a mixture of DDO and HYD pathway. Reaction conditions: 573K and 4482kPa. WHSV of 235h<sup>-1</sup> of phenol 0.5M in decalin, GHSV of 970 h<sup>-1</sup> hydrogen. ....</i>	38
<i>Table 2. 6 KIE for direct deoxygenation of phenol diluted with D<sub>2</sub>O instead of water.. Reaction conditions: 573K and 4482kPa Ru/TiO<sub>2</sub>-Rutile <sup>57</sup>. WHSV of 235h<sup>-1</sup> of phenol 0.5M in decalin, GHSV of 970 h<sup>-1</sup> hydrogen. Co-feed of 27 h<sup>-1</sup> of water and D<sub>2</sub>O. Conversion &lt; 15%. ....</i>	44
<i>Table A. 1 Gas price in some countries of the world in dollars per gallon.<sup>76</sup> .....</i>	69
<i>Table A. 2 Properties from popular biofuels compared to gasoline. <sup>79</sup> .....</i>	71
<i>Table A. 3 Chemical abbreviations for HMF hydrodeoxygenation products. ....</i>	74
<i>Table A. 4 Reaction conditions extracted from bibliography <sup>83</sup>, with respective values of yield and conversion if reported. Reaction performed at 130°C and 1 MPa with a Ni/Co<sub>3</sub>O<sub>4</sub> synthesized by an hydrothermal method, using THF as a solvent. ....</i>	76

*Table A. 5 Reaction conditions extracted from bibliography <sup>82</sup>, with respective values of yield and conversion if reported. Reaction performed at 130°C and 1 MPa with a Ru-Co<sub>3</sub>O<sub>4</sub> synthesized by a co-precipitation method using THF as a solvent. .... 76*

*Table A. 6 Reaction conditions extracted from bibliography, with respective values of yield and conversion if reported. Reaction performed at 130°C and 1 MPa with a Ru-Co<sub>3</sub>O<sub>4</sub> synthesized by a co-precipitation method using THF as a solvent. .... 77*

*Table A. 7 Summary of general catalytic runs results. Reaction conditions with respective values of yield and conversion. Reaction performed at 130°C and 3.4 MPa with catalysts synthesized by a co-precipitation method using THF as a solvent. .... 85*

*Table A. 8 Concentrations in input and output. Reaction performed at 130°C and 3.4 MPa with catalysts synthesized by a co-precipitation method using THF as a solvent. .... 86*

*Table B. 1 Results for the CO chemisorption analysis over Ru/TiO<sub>2</sub>-P25, UM catalyst..... 92*

*Table B. 2 List of all the experiments analyzed by Aspen Plus™, given the input of total moles (mol/h) in, the output of the simulation is the distribution of all the reactants flowrates in the gas and liquid phase in kmol/h going through the reactor column. .... 96*

## LIST OF FIGURES

<i>Figure 1. 1 Mechanism of deoxygenation of m-cresol over Ni, Fe and Ni-Fe Catalysts. Adapted from <sup>14</sup>.....</i>	5
<i>Figure 1. 2 Mechanism of phenolic model compound adsorption over silica supports. Adapted from ref. <sup>17</sup>.....</i>	8
<i>Figure 1. 3 Hydrodeoxygenation mechanism of oxygenated compounds over metallic catalysts with active supports. Extracted from. <sup>33,36</sup>.....</i>	8
<i>Figure 1. 4 Hydrodeoxygenation of phenol over Pd/SiO<sub>2</sub> or Pd/ZrO<sub>2</sub> via the tautomerization method, Adapted from. <sup>21</sup>.....</i>	11
<i>Figure 1. 5 Hydrodeoxygenation mechanism of anisole and the formation of the tautomer cyclohexadienes to further conversion into benzene. Adapted from. <sup>45</sup>.....</i>	12
<i>Figure 2. 1 Reaction pathways for phenol hydrodeoxygenation. In the direct deoxygenation pathway (DDO) phenol is converted directly to benzene. ....</i>	14
<i>Figure 2. 2 Proposed molecular mechanism of DDO pathway for phenol over Ru/TiO<sub>2</sub>. <sup>57</sup>.....</i>	15
<i>Figure 2. 3 Schematic diagram of the hydrogenation biphasic reactor. ....</i>	20
<i>Figure 2. 4 Picture of the Hydrogenation biphasic reactor built at UMaine Catalysis Laboratory. ....</i>	21
<i>Figure 2. 5 Illustration of how the catalyst was packed, with a small bed of catalyst in the middle, quartz wool to keep it in place and silica chips to decrease the dead volume. ....</i>	21
<i>Figure 2. 6 DDO (a) and HYD (b) rates in moles per gram of catalyst per minute as a function of time-on-stream in h.....</i>	30
<i>Figure 2. 7 Natural logarithm of DDO rates in moles per gram of catalyst per minute shown as a function of time-on-stream in h.....</i>	31
<i>Figure 2. 8 Initial conversion at different values of inverse WHSV. WHSV (h<sup>-1</sup>) values were reached by varying the amount of Ru/TiO<sub>2</sub>-P25. ....</i>	33
<i>Figure 2. 9 Initial DDO rates evaluated at similar condition with and without co-feed of water, for different Ru/TiO<sub>2</sub> catalysts.....</i>	39
<i>Figure 2. 10 Rates of direct deoxygenation of phenol with respect to the initial liquid composition of water on a log-log scale. ....</i>	40

<i>Figure 2. 11 Rates of direct deoxygenation (a) and hydrogenation (b) of phenol with respect to partial pressure of water on a log-log scale.....</i>	<i>41</i>
<i>Figure 2. 12 Rates of direct deoxygenation (a) and hydrogenation (b) of phenol with respect to partial pressure of water on a log-log scale.....</i>	<i>41</i>
<i>Figure 2. 13 Rates of direct deoxygenation (a) and hydrogenation (b) of phenol with respect to partial pressure of phenol on a log-log scale.....</i>	<i>42</i>
<i>Figure 2. 14 Rates of direct deoxygenation (a) and hydrogenation (b) of phenol with respect to partial pressure of phenol on a log-log scale.....</i>	<i>43</i>
<i>Figure 2. 15 Updated molecular mechanism of DDO pathway for phenol over Ru/TiO<sub>2</sub>, with a mechanism consistent with isotopic trace experiments and kinetic results. ....</i>	<i>45</i>
<i>Figure 2. 16 Schematic representation of all the possible active sites used in the derivation for the rate expression. Pictures based on Figure 2.2.....</i>	<i>49</i>
<i>Figure A. 1 Gasoline price distribution around the world. <sup>76</sup> .....</i>	<i>69</i>
<i>Figure A. 2 Range of end products derived from HMF. Extracted from. <sup>80</sup>.....</i>	<i>72</i>
<i>Figure A. 3 Reduced two-step fructose dehydration to HMF reaction scheme. <sup>46</sup>.....</i>	<i>73</i>
<i>Figure A. 4 Proposed reaction pathway for HMF HDO over Ru-C<sub>3</sub>O<sub>4</sub> catalyst. <sup>82</sup>.....</i>	<i>73</i>
<i>Figure A. 5 Proposed reaction pathway for HMF HDO over Ni/Co<sub>3</sub>O<sub>4</sub> catalyst <sup>83</sup>.....</i>	<i>74</i>
<i>Figure A. 6 Proposed reaction pathway for further HMF hydrodeoxygenation, including hydrogenation and hydrogenolysis reactions. <sup>84</sup>.....</i>	<i>74</i>
<i>Figure A. 7 HMF hydrodeoxygenation over time. Reaction conditions: 0.04g HMF with 0.04g catalyst diluted in 10g of butanol. Reaction temperature 105°C, and 3.4 MPa. ....</i>	<i>82</i>
<i>Figure A. 8 HMF hydrodeoxygenation over time. Reaction conditions: 0.04g HMF with 0.04g catalyst diluted in 10g of butanol. Reaction temperature 120°C, and 3.4 MPa. ....</i>	<i>83</i>
<i>Figure A. 9 HMF hydrodeoxygenation over time. Reaction conditions: 0.04g HMF with 0.04g catalyst diluted in 10g of butanol. Reaction temperature 135°C, and 3.4 MPa. ....</i>	<i>83</i>
<i>Figure A. 10 Effect of temperature in HMF hydrodeoxygenation. Reaction conditions: 3.4 MPa and 0.08 h<sup>-1</sup> WHST.....</i>	<i>84</i>

<i>Figure A. 11 Reaction pathway with respect to WHSV for Ru-Co<sub>3</sub>O<sub>4</sub>(2) catalyst. Reaction performed at 130°C and 3.4 MPa with catalysts synthesized by a co-precipitation method using THF as a solvent.....</i>	<i>88</i>
<i>Figure A. 12 Effect of catalyst metal for HMF hydrodeoxygenation. Ru-Co<sub>3</sub>O<sub>4</sub> and Ni-Co<sub>3</sub>O<sub>4</sub> catalysts are compared. Reaction conditions: 3.4 MPa and. 0.0053 h<sup>-1</sup> WHST. ....</i>	<i>89</i>
<i>Figure B. 1 Adsorption isotherm data for Ru/TiO<sub>2</sub>-P25, UM catalyst .....</i>	<i>92</i>
<i>Figure B. 2 Thermogravimetric analysis performed in 117.218 mg Ru/TiO<sub>2</sub> –P90 catalyst, after being deactivated by a phenol HDO reaction, in decalin.....</i>	<i>93</i>
<i>Figure B. 3 TEM analysis performed in a Ru/TiO<sub>2</sub> catalyst, before (a) and after (b) being calcined in a phenol HDO reaction. Insrument JEOL 2010 Advanced High Performance TEM.....</i>	<i>94</i>
<i>Figure B. 4 Calibration curves obtained for (a) cyclohexane at 2.3 min, (b) cyclohexene at 3.2 min (c) benzene at 5.7 min (d) cyclohexanone at 13.1 min (e) cyclohexanol at 14.7 min and (f) phenol at 21.4 min. Method DB-624 used in a Agilent DB-WAX column (30 m × 0.53 mm, 1 μm). ....</i>	<i>95</i>
<i>Figure B. 5 Partial pressure of (a) water and (b) phenol with respect to their respective liquid phase composition, times their saturation pressure. The slope represents the activity coefficient for each case. ....</i>	<i>97</i>
<i>Figure B. 6 Initial Benzene selectivity for phenol hydrodeoxygenation at different water concentrations. ....</i>	<i>100</i>
<i>Figure B. 7 Deactivation constant for phenol hydrodeoxygenation at different water concentrations.....</i>	<i>100</i>
<i>Figure B. 8 Initial Site time yield (STY) for phenol hydrodeoxygenation at different water concentrations.....</i>	<i>101</i>
<i>Figure B. 9 Initial Benzene selectivity for phenol hydrodeoxygenation at different water concentrations. ....</i>	<i>102</i>
<i>Figure B. 10 Deactivation constants for phenol hydrodeoxygenation at different water concentrations. ....</i>	<i>102</i>
<i>Figure B. 11 Estimated initial TOF for phenol hydrodeoxygenation at different water concentrations. ....</i>	<i>103</i>
<i>Figure B. 12 Initial Benzene selectivity for phenol hydrodeoxygenation at different water concentrations at 350°C.....</i>	<i>104</i>
<i>Figure B. 13 Deactivation constants for phenol hydrodeoxygenation at different water concentrations at 350°C.....</i>	<i>104</i>
<i>Figure B. 14 Estimated initial TOF for phenol hydrodeoxygenation at different water concentrations at 350°C.....</i>	<i>105</i>

<i>Figure B. 15 Initial Benzene selectivity for phenol hydrodeoxygenation at different water concentrations at 400°C.....</i>	<i>106</i>
<i>Figure B. 16 Deactivation constants for phenol hydrodeoxygenation at different water concentrations at 400°C.....</i>	<i>106</i>
<i>Figure B. 17 Estimated initial TOF for phenol hydrodeoxygenation at different water concentrations at 400°C.....</i>	<i>107</i>

## CHAPTER 1: C-O HYDROGENOLYSIS

C-O bond cleavage in aromatics is a widely used reaction for lignin depolymerization to phenolic compounds and thus deoxygenation to most suitable chemicals. In this context, hydrogenolysis of lignocellulosic compounds has been previously studied and reviewed<sup>2-10</sup>. Model compounds from lignin-derived bio-oils were widely used; the most common are phenol, m-cresol, guaiacol, anisole, vanillin and eugenol<sup>3</sup>.

Research<sup>2,11</sup> indicates that noble metals, such as Ru, Pt, Pd and Ni, are favorable for this reaction. Bimetallic systems can also be highly selective for oxygen removal. Combinations of noble metals with first-row and late transition metals like Fe, Ni, Cu, Zn or Sn form highly selective catalysts.<sup>3,12,13</sup> Also, alloying group VIII metals with oxophilic metals such as Sn, Re, or Fe will decrease the interaction with the ring and enhance the interaction with the carbonyl or hydroxyl group.<sup>14</sup>

The selectivity for hydrodeoxygenation (HDO) can be influenced by the properties of the support.<sup>15</sup> Noble metals supported on acidic materials can offer good selectivity for direct deoxygenation (DDO) of the C-O bond, but also oxophilicity, metal dispersion, strength of metal-support interactions and deactivation effects by coking formation needs to be considered for the selection of the right metal-support combination.

Based on Sabatier's rule, an oxide support with moderate metal-oxygen bond strength is the optimal support of choice if the substrate reacts at the interface.<sup>8</sup> If the metal-oxygen bond is too strong, it is difficult to create surface vacancies for oxygenated group adsorption, but if the metal-

oxygen bond strength is too low it would make the catalyst unable to abstract oxygen effectively.<sup>7</sup> In terms of oxygen bond strength, metals were evaluated as follows: Mg > Al > Zr > Ti > W > Cr > Zn > V > Sn > Fe > Ge > Mn > Ni > Bi > Cu > Pb.<sup>3</sup> Therefore, mild to moderate acidic supports such as TiO<sub>2</sub>, ZrO<sub>2</sub>, zeolites, Al<sub>2</sub>O<sub>3</sub> and CeO<sub>2</sub> are often used for the HDO process due to their ability to catalyze C-O bond hydrogenolysis with minimal coking effects.<sup>7</sup> Basic support (CoMo/MgO) catalysts are more likely to resist sintering and coking effects but offer significantly lower HDO activity.<sup>3</sup>

Some metal-support combinations in heterogeneous catalysts are known to exhibit metal-support interactions and present physicochemical properties that were not present when metals and supports were just physically mixed. Metal-support interactions generally arise due to the electronic perturbation of metallic atoms by surrounding atoms from the support, which would result in the change of electronic properties of the metal catalyst.<sup>3</sup> For selective HDO catalyst, surface oxide-metal interactions are not desired.

A general mechanism for C-O bond cleavage in aromatics can be established as follow.<sup>16</sup>

1. Oxygenated groups can be adsorbed through Lewis acid/base interaction and activated on the following sites. An aromatic species with more than one oxygen atom may adsorb at different sites.<sup>17</sup>
  - Reduced metal sites
  - Oxygen vacancies on the support
  - Exposed cations on the support

- Coordinatively unsaturated metal sites: for bimetallic catalysts the second metal can also adsorb the oxygenated group. <sup>18</sup>
2. At the same time, the aromatic ring is easily bonded to the metallic surface. <sup>19</sup>
  3. Proton donation to the oxygenated group donation, which is available directly from:
    - Phosphides, carbides and nitrides
    - Brønsted acids, -OH groups
    - SH groups
    - Metals and noble metals by H spillover: Adsorbed H<sub>2</sub> atoms spill over from noble metals to an adsorbed oxygen atom. <sup>8</sup> Noble metals are particularly efficient catalysts in activating molecular hydrogen.

Some heterogeneous catalysts that favor DDO are presented as follows:

Cresol deoxygenation over Pt/Al<sub>2</sub>O<sub>3</sub> catalysts at atmospheric pressure generates toluene and benzene, but methylcyclohexane remains the main reaction product. <sup>20</sup> In the conversion of *m*-cresol over Pd/SiO<sub>2</sub>, hydrogenation of the aromatic ring is favored, but using ZrO<sub>2</sub> as a support helps by creating oxophilic sites favoring the DDO mechanism. <sup>21</sup> As another example, Ni/SBA-15 catalyst exhibits higher catalytic performance for hydrodeoxygenation of the aromatic ring (HYD) of anisole, On the contrary, the direct hydrogenolysis of the methoxy group is favored over Co/SBA-15, leading to much higher aromatic selectivity. <sup>22</sup> For Ga particles, in general, despite steric effects and mass transfer limitations, the higher acid support strength (SiO<sub>2</sub> < HBeta ≈ HZSM-5) is generally associated with higher C-O bond cleavage activity. <sup>23</sup>

A mechanism for HDO of 2-ethylphenol over a CoMoS/Al<sub>2</sub>O<sub>3</sub> catalyst was proposed.<sup>24</sup> On MoS/Al<sub>2</sub>O<sub>3</sub> catalysts, vacancy sites are created by the removal of H<sub>2</sub>S in the presence of H<sub>2</sub>.<sup>8</sup> H<sub>2</sub> is activated by heterolytic dissociation forming one S-H and one Mo-H group; the oxygenated group is adsorbed on those vacancy sites formed an adsorbed carbocation after receiving a proton from the S-H group. This intermediate undergoes direct C-O bond cleavage and generates ethylbenzene. The vacancy site is recovered by the formation of H<sub>2</sub>O from the adsorbed OH and H groups.<sup>24</sup> The addition of cobalt to this catalyst CoMoS/Al<sub>2</sub>O<sub>3</sub> enhances the direct C-O bond scission, because of an increment in the number of active sites, some of them being new sulfur vacancies.<sup>24</sup>

ReS<sub>2</sub>/ZrO<sub>2</sub> is highly active for guaiacol DDO. Reaction with H<sub>2</sub> breaks in the first instance the C-O bond of the methoxy group and then breaks the formed hydroxyl group, producing mostly catechol and phenol. Here, demethoxylation occurs on the vacancies of the sulfide metal ReS<sub>2</sub>. The use of sulfated ZrO<sub>2</sub> as a support provides a stronger interaction with the Re precursor leading to a highly dispersed catalyst.<sup>25</sup> The mechanism for HDO over sulfided NiW<sup>26</sup> is similar to that proposed by Romero et al.<sup>24</sup>

Bifunctional catalyst have been studied recently for DDO reactions. The presence of Fe and Ni-Fe bimetallic catalysts supported on SiO<sub>2</sub> promotes the hydrogenation of the C-O group of m-cresol. On the mixed Ni-Fe catalysts, hydrogenation of the non-aromatic tautomer produces a reactive alcohol, which is easily dehydrated (Figure 1.1). The favorable sites for this process come from Lewis acids associated with the incomplete reduction of Fe and/or Ni-Fe cations.<sup>14</sup> Here, the aromatic ring is repulsed from the catalyst surface, while the oxygenated group strongly interacts

with the acid sites, promoting the oxygen removal reaction pathway.<sup>14</sup> Otherwise, in pure Ni catalysts, HYD is favored, forming 3-methyl-cyclohexanol and 3-methyl-cyclohexanone showed in Figure 1.1.

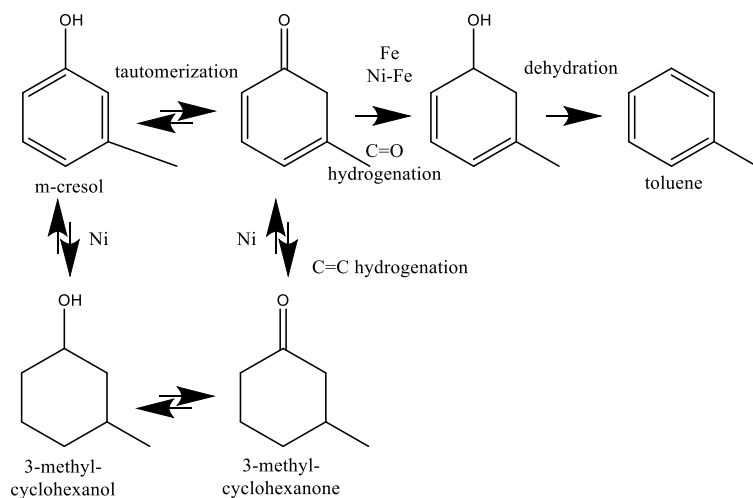


*Figure 1. 1 Mechanism of deoxygenation of m-cresol over Ni, Fe and Ni-Fe Catalysts. Adapted from ref.<sup>14</sup>*

When studying HDO of m-cresol over Pt/C and Pt-WO<sub>x</sub>/C, the latter was much more active and selective towards DDO.<sup>27</sup> The HDO reaction on Pt-WO<sub>x</sub>/C proceeds selectively for *m*-cresol, because of the synergetic effect between the Pt and the redox supported WO<sub>x</sub> complexes. Pt stabilizes the partially reduced tungsten-oxide sites and favors the formation of oxygen vacancies, where the hydroxyl group is adsorbed, by forming a Pt-W bond. These sites are very important for selective C–O scission, because they limit the interaction of the aromatic ring with the Pt surface, avoiding its parallel adsorption that could cause ring hydrogenation.<sup>27</sup>

Selective C-O hydrogenolysis of vanillin was also found over Au-Pt/CeO<sub>2</sub> using formic acid as the hydrogen source. Pt interacts with Au forming Au-Pt alloys showing excellent performance. The presence of small nanoparticles, the CeO<sub>2</sub> support, the good dehydrogenation ability of formic acid and the hydrogenolysis of C=O species are also key factors for this reaction. The strong activity of this catalyst is, again, because of oxygen vacancies that interact with the hydroxyl group, which facilitates the C-O bond cleavage. The remaining oxygen is removed by hydrogenation, forming water and thus leading to the formation of new oxygen defects <sup>28</sup>.

The activity of transition metal carbides (TMC) and nitrides (TMN) depends on the surface structure, metal oxidation state, and N and C deficiency. <sup>29</sup> Increasing the concentration of molybdenum oxynitride species reduces the overall HDO activity but favors the formation of Mo<sub>2</sub>N species. Oxynitride species are formed by reactions between the unsaturated Mo sites and the oxygen that is available either on the support surface or on the subsurface of the Mo<sub>2</sub>N species. <sup>8,29</sup> Tungsten carbides, W<sub>x</sub>C, exhibit an impressive activity for hydrogenolysis of the aryl ether oxygen of guaiacol. Here, the activation of both H<sub>2</sub> and guaiacol on the surface of the catalyst is necessary for the cleavage. <sup>30</sup>

Some supports are discovered to be active in the molecular mechanism of C-O bond hydrogenolysis; those will be called active supports and their performance were in some cases very well studied. <sup>17,31-36</sup>

Improvements of inert supports like carbon modified into a nitrogen-doped hierarchical porous carbon (NHPC), has also been developed, reaching higher performances for C-O cleavage. A direct hydrogenation-hydrogenolysis reaction mechanism for vanillin was proposed. Here,

Ni/NHPC favors full oxygen removal of a broad set of oxygenated aromatics. The reason for its high activity is the structure of the modified nickel interacting with nitrogen dopant contributed by the hierarchical porous structure of the carbon.<sup>31</sup>

A strontium (Sr)-substituted lanthanum cobaltite ( $\text{La}_{0.8}\text{Sr}_{0.2}\text{CoO}_3$ ) was recently found to be selective towards C-O and C-C hydrogenolysis on anisole by stabilizing the  $\text{Co}^0/\text{Co}^{\text{II}}$  sites. This stabilization effect plays an important role on the activity of the catalyst.  $\text{Co}^{\text{II}}$  sites were favored at low temperatures and performed selective C-O hydrogenolysis by the existence of oxygen vacancies generated by Sr-substitution. With the participation of  $\text{Co}^0$  sites in close proximity to  $\text{Co}^{\text{II}}$  sites, the adsorbed anisole can also form H-deficient intermediates.<sup>32</sup>

Phenolic compounds could be very strongly adsorbed on oxides. Adsorption of phenolic compounds over  $\text{SiO}_2$  and  $\text{Al}_2\text{O}_3$  was studied. As seen in Figure 1.2, over silica the main interaction mechanism is H-bonding, while over alumina the main adsorption mode is chemisorption.<sup>17</sup> Despite the fact that a hydroxyl on the surface could be beneficial for HDO processes, the strong interaction between the phenolic compounds and the alumina support could also generate severe catalyst poisoning.<sup>33</sup>



Ru/TiO<sub>2</sub> demonstrated an outstanding performance: unusual and high selectivity towards the direct deoxygenated product, without hydrogenation of the aromatic ring<sup>40</sup>. This is due to the active nature of the support TiO<sub>2</sub> and requires small (<2nm) Ru nanoparticles. Different groups<sup>40,41</sup> have investigated the catalytic conversion on different model compounds over this catalyst. It has been demonstrated that the direct deoxygenation pathway of phenol and guaiacol on titania involves a bifunctional catalyst, where the metal-support interface is participating in the reaction, while there is no apparent support, pore size, or morphology effects for the HYD pathway<sup>19</sup>.

For the DDO pathway, the overall activity and selectivity is higher for catalysts with more interfacial sites.<sup>40,41</sup> The following research<sup>19,42</sup> demonstrates the interfacial direct deoxygenation mechanism.

Under this mechanism, it has been proposed that the presence of a water molecule in close proximity to the interface avoids the formation of oxygen vacancy sites and generates the surface hydroxyl groups that favor acidic direct deoxygenation pathway, lowering the activation barrier of the process. Water acts as a co-catalyst for the reaction, favoring the hydrogen spillover and stabilizing the adsorbed molecule of phenol at the interface<sup>42</sup>.

The enhancement in DDO activity of TiO<sub>2</sub> was also proposed for other metals, even if the reaction mechanism is not demonstrated to happen at the interface. The use of gold supported on TiO<sub>2</sub> shows a preferential activation of C-O bond. Oxygenated aromatics form activated complexes with this catalyst, proposed by transition state theory. The kinetics studies led these authors to propose

that phenol hydrogenolysis and hydrogenation are the respective rate-limiting steps for DDO and HYD pathways respectively.<sup>43</sup>

Physical mixtures of Ni on different supports were investigated for HDO of guaiacol. High selectivities to C-O hydrogenolysis were obtained only for Ni over TiO<sub>2</sub> anatase because of the appearance of strong interactions between them.<sup>44</sup> Here, two types of Ni species are present. One type consisted of a cluster of Ni atoms affected by strong metal-support interactions (SMSI) after the reduction pretreatment, leaving a TiO<sub>2</sub> overlayer making the Ni particles completely inactive. Conversely, small amounts of Ni migrates onto the support, forming highly dispersed Ni, generating a new type of catalytic site that was highly selective for hydrodeoxygenation.<sup>44</sup>

Other studies on oxophilic supports have shown that direct deoxygenation mechanism is favored through tautomerization of phenolics.<sup>14,15,21</sup> Pd/ZrO<sub>2</sub> and Pd/TiO<sub>2</sub> catalysts exhibit high selectivity to deoxygenated products that can be explained by a mechanism that involves a keto-intermediate tautomer favored by oxophilic sites on the support.<sup>21</sup> Over Pd/SiO<sub>2</sub>, *m*-cresol is tautomerized to an unstable ketone intermediate and then the carbonyl group is hydrogenated, leading to C-O bond cleavage. This mechanism also competes with the ring hydrogenation mechanism.<sup>21</sup>

For Pd/ZrO<sub>2</sub> catalysts, the oxophilic sites are incompletely coordinated Zr<sup>4+</sup> cations (Lewis acid sites) near the perimeter of the metal. These sites favor the interaction of the tautomer oxygen group with the catalyst surface favoring the hydrogenation of the C=O bond. Therefore, carbonyl group hydrogenation is favored on the metal particles at the interface.<sup>15,21</sup> The mechanism of phenol as a model compound is shown in Figure 1.4.

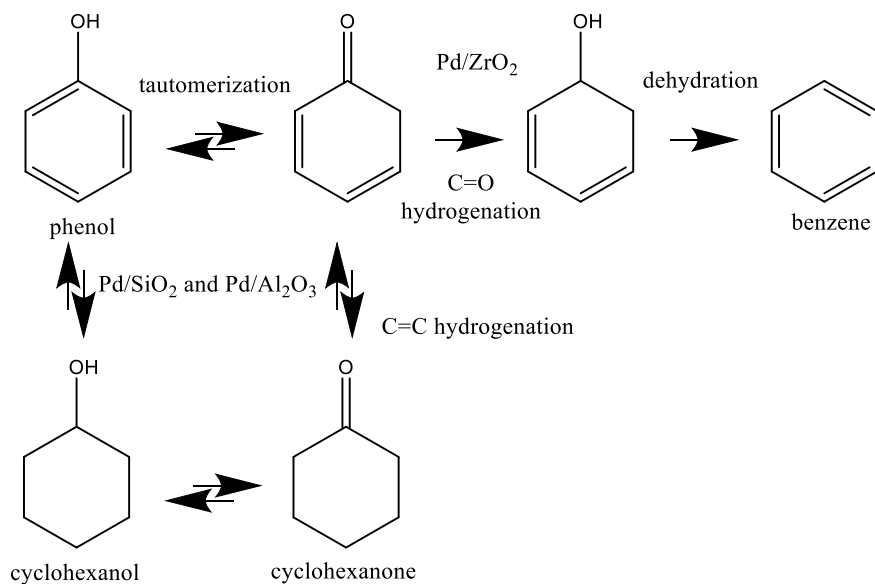
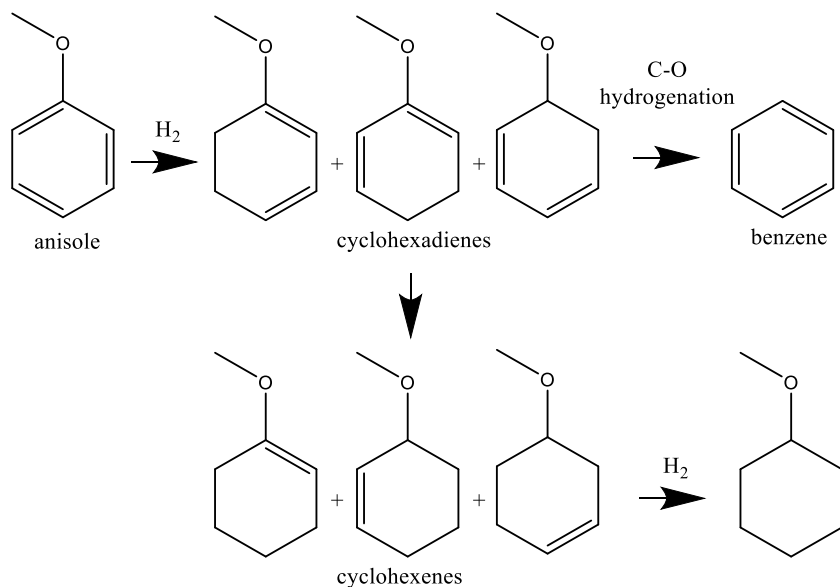


Figure 1. 4 Hydrodeoxygenation of phenol over Pd/SiO<sub>2</sub> or Pd/ZrO<sub>2</sub> via the tautomerization method, Adapted from.<sup>21</sup>

In zeolites, this same tautomerization mechanism was proposed. It was suggested that the formation of a pool of oxygenated intermediates adsorbed on the surface may influence the reaction pathway. Here, *m*-cresol and other phenolic compounds are trapped inside the zeolite. These trapped species can undergo several reaction paths, including condensation to heavier products (deactivation), decomposition to other aromatics, hydrogenolysis, and formation of molecular aggregates.<sup>23</sup> H<sub>2</sub> plays an important role in this reaction, because it keeps Ga species in its reduced form and stabilizes GaH<sup>2+</sup> species, promoting hydride transfer to the C-C and C-O bond of the condensation product, generating lighter aromatics.<sup>23</sup>

Tautomerization mechanism was also proposed in a more recent study<sup>45</sup>. Reaction of different model compounds over Ru/C in acetic acid shows that C–O bond cleavage does not proceed via a direct hydrogenolysis reaction of C–O bonds, but occurs due to side-reactions of the highly

reactive intermediates formed during hydrogenation such as cyclohexadiene- and cyclohexene-based enols, enol ethers, and allyl ethers. The hydrogenation of anisole with metallic Ru/C catalysts proceeds in a stepwise fashion via cyclohexadiene and cyclohexene intermediates as shown in Figure 1.5.<sup>45</sup>



*Figure 1. 5 Hydrodeoxygenation mechanism of anisole and the formation of the tautomer cyclohexadienes to further conversion into benzene. Adapted from.<sup>45</sup>*

In conclusion, it is important to notice that many different mechanisms have been proposed for direct deoxygenation of aromatic oxygenates. Some of them are in close agreement with each other, like the presence of an oxygen vacancy site that favors the adsorption of the oxygenated group. Other groups<sup>14,46-48</sup> have proposed the tautomerization mechanism as a different point of view for this reaction. This mechanism it still catching the attention of researchers, and it is expected that new insights will appear in upcoming publications.

## CHAPTER 2: PHENOL HYDRODEOXYGENATION

### 2.1. Introduction

While petroleum is currently the principal source of fuels and chemicals on the world stage, recent changes in global policy and concerns about sustainability have driven research focused on biobased fuels and chemicals.<sup>49,50</sup> Biomass is forecasted to comprise between 8 and 35%, under mitigation scenarios, of total primary energy supply by 2050.<sup>51</sup> This shift in focus has coincided with a change in the distribution of petroleum resources in the United States, where the shale gas boom has led to an abundance of light hydrocarbons, making biomass particularly useful as a source for liquid aromatics.

Pyrolysis is a thermochemical process to upgrade lignin into bio-oil and biochar, heating it up to 300 to 800°C in absence of oxygen. The feedstock, heating temperature, and rate of heat transfer determine the composition of the pyrolyzed product<sup>52</sup>. Bio oil production is still in a developing stage<sup>50</sup> and pyrolysis oil upgrading is desired. Fast pyrolysis at medium temperature (400 to 650°C) will lead to the higher content of bio-oils; unfortunately those bio-oils are highly oxygenated aromatic mixtures, diminishing its properties as a biofuel and having a low heating value of 16–18 MJ/kg.<sup>53</sup> Future efforts are needed to develop new feasible technology and methods for pyrolysis oil upgrading.<sup>54</sup> Finding a way to efficiently remove oxygen, without hydrogenating the aromatic ring, will increase the applicability of biomass for biofuels production.

Hydrodeoxygenation (HDO) is one of the most common processes for removal of oxygen from biomass<sup>55,56</sup>, whereby hydrogen is added to the molecule, reacting with oxygen atoms to release

water. Phenol can be used as a model compound to represent the complex mixture of oxygenated aromatics present in bio-oils, because cleavage of the last hydroxyl group in these molecules has been reported to be the most challenging <sup>8</sup>.

Nelson and coworkers have shown that phenol can undergo deoxygenation via two different mechanisms. One possible reaction pathway is called direct deoxygenation (DDO), which is a direct C-O hydrogenolysis reaction that converts phenol to benzene in a single step, as seen in Figure 2.1. Conversely, the catalytic step with the lower activation energy is the hydrogenation of the aromatic ring to yield cyclohexanol and cyclohexanone. Subsequent dehydration of cyclohexanol generates cyclohexene, which is rapidly reduced to cyclohexane. This overall sequence of steps is called hydrogenation (HYD), as shown in Figure 2.1. <sup>42</sup>

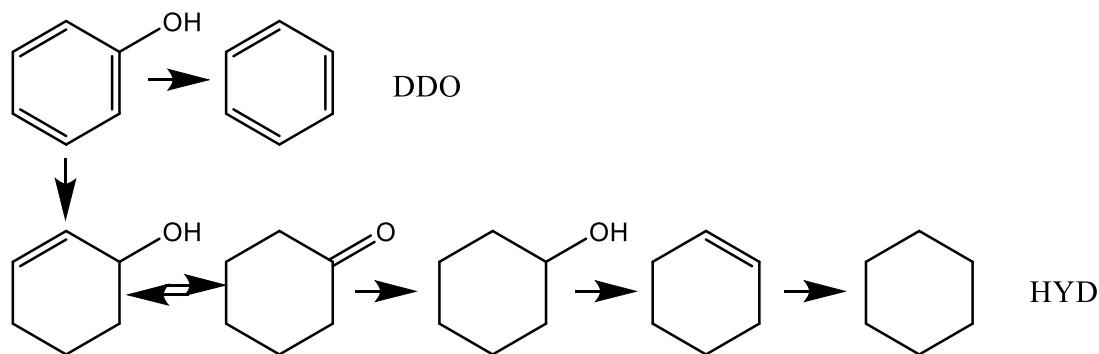


*Figure 2. 1 Reaction pathways for phenol hydrodeoxygenation. In the direct deoxygenation pathway (DDO) phenol is converted directly to benzene. In the hydrogenation pathway (HYD), phenol is hydrogenated and dehydrated into cyclohexanone, cyclohexanol, cyclohexene, and cyclohexane. <sup>42</sup>*

That the ring is not reduced in the DDO pathway makes this process much more efficient in terms of hydrogen consumption,<sup>40</sup> although it is also possible that benzene hydrogenates into cyclohexane under some conditions. Therefore, catalysts that favor the DDO pathway into benzene are desired. Newman and coworkers have demonstrated Ru/TiO<sub>2</sub> to achieve unusually high selectivity for DDO<sup>40</sup>. This has been hypothesized to be due the amphoteric nature of the TiO<sub>2</sub> support and its participation in metal-support interfacial sites<sup>19</sup>.

For the DDO pathway, the overall activity and selectivity is higher for catalysts with lower particle size related to more interfacial sites.<sup>40,41</sup> Subsequent publications from Nelson et al. and Omotoso et. al.<sup>19,42</sup> have proposed the interfacial direct deoxygenation mechanism.

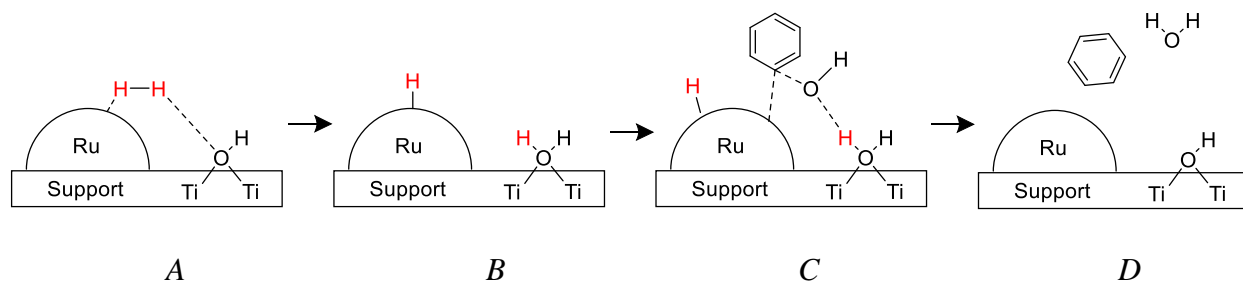


Figure 2. 2 Proposed molecular mechanism of DDO pathway for phenol over Ru/TiO<sub>2</sub>.<sup>57</sup>

The mechanism shown in Figure 2.2. starts with a hydroxyl on the TiO<sub>2</sub> surface in the vicinity of the Ru nanoparticle that acts as a Brønsted base. This hydroxyl helps facilitate the heterolytic cleavage of H<sub>2</sub> (A in Figure 2.2). This step forms a Brønsted acid on the support in close proximity to the interface, while the Ru hydride remains mobile in the metal (B in Figure 2.2). The DDO of phenol begins with its adsorption at the interfacial site as shown in C of Figure 2.2. Here the surface

hydroxyl protonates the phenolic oxygen, thereby weakening the C-O bond. Finally, the weakened C-O bond undergoes cleavage, while the released hydroxyl group leaves with a proton from the surface  $\text{Ti-OH}_2^+$  species generating a neutral water molecule. The adsorbed phenyl group is hydrogenated by the remaining hydride and subsequently desorbs as benzene (*D* in Figure 2.2).

57,58

Competing mechanisms in the literature suggest that the reaction occurs at oxygen vacancy sites in the  $\text{TiO}_2$  surface, generated by reduction with spilled-over hydrogen.<sup>42</sup> Indeed, calculations presented by Nelson and workers show that at near-zero water partial pressures, oxygen vacancies should exist and the reaction would occur at interface sites that incorporate these vacancies, rather than the hydroxyl groups described above. However, the intrinsic activation barrier for this pathway is 0.24 eV higher than that for the pathway shown in Figure 2.2.<sup>42</sup> Moreover, at non-zero water pressures, the oxygen vacancies will dissociate water, forming the active sites shown in Figure 2.2.

The influence of water on the reaction mechanism suggests there could be a substantial effect of water on the reaction rates, and such an effect has been observed by several authors. In particular, the selectivity for DDO of phenolic compounds can be increased by one order of magnitude when water is added.<sup>42,57</sup> This increase could be due to the competing mechanisms described above, although it could also be due to the presence of a water molecule in close proximity to the interface site, potential lowering the activation barrier for the reaction.

In this work, we have performed a rigorous kinetic study to obtain new and substantial evidence for the DDO mechanism. We show reaction orders with respect to water and phenol and use this information to define a consistent rate expression.

## **2.2. Objectives**

### **2.2.1 General Objective**

Elucidate kinetics and effect of water in the hydrodeoxygenation of phenol over Ru/TiO<sub>2</sub> catalyst.

### **2.2.2 Specific Objectives**

- Elucidate the influence of water on reactivity of phenol.
- Elucidate the influence of the crystal structure of the support TiO<sub>2</sub> on reactivity of phenol.
- Determine the reaction mechanism of phenol HDO.

## **2.3. Methodology**

### **2.3.1 Materials**

TiO<sub>2</sub> P-25 was donated by Evonik, TiO<sub>2</sub> rutile was purchased from US Research Nanomaterials and TiO<sub>2</sub> anatase was purchased from Nanografi. RuCl<sub>3</sub>·3H<sub>2</sub>O, was purchased from Sigma-Aldrich. Phenol (99.5%, extra pure, loose crystals, unstabilized, ACROS Organics™), and Decalin (Decahydronaphthalene, Mixture of cis + trans, 98%, Reagent Grade, Decalin™, Honeywell™) was purchased from Fisher Scientific. Fused silicon dioxide (4-20 mesh, 99.9% trace metals basis,

Aldrich) was used to fill the dead volume of the reactor column. The H<sub>2</sub> was Matheson, 99.999%. Also, for calibration purposes benzene (Sigma-Aldrich for HPLC  $\geq 99.9\%$ ) cyclohexane (Fisher Scientific HPLC grade), cyclohexene (Acros, 99% pure), cyclohexanol (Sigma Aldrich, Reagent Plus 99%) and cyclohexanone (Sigma Aldrich, Reagent Plus 99.8%) were used. D<sub>2</sub>O (Deuterium oxide, for NMR. 100.0 atom% D) was used for the kinetic isotope effect experiments.

### **2.3.2 Catalyst Preparation**

The catalysts used consisted of a 1.5 wt. % Ru on TiO<sub>2</sub>, with different TiO<sub>2</sub> structures, P25 (particle size of 1.8 +/- 0.5 nm), rutile (particle size of 2.0 +/- 0.5 nm) and anatase (particle size of 1.7 +/- 0.6 nm). Catalysts were synthesized and characterized by our collaborators.<sup>57</sup> Catalysts were prepared by co-precipitation on a 5 g scale. The metal precursor was RuCl<sub>3</sub>·3H<sub>2</sub>O and the mixtures were dried overnight at 90°C. The catalyst were further crushed and diluted in a 9:1 ratio with fused silica for more than 30 min.

### **2.3.3 High Pressure Flow Reactor Experiments**

The liquid phase reactor design was based on that published by Roman-Leshkov et al.<sup>59</sup> The design is shown in Figure 2.3 and some pictures of the actual reactor are presented in Figures 2.4 and 2.5. The liquid flow reactor includes a liquid delivery system, a gas delivery system, a reactor system with a separator, a manual sampling system and a pressure measurement system.

The gas delivery system consists of two Mass Flow Controllers to feed a constant flowrate of Ar (MFC#1) and/or H<sub>2</sub> (MFC#2) into the system and to pressurize it with help of a back-pressure regulator located downstream of the reactor and a safety relief valve.

A constant liquid flowrate of phenol, water and decalin as a solvent is sent to the reactor through an HPLC pump and is mixed with the H<sub>2</sub> flow before going to the reactor system. Both reactants move in up flow mode through the reactor system, which consisted of a ¼” stainless steel column packed with catalyst. The reactor heater was a heat tape wrapped around a cylindrical aluminum block that covers the column connected to a temperature controller.

The diluted catalysts were packed between two plugs of quartz wool in a quarter-inch outside diameter (OD) stainless steel tube. Prior to the reaction kinetics measurements, the catalyst was reduced at 573 K (5 K min<sup>-1</sup>) for at least one hour in 40 sccm flowing H<sub>2</sub>. Gas flow was controlled by a mass flow controller (Brooks 5850E). The reactor temperature was measured by a K-type thermocouple (Omega), and temperature control was provided by a PID controller (Automation Direct). Following reduction, a 0.53 M stream of phenol diluted in decalin was introduced to the reactor using an HPLC pump (Chromtech M-1), and the production rate of benzene was measured (i.e., the rate of DDO). The dead volume of the reactor was estimated to be 1.5mL before reaching the catalyst bed.

For experiments with water, mixtures of 90, 85, 80, and 75 wt.% phenol and respective 10 to 25 wt.% water (18 MΩ) were fed to the reactor, and a second HPLC pump was used to co-feed decalin at a flowrate sufficient to keep the net phenol concentration constant (0.53 M). for experiments

with respect to phenol, solutions of 0.53, 0.25, 0.12 and 0.05 M were fed to the reactor at different flowrates keeping constant the amount of phenol fed to the reactor and the volumetric ratio of hydrogen flowrate (scm) vs liquid flowrate (ml/min) at a value of 250, the same ratio reached in the set of experiments described above.

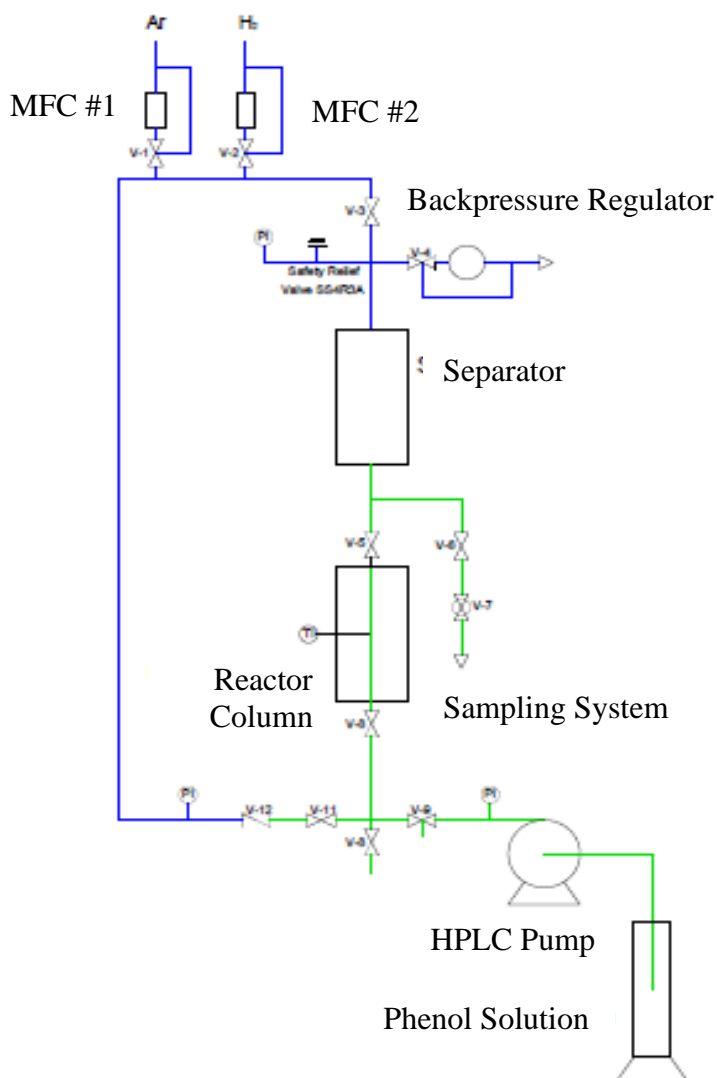
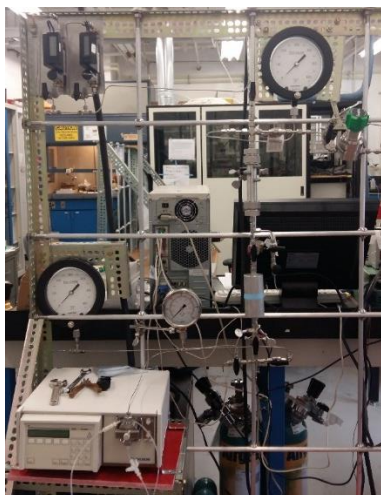


Figure 2. 3 Schematic diagram of the hydrogenation biphasic reactor.



*Figure 2. 4 Picture of the Hydrogenation biphasic reactor built at UMaine Catalysis Laboratory, showing HPLC pumps, pressure gauges, aluminum block, mass flow controller and the pressure regulator.*



*Figure 2. 5 Illustration of how the catalyst was packed, with a small bed of catalyst in the middle, quartz wool to keep it in place and silica chips to decrease the dead volume.*

Products are accumulated in the separator and periodically collected as a liquid batch sample through the sampling system. The sampling system consisted of a needle valve and a ball-valve

installed in series between the reactor and the separator. Liquid samples are further injected in a GC-FID. Concentrations of species in solution were measured using a gas chromatograph equipped with a flame ionization detector (Agilent 7820A). Separation was achieved using an Agilent DB-WAX column (30 m × 0.53 mm, 1 μm) and an method defined as follow. Oven: 313K for 5 min, then 313 to 533K at 10K/min, and 533K for 3 min. Carrier of helium at 30cm/s at 313 K. Injector: Split 1:10, 523K. Detector: FID, 573K. Retention times were 2.3 min for cyclohexane, 3.2 min for cyclohexene, 5.7 min for benzene, 13.1 min for cyclohexanone, 14.7 min for cyclohexanol and 21.4 min for phenol. Calibration curves for each compound are shown in Appendix B.3.

## **2.4. Determination of Reaction Conditions**

The desired reactor configuration for this system is called a bubble flow reactor,<sup>60</sup> where the reaction happens in the liquid phase with bubbles of gas flowing through the liquid allowing proper dilution of H<sub>2</sub> in the liquefied phenol. In terms of the gas delivery system, the gas flowrate was varied between 10 and 100 sccm and the H<sub>2</sub> concentration was modified by co-feeding Ar through a second MFC. The goal was to find a condition where the liquid phase existed and the diluted H<sub>2</sub> was in stoichiometric excess.

In terms of the liquid delivery system, other parameters need to be taken into consideration. In the first instance, phenol is a solid crystal at ambient temperature; therefore, the use of a solvent is necessary. Since we were interested in evaluating the effect of water in the reaction, water was not

a possible solvent. Tetrahydrofuran (THF) appeared to be a suitable solvent but it reacts with the catalyst leading to rapid deactivation. Decalin (decahydronaphthalene) was observed to be inert during the reaction, but the solubility of phenol in it is low and it is not miscible with water.

Therefore, a second pump was added for experiments where co-feeding water was needed. One pump supplied a mixture of phenol diluted in water and the other provided pure decalin to keep the desired total concentration in the final liquid phase. The total liquid flowrate should not influence the reaction rate, but it will modify the weight hourly space velocity (WHSV), defined as mass flowrate of reactant (usually pure phenol) per mass of Ru/TiO<sub>2</sub> catalyst and is necessary to calculate the reaction rate. In addition, the gas flowrate needed to be set proportionally. Finally, different reactants and concentrations in the liquid phase were evaluated in this reactor.

Regarding the catalyst itself, it has been demonstrated that the crystal structure of TiO<sub>2</sub> has a significant effect on the DDO rate,<sup>61</sup> therefore different catalysts were evaluated. A proper packing of the columns will prevent external mass transfer limitations. We evaluated different ways to pack the column and dilute the catalyst to enlarge the catalyst bed. (See appendix C for details)

### **2.4.1 Pretreatment**

The catalyst pretreatment was performed by *in situ* reduction under hydrogen, as expected. The catalyst was heated under flowing H<sub>2</sub> at atmospheric pressure until the reduction temperature was reached. After 4 h of reduction time, the system was pressurized and the liquid reactant was fed to the reactor, which is referred to as zero time-on-stream.

The rate of benzene production was also measured using a catalyst (Ru/P25) that was soaked in phenol to mimic the pretreatment used in the batch reactor experiments performed by our collaborators.<sup>57</sup> The catalyst was first reduced at 573 K, then cooled to room temperature in flowing H<sub>2</sub>. The sweep gas was switched to Ar (Matheson, 99.5%), and a stream of 90 wt.% phenol and 10 wt.% water was fed to the reactor while the temperature was increased to 573 K (5 K min<sup>-1</sup>). Once the reactor reached 573 K, the sweep gas was switched back to H<sub>2</sub> (40 sccm) and the rate of DDO was again measured. No significant difference was observed in the rate of DDO following this pretreatment: DDO rates were 0.380 ± 0.032 mol/gcat/min for the soak in phenol pretreatment and 0.400 ± 0.004 mol/gcat/min for the clean surface pretreatment, while HYD rates were 0.172 ± 0.05 mol/gcat/min for the soak in phenol pretreatment and 0.162 ± 0.004 mol/gcat/min for the clean surface pretreatment.

## 2.4.2 Non-Ideality

Because the liquid phase contains both alkanes and water, it is expected to see two liquid phases and one gas phase, all in chemical equilibrium.<sup>62</sup> Biphasic liquid systems arise from significant thermodynamic non-ideality, and by definition,<sup>63</sup> reaction rate expressions are proportional to activities ( $a_i$ ) or fugacities ( $f_i$ ) as shown in Equations 2.1 and 2.2. Thus, we must account for the influence of thermodynamic non-ideality on our reaction system.

$$r = k * a_A^x * a_B^y * a_C^z \quad (2.1)$$

$$a_i = \frac{f_i}{f_i^0} \quad (2.2)$$

Fugacities in the liquid phase  $\hat{f}_i^L$  can be expressed as functions of liquid mole fractions,  $x_i$ , activity coefficients,  $\gamma_i$ , and fugacities of pure components,  $f_i$ . Conversely, fugacities in the vapor phase,  $\hat{f}_i^V$ , can be expressed in terms of the vapor mole fraction, fugacity coefficient  $\phi$  and total pressure  $P$ .<sup>62</sup> At chemical equilibrium, the liquid and vapor fugacities are equivalent, as shown in Equation 2.3.

$$\hat{f}_i^L = x_i \gamma_i^L f_i^L = \hat{f}_i^V = y_i \hat{\Phi}_i^V P \quad (2.3)$$

The expression in Equation 2.3 can be simplified for ease of use. First, it is a good approximation to express fugacities of pure components in the liquid phase with respect to saturation parameters, as shown in Equation 2.4. Correspondingly, the fugacity coefficient for species  $i$ ,  $\phi_i$ , can be combined with the saturation fugacity coefficient,  $\phi_i^{sat}$ , and expressed as a ratio,  $\Phi_i$ , (Equation 2.5), which leads to the so-called gamma-phi formulation<sup>62</sup> of vapor-liquid equilibrium (Equation 2.6).

$$f_i^L \approx \phi_i^{sat} P_i^{sat} \quad (2.4)$$

$$\Phi_i = \frac{\hat{\Phi}_i^V}{\phi_i^{sat}} \quad (2.5)$$

$$\hat{f}_i = y_i \Phi_i P = x_i \gamma_i P_i^{sat} \quad (2.6)$$

This formulation can be further simplified for our system. It is possible to assume that for our conditions (650 psi and 300°C) the vapor phase behaves as an ideal gas, and  $\Phi_i = 1$ , even though the liquid is highly non-ideal. So, from Equation 2.6, we see that the fugacities in this system reduce to the vapor-phase partial pressures (Equation 2.7):

$$\hat{f}_i = y_i P = x_i \gamma_i^L P_i^{sat} \quad (2.7)$$

It could be the case that the vapor phase is indeed non-ideal. In this case, Equation (2.5) will strictly need to be applied.

### 2.4.3 Mass Transfer Limitations

Different parameters were calculated to assure the absence of mass and heat transfer limitations, for gas and liquid phase. The parameters and relevant criteria are as follows <sup>64</sup>:

Weiss-Prater (WP) criteria for intraparticle mass transfer:

$$\frac{r''' r_p^2}{C_s D_{eff}} < \frac{1}{|n|} \quad (2.8)$$

Interphase mass transfer criteria:

$$\frac{r''' r_p}{C_B k_c} < \frac{1}{|n|} \quad (2.9)$$

Mears criteria for intraparticle heat transfer:

$$\frac{|\Delta H| r''' r_p^2}{\lambda T_s} < \frac{T_s R}{E_{app}} \quad (2.10)$$

Combined criteria for intraparticle heat and mass transfer:

$$\left| \frac{n r''' r_p^2}{C_S D_{eff}} - \frac{(-\Delta H) r''' r_p^2 E_{app}}{\lambda R T_s^2} \right| < 1 \quad (2.11)$$

Where

$r'''$  = reaction rate per volume of catalyst (mol/m<sup>3</sup>s)

$r_p$  = particle radius (m)

$n$  = reaction order per each component

$C_S$  = component concentration at the surface of the pore in the respective phase (mol/m<sup>3</sup>)

$C_B$  = component concentration at the bulk phase in the respective phase (mol/m<sup>3</sup>)

$D_{eff}$  = effective diffusivity in the porous catalyst (m<sup>2</sup>/s)

$k_c$  = mass transfer coefficient between gas and solid particle (cm/s)

$\Delta H$  = heat of chemical reaction (J/mol)

$\lambda$  = thermal conductivity of particle (J/msK)

$T_s$  = Absolute temperature at the surface of the particle (K)

$R$  = Gas constant (J/molK)

$E_{app}$  = Apparent activation energy (J/mol) obtained from DFT calculations <sup>42</sup>

#### **2.4.4 Thermodynamic equilibria analysis**

In order to do a thermodynamic analysis of the reaction pathways, a Gibbs reactor in Aspen was used to obtain the equilibrium conditions for respective reactant and products. Empirical molar flowrates for phenol, water, decalin and H<sub>2</sub> were introduced, 650 psi and 300°C were set as reaction conditions for the Gibbs reactor. Decalin was defined as an inert.

Also, an equilibrium reactor was used to determine what would be the maximum possible conversion for DDO and HYD pathway as they were two independent mechanism and as both reaction pathways happen in parallel in a mixed mechanism. This calculation was made to elucidate if both reactions are energetically favorable under our current conditions.

#### **2.4.5 Benzene and Cyclohexane interconversion**

Independent experiments were done to elucidate if benzene and cyclohexane were interconverted under current conditions. In one experiment, 0.1 M benzene solution in decalin was fed to the

reactor at a 1 mmol/h, at 573K and 4482kPa. Here, we looked for the production of cyclohexane and cyclohexene through GC-FID. Analogously, a second experiment was carried out in the same defined conditions but by feeding a solution of 0.1M of cyclohexane.

#### **2.4.6 Kinetic isotope effect (KIE)**

In order to get more information about the influence of water, an experiment was run by co-feeding D<sub>2</sub>O instead of water. This data was compared with an experiment with co-fed of H<sub>2</sub>O under the same reaction conditions. Kinetic isotope effect correspond be the ratio of the regular DDO reaction rate with respect to the reaction rate performed in presence of the isotope.

### **2.5. Results**

#### **2.5.1 Data Treatment**

The catalysts used in this work exhibited first-order deactivation, defined in Equation 2.12.

$$r_{observed} = r_{initial}e^{-kat} \quad (2.12)$$

Figure 2.6 shows DDO and HYD observed rates as a function of time-on-stream. DDO corresponds to the rate of benzene produced in moles per grams of catalyst per hour, and HYD

rate corresponds to the sum of cyclohexane plus cyclohexene, cyclohexanol and cyclohexanone produced in the same units.

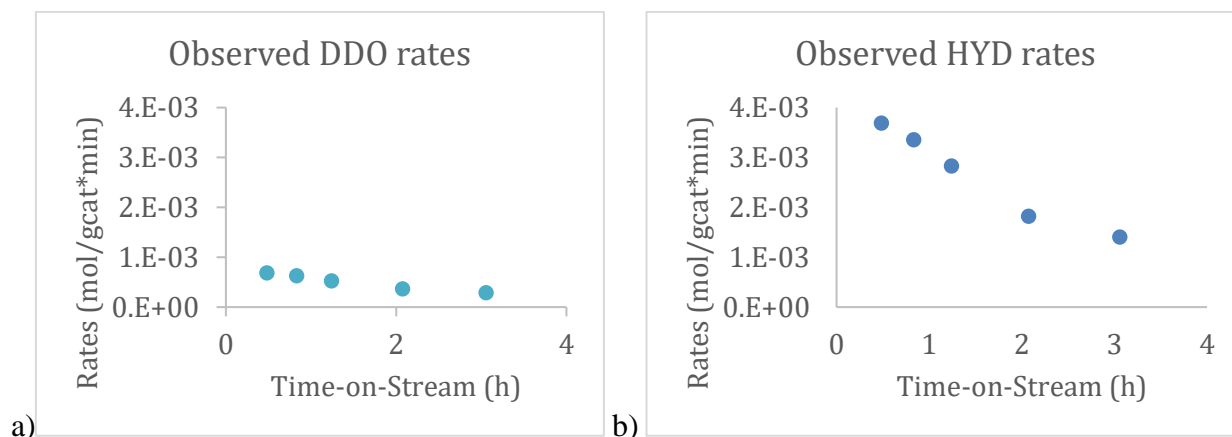


Figure 2. 6 DDO (a) and HYD (b) rates in moles per gram of catalyst per minute as a function of time-on-stream in h. DDO is the amount of benzene produced and HYD is the amount of cyclohexane plus cyclohexene, cyclohexanol and cyclohexanone produced in the same units. Reaction conditions: 573K and 4482kPa Ru/TiO<sub>2</sub>-Anatase NG<sup>57</sup>. WHSV of 235h<sup>-1</sup> of phenol 0.5M in decalin, GHSV of 970 h<sup>-1</sup> hydrogen. Conversion < 15%.

Figure 2.7 shows the natural logarithm of the DDO rates as a function of time-on-stream. From the figure, it is apparent that the system deactivates in a first-order fashion with respect to time-on-stream. It is possible to see a decrease in catalytic activity over time because of deactivation artifacts. Since the data are linear on a semi-log plot, then by definition the data exhibit first-order deactivation, as seen in Figure 2.7. By doing this mathematical treatment it is possible to calculate something that will be called the “initial rate”, which be the extrapolation at time zero. This value would correspond with good accuracy to a reaction rate that is not influenced by any deactivation

mechanism. Further results will only report initial reaction rates extrapolated from independent experiments conducted for at least 2h of time-on-stream.

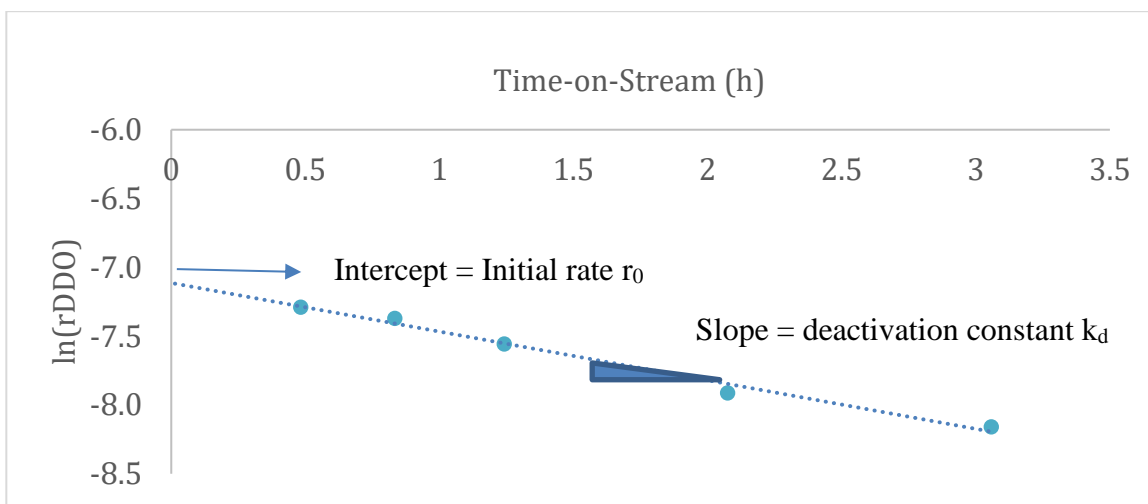


Figure 2. 7 Natural logarithm of DDO rates in moles per gram of catalyst per minute shown as a function of time-on-stream in h. The intercept obtained from extrapolation to time zero corresponds to the natural logarithm of the initial rate, in absence of deactivation mechanisms. The slope obtained from the trend line corresponds to the deactivation constant with respect to time, this value will not be reported on this thesis. Reaction conditions: 573K and 4482kPa Ru/TiO<sub>2</sub>-Anatase NG<sup>57</sup>. WHSV of 235h<sup>-1</sup> of phenol 0.5M in decalin, GHSV of 970 h<sup>-1</sup> hydrogen. Conversion < 15%.

Some analyses were done over our deactivated catalyst in order to understand our deactivation mechanism. Our TEM and TGA analyses are consistent with a deactivation mechanism governed by carbon deposition (See Appendix B).

Also, it is possible to obtain a deactivation constant, which will be the slope of the reaction rates on a semi-logarithmic plot. This will represent the exponential deactivation factor that governs the deactivation reaction over time as shown in Equation 2.12.

Since the goal of this project is elucidating the kinetics of DDO mechanism and there is not enough kinetic data to elucidate the conversion mechanism between all the HYD products, the sum of all possible products coming from the hydrogenation pathway will be reported as the HYD rate.

## 2.5.2 Differential Conditions

The mass balance for a packed bed reactor can be reduced to Equation 2.13. For packed bed reactors operating under differential conditions, the fractional conversion should depend inversely on WHSV as discussed extensively in the literature<sup>65</sup>. Phenol conversion (extrapolated to zero time-on-stream) was measured at several values of WHSV and, as shown in section 2.5.1, the reactor behaved according to the differential approximation at conversions as high as 20%. Consequently, all of the reaction kinetics data presented below were measured at phenol conversions of less than 20%.

$$-r'_A \left( \frac{g}{h*gcat} \right) = \frac{1}{MM_A} \frac{dX_A}{d\left(\frac{W}{m_{A0}}\right)} \sim \frac{\Delta X_A}{\Delta\left(\frac{1}{WHSV}\right)} \quad (2.13)$$

Reaction conditions at different combinations between phenol flowrate and mass of catalyst were tested leading to different values of 1/WHSV and obtaining its respective phenol total conversion based on the amount of product formed, which is justified because mass balance closed to within 7%.



By choosing a combination of mass of catalyst and liquid flowrates that lies under this linear trend, it can be assured that the reactor was run in a differential mode. Here it is possible to see that differential conditions are reached under different masses of catalysts as long as the liquid flowrate is high enough. At lower flowrates (i.e., larger inverse WHSVs), deviation from the ideal flow regime was seen, possibly due to channeling into the catalyst bed.

### **2.5.3 Mass Transfer Limitations**

Table 2.1 calculated values of the parameter needed for the calculation of the mass and heat transfer limitation criteria for all the possible reactants and phases in the system. Table 2.2 shows the final values of those criteria. All the values in Table 2.2 were below the upper limit transfer limitation, meaning that the experimental data were collected in a kinetically controlled regime. It is noticeable that for water in the liquid phase the Weiss-Prater criterion was relatively large, being right at the limit, this is mostly because the very low water concentration reached under experimental conditions. A Madon-Boudart test needs to be done in future work to discard any possible internal mass transfer limitation.

The possibility of interfacial mass transfer limitations was also evaluated, laying far away from the limit. Mears' criterion for intraparticle heat transfer was calculated to discard any heat effect. The last combined parameter is a mixture of the WP and Mears criteria, and the value for water in the liquid phase is again relatively large because of the low water concentration reached.

Unit Particle radio (m)		2.25x10 <sup>05</sup>
rate (mol/m <sup>3</sup> /s)		135
Mole concentration liquid (mol/m <sup>3</sup> )	H2	968.00
	PHENOL	104.56
	WATER	6.63
	DECALIN	2499.00
Mole concentration gas (mol/m <sup>3</sup> )	H2	799.20
	PHENOL	33.77
	WATER	45.08
	DECALIN	59.99
Diffusivity phenol mixture (m <sup>2</sup> /s)	H2	5.95 x10 <sup>-08</sup>
	PHENOL	1.14 x10 <sup>-08</sup>
	DECALIN	8.62 x10 <sup>-09</sup>
	WATER	3.88 x10 <sup>-08</sup>
Thermal conductivity (m/s)	H2	24.72
	PHENOL	8.21
	DECALIN	6.82
	WATER	18.61
Diffusivity liquid (m <sup>2</sup> /s)	H2	2.89 x10 <sup>-08</sup>
	PHENOL	2.89 x10 <sup>-08</sup>
	DECALIN	1.21 x10 <sup>-06</sup>
	WATER	7.28 x10 <sup>-08</sup>
Diffusivity gas (m <sup>2</sup> /s)	H2	1.93 x10 <sup>-06</sup>
	PHENOL	5.59 x10 <sup>-07</sup>
	DECALIN	1.16 x10 <sup>-06</sup>
	WATER	1.77 x10 <sup>-06</sup>

*Table 2.1 Intermediate parameter calculated for mass and heat transfer limitation parameters, for phenol, hydrogen and water in both liquid and gas phase.*

Test	Intraparticle Mass Weiss-Prater		Intephase Mass		Intraparticle Heat Mears		Intraparticle Heat + Mass	
	Liquid	Gas	Liquid	Gas	Liquid	Gas	Liquid	Gas
Phenol	5.7E-02	9.2E-04	4.3E-05	1.9E-05	4.0E-06	4.0E-06	0.18	2.8E-02
H <sub>2</sub>	1.2E-03	1.7E-05	1.0E-06	1.8E-07	4.0E-06	4.0E-06	1.3E-02	2.8E-04
Water	0.27	1.6E-04	1.6E-04	3.3E-06	4.0E-06	4.0E-06	0.6	3.5E-03
Target	< 0.3	< 0.3	< 0.15	< 0.15	< 0.075	< 0.075	< 1	< 1
Equation	11		12		13		14	

*Table 2.2 Results for calculation of mass and heat transfer parameters for phenol, hydrogen and water in both liquid and gas phase. All of the parameters meet the criteria but it is also noticeable that water in the liquid phase presents a significant value of the Weiss-Prater number that needs to be considered.*

Considering the absence of any heat and mass transfer limitations, it is reasonable to assume that catalyst pores are filled with liquid and that the reaction happens in the liquid phase that is in equilibrium with the vapor phase.

#### 2.5.4 Benzene and cyclohexane interconversion

From Table 2.3 it is possible to see that by feeding pure benzene and pure cyclohexane through the reactor, less than 10% of each is converted into cyclohexane and benzene, respectively, demonstrating that under current reaction conditions interconversion between cyclohexane and benzene is insignificant and will not be affecting our kinetics measurements.

Experiment	Flow rates per catalyst (mol/h*gcat)			
	Benzene in	Benzene out	Cyclohexane in	Cyclohexane out
0.1M Benzene	0.57	0.415		0.034
0.1M Cyclohexane		0.002	0.358	0.305

*Table 2.3 Benzene and cyclohexane flowrates, out of a reactor fed by a solution of 0.1 M of benzene or cyclohexane in decalin. Reaction conditions: 573K and 4482kPa Ru/TiO<sub>2</sub>-Rutile. WHSV of 19530 h<sup>-1</sup> for benzene and 12620 h<sup>-1</sup> for cyclohexane respectively, GHSV of 970 h<sup>-1</sup> hydrogen. Conversion < 15%.*

#### 2.5.5 Thermodynamics equilibria analysis

Table 2.4 shows the results of the thermodynamics equilibria analysis from Aspen's Gibbs reactor. At equilibrium, phenol hydrodeoxygenation is exergonic for DDO and HYD, leading to a 100% conversion of phenol for all cases, i.e. both reaction pathways are thermodynamically downhill.

Considering the mixed scenario, where DDO and HYD happen in parallel, the product distribution favors cyclohexane production, which is reasonable considering the hydrogenation of benzene. Current reaction rates indicated that from a thermodynamic standpoint the residence time is not enough to reach equilibrium.

Mechanism	Phenol → Benzene	Phenol → Cyclohexane	Phenol → DDO + HYD
H2 Conversion	5.5%	5.5%	5.5%
Phenol Conversion	100%	100%	100%
DDO Selectivity	100%	-	0.005%
HYD Selectivity	-	100%	99.995%

*Table 2. 4 Results of energy analysis estimates with Aspen Plus™. Conversion and selectivity from a Gibbs reactor estimated for just benzene, just cyclohexane and both DDO and HYD pathway. Reaction conditions: 573K and 4482kPa. WHSV of 235h<sup>-1</sup> of phenol 0.5M in decalin, GHSV of 970 h<sup>-1</sup> hydrogen.*

Table 2.5 shows the product distribution at equilibrium. Results show that at equilibrium the reaction is 99% selective for cyclohexane, being different than current results that produce an even distribution of all possible products. That means that under current conditions, the product distribution is not governed by thermodynamics but rather reaction kinetics.

Component	Mol Fr.	Selectivity (%)
BENZENE	1.29E-07	0.01%
CYCLOHEXANE	0.002179	99.99%
CYCLOHEXENE	3.85E-08	0.00%
CYCLOHEXANOL	8.43E-16	0.00%
CYCLOHEXANONE	1.20E-15	0.00%
Products	2.18E-13	

*Table 2. 5 Results of energy analysis estimates with Aspen Plus™. Product distribution from a Gibbs reactor estimated for a mixture of DDO and HYD pathway. Reaction conditions: 573K and 4482kPa. WHSV of 235h<sup>-1</sup> of phenol 0.5M in decalin, GHSV of 970 h<sup>-1</sup> hydrogen.*

The analysis presented in sections 2.5.1 to 2.5.5 demonstrates from both experimental and theoretical aspects of reactor design, that at the conditions used here the flow reactor was running in a kinetically controlled regime. High pressure (650 psi) and high flowrate of pure H<sub>2</sub> was chosen (between 40 to 170 sccm), in accordance with a high liquid flowrate allowing the collection of samples in a convenient way (between 0.15 to 1.50 mL/min).

Phenol concentration in the liquid feed was varied between 0.5M and 0.05M, and the water concentration was varied by using two pumps in parallel. Different catalysts were evaluated, presenting in this work the results of Ru/TiO<sub>2</sub>-Anatase (Nanografi), Ru/TiO<sub>2</sub>-Rutile USR and Ru/TiO<sub>2</sub>-P25.<sup>57</sup>

### **2.5.6 Effect of water on DDO kinetics**

Previously, our collaborators determined experimental evidence for enhancement in DDO activity in presence of water. By switching to a 10% wt. water condition, they saw a 10-fold enhancement in DDO/HYD activity data.<sup>42</sup>

In addition, Omotoso et al.<sup>19</sup> saw the same enhancement effect of water using different Ru loadings and different TiO<sub>2</sub> supports. They evaluated the conversion of *m*-cresol in the gas phase at 400°C. By having a high ratio of active sites with respect to water, they saw a bigger

enhancement effect on P25 and anatase, they also reported no significant influence of the crystal structure of the support.

For this project, experiments in absence and in presence of water for Ru/TiO<sub>2</sub> rutile, anatase and P25 were evaluated. Here a positive enhancement in DDO rates for the three catalyst was seen, under similar conditions as shown in Figure 2.9.

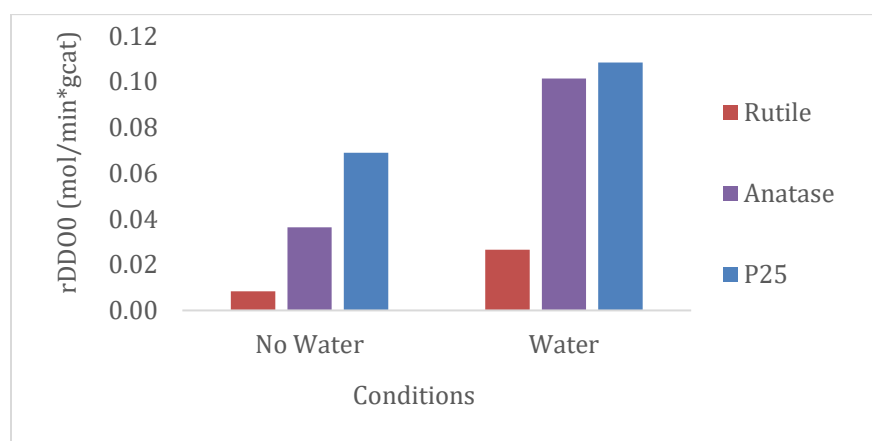


*Figure 2. 9 Initial DDO rates evaluated at similar condition with and without co-feed of water, for different Ru/TiO<sub>2</sub> catalysts. DDO is the amount of benzene produced in moles per grams of catalyst per hour. Reaction conditions: 573K and 4482kPa Ru/TiO<sub>2</sub>-Rutile, Anatase NG and P25<sup>57</sup>. WHSV of 235h<sup>-1</sup> of phenol 0.5M in decalin, GHSV of 970 h<sup>-1</sup> hydrogen. Co-feed 60h<sup>-1</sup> of water. Conversion < 15%.*

Figure 2.10 shows rates of DDO as a function of the inlet liquid water composition, for Ru/rutile and Ru/anatase, both on a log-log scale; there is no clear mechanistically-interpretable trend in the data analyzed in tis way. Therefore, it was necessary to account for the thermodynamically non-ideal phase separation inside the reactor.

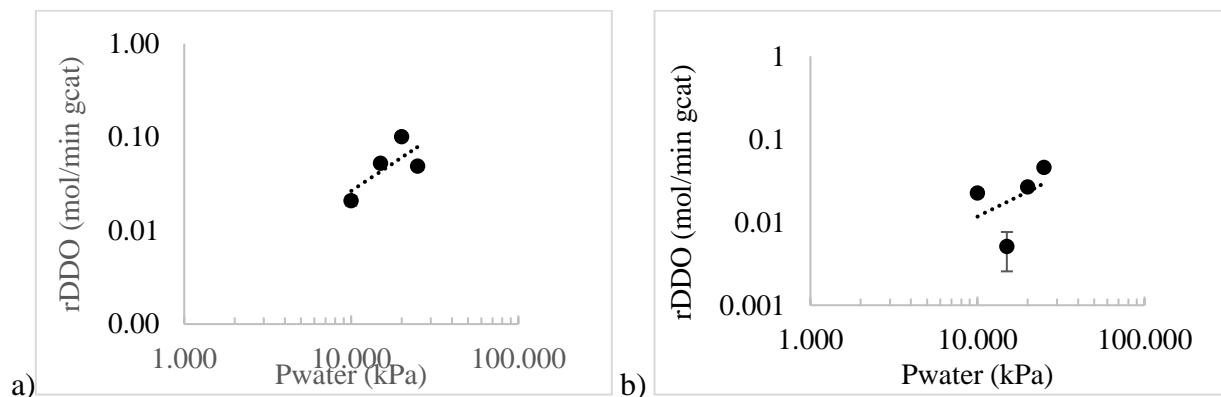


Figure 2.10 Rates of direct deoxygenation of phenol with respect to the initial liquid composition of water on a log-log scale for (a) Ru/TiO<sub>2</sub>-Anatase<sup>57</sup> and (b) 4482kPa Ru/TiO<sub>2</sub>-Rutile<sup>57</sup>. Reaction conditions: 573K and 4482kPa Ru/TiO<sub>2</sub>-Rutile<sup>57</sup>. WHSV of 235h<sup>-1</sup> of phenol 0.5M in decalin, GHSV of 970 h<sup>-1</sup> hydrogen. Co-feed between 27 and 80h<sup>-1</sup> of water. Conversion < 15%.

After defining the correct method to determine the liquid and gas phase distribution, results were presented with respect to the newly calculated water partial pressure.

From Figure 2.11 it is possible to see rates of DDO (a) and HYD (b) as a function of water partial pressure, in the gas phase both on a logarithmic scale. The water partial pressure was calculated as defined in section 2.4.2. For Ru/rutile, as expected, an increase in the DDO pathway with respect to water is found, suggesting that at higher concentrations of water the number transition states available on the surface increased. The same trend was found for the HYD pathway.

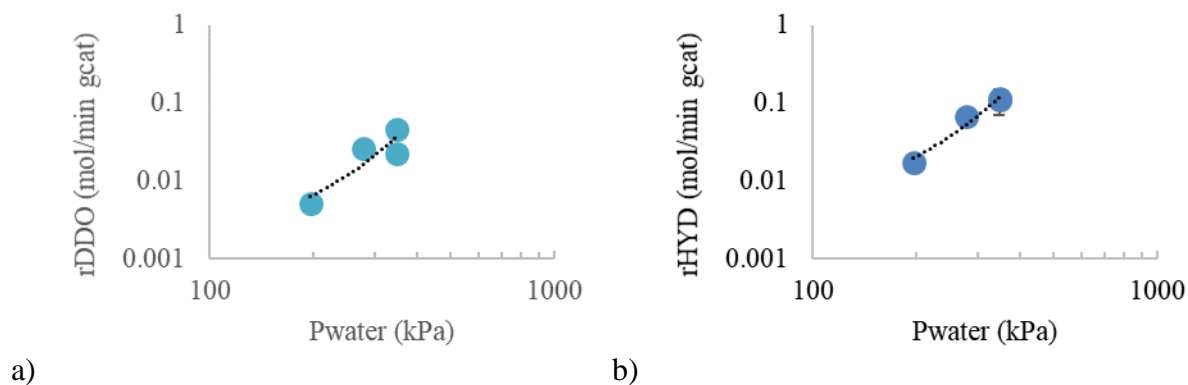


Figure 2. 11 Rates of direct deoxygenation (a) and hydrogenation (b) of phenol with respect to partial pressure of water on a log-log scale. Reaction conditions: 573K and 4482kPa Ru/TiO<sub>2</sub>-Rutile<sup>57</sup>. WHSV of 235h<sup>-1</sup> of phenol 0.5M in decalin, GHSV of 970 h<sup>-1</sup> hydrogen. Co-feed between 27 and 80h<sup>-1</sup> of water. Conversion < 15%.

Surprisingly, for Ru/Anatase, the results follow an opposite trend, and for the current set of experiments shown, co-feeding a higher concentration of water decreased the activity for both DDO and HYD pathway, as seen in Figure 2.12.

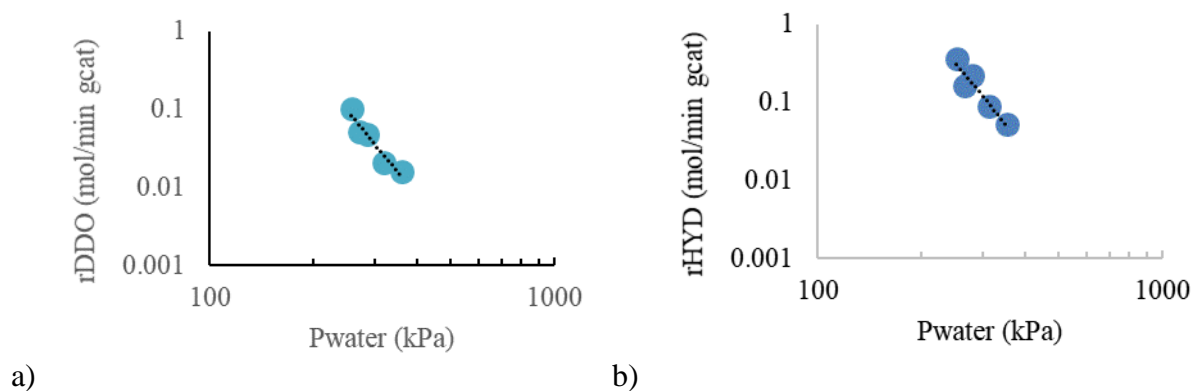


Figure 2. 12 Rates of direct deoxygenation (a) and hydrogenation (b) of phenol with respect to partial pressure of water on a log-log scale. Reaction conditions: 573K and 4482kPa Ru/TiO<sub>2</sub>-

Anatase NG<sup>57</sup>. WHSV of 235h<sup>-1</sup> of phenol 0.5M in decalin, GHSV of 970 h<sup>-1</sup> hydrogen. Co-feed between 27 and 80h<sup>-1</sup> of water. Conversion < 15%.

### 2.5.7 Effect of phenol for rutile and anatase

To get more information for the reaction pathway, experiments were done at different concentrations of phenol keeping the same vapor/liquid ratio. Reaction orders with respect to phenol are significantly different between Ru/TiO<sub>2</sub> rutile and anatase, as seen in Figures 2.13 and 2.14.

For DDO pathway, reaction order shifts with respect to phenol for rutile, but it is constant for anatase. On the other hand, reaction orders of HYD rates with respect to phenol comparable for the DDO trend on rutile and fractional order for anatase.

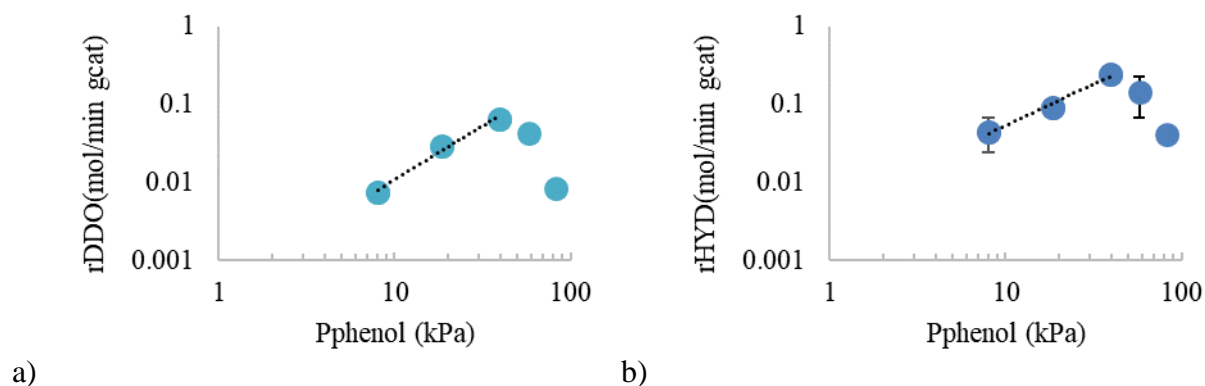


Figure 2. 13 Rates of direct deoxygenation (a) and hydrogenation (b) of phenol with respect to partial pressure of phenol on a log-log scale. Reaction conditions: 573K and 4482kPa Ru/TiO<sub>2</sub>-

Rutile <sup>57</sup>. WHSV of 235h<sup>-1</sup> of phenol 0.05 to 0.5M in decalin, GHSV of 970 to 9700 h<sup>-1</sup> hydrogen.

Conversion < 15%.

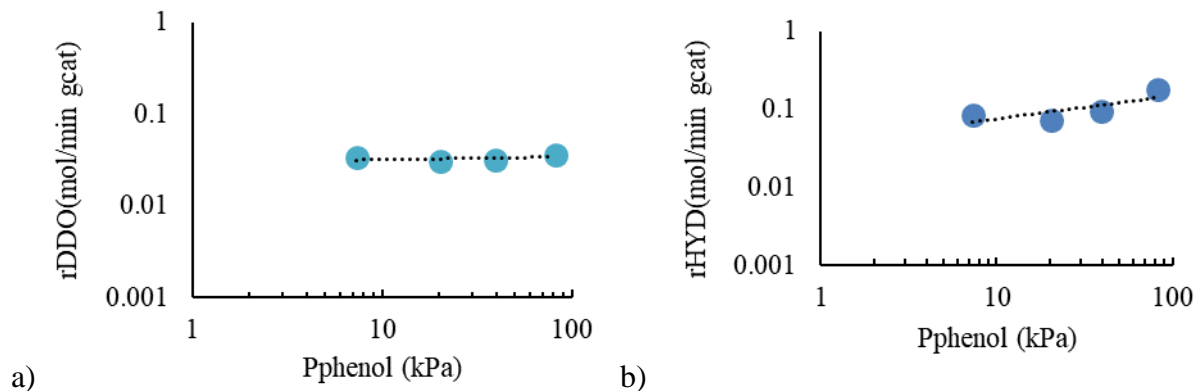


Figure 2. 14 Rates of direct deoxygenation (a) and hydrogenation (b) of phenol with respect to partial pressure of phenol on a log-log scale. Reaction conditions: 573K and 4482kPa Ru/TiO<sub>2</sub>-Anatase NG. <sup>57</sup> WHSV of 235h<sup>-1</sup> of phenol 0.05 to 0.5M in decalin, GHSV of 970 to 9700 h<sup>-1</sup> hydrogen. Conversion < 15%.

### 2.5.8 Kinetic isotope effect (KIE)

In order to get more information about the influence of water, an experiment was run by co-feeding D<sub>2</sub>O (Deuterium oxide, for NMR. 100.0 atom% D) instead of water. This data was compared with an experiment with co-fed of H<sub>2</sub>O under the same reaction conditions. Kinetic isotope effect correspond be the ratio of the regular DDO reaction rate with respect to the reaction rate performed in presence of the isotope. The values are presented in Table 2.6.

	KIE DDO
--	---------

Anatase 10% H <sub>2</sub> /D <sub>2</sub> O	1.00
Anatase 10% regular	1
Rutile 10% H <sub>2</sub> /D <sub>2</sub> O	2.51
Rutile 10% regular	1

Table 2. 6 KIE for direct deoxygenation of phenol diluted with D<sub>2</sub>O instead of water.. Reaction conditions: 573K and 4482kPa Ru/TiO<sub>2</sub>-Rutile<sup>57</sup>. WHSV of 235h<sup>-1</sup> of phenol 0.5M in decalin, GHSV of 970 h<sup>-1</sup> hydrogen. Co-feed of 27 h<sup>-1</sup> of water and D<sub>2</sub>O. Conversion < 15%.

## 2.6. Discussion

### 2.6.1 Effect of water and crystal structure of the support

We discovered significant differences with the crystal structure of our supports that were related to the amount of water adsorbed in the support, and to the enthalpy of adsorption of those water molecules in the support.<sup>66</sup>

Based on kinetics experiments and results of isotopic trace experiments, we propose an updated mechanism where adsorbed water will favor proton shuttling in a mechanism consistent with the Ru/rutile trend instead of the one proposed by Nelson et al.<sup>42</sup>

The updated mechanism is shown in Figure 2.15. We propose that weakly adsorbed water at the surface participates in the transition state for C-O bond scission. Those molecules stabilized by hydrogen bonding with other water molecules act as Brønsted acids, transfer a proton to the phenolic hydroxyl, facilitating C-O cleavage, in one elementary step (corresponding to the RDS).

In the meantime, water is re-protonated by spilled-over hydrogen, reconstructing the interfacial active sites.

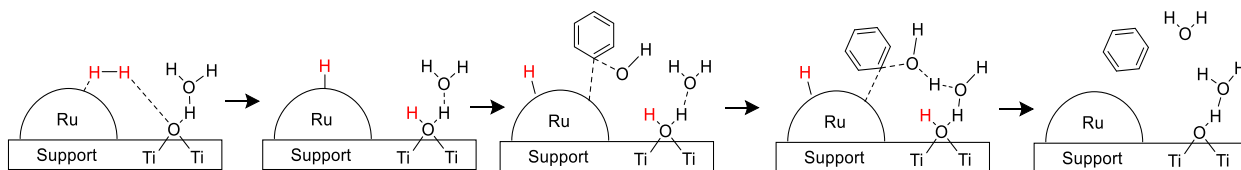


*Figure 2. 15 Updated molecular mechanism of DDO pathway for phenol over Ru/TiO<sub>2</sub>, with a mechanism consistent with isotopic trace experiments and kinetic results. Mechanism is proposed for experiments in presence of water as a co-reactant.*

Our mechanism account on C-O scission step as rate determining. Based on DFT calculations generated from our collaborators, it was concluded that even since the activation energy for C-O bond scission (0.48 eV) was not the highest in the sequence, its corresponding Gibbs free energy under moderate reaction conditions resulted in negligible values for the adsorption and desorption steps.<sup>42</sup>

Water can be easier adsorbed on protonated hydroxyls groups at the interface rather than metal hydrides.<sup>67</sup> The proton shuttling effect was proposed in Saavedra's work, for CO oxidation over Au/TiO<sub>2</sub>, where water molecules adsorbed on the protonated hydroxyls groups from the support act as amphoteric site in a similar way as the way proposed by earlier work.<sup>42</sup>

We believe that under this mechanism the surface hydroxyls do not play a direct role in the reaction, but they help in anchoring water to the support surface through hydrogen bonding and

transferring protons from the support through water as proposed by Saavedra's work.<sup>68</sup> Water participates in the transition state; changing the water concentration changes the number of transition states, and therefore the reaction rates. Saavedra's kinetics studies showed that water did not affect the rate constant, but it affected the coverage of weakly adsorbed water at the MSI affecting the rate expression.<sup>66,68-70</sup> Based on our previous premises the type of support will not be directly important for the mechanism, and it will only influence the amount of adsorbed water available.

Besides CO oxidation, other C-O bond cleavage reactions were reported with consistent evidence to our proposed reaction mechanism. For furfural liquid hydrodeoxygenation<sup>47</sup> over a Pd catalyst, it was proposed a water-mediated protonation mechanism favoring C-O bond hydrogenolysis, which was the kinetically relevant step under water-rich environments. Their work proposed a stabilization effect of water.

The negative reaction order with respect to water for DDO over Ru/anatase is more difficult to explain, but we believe that the originally proposed mechanism (Figure 2.2) should govern the reaction performance under this case.

The negative effect of water can be related to the hydrophilicity of anatase and therefore water could be a MASI for this mechanism. Anatase surface is more hydrophilic than rutile surfaces, and it would lead to higher water adsorption at the catalyst interface. Stone and coworkers<sup>1</sup> performed microcalorimetry measurements of water adsorption on anatase and rutile powders indicating that

water adsorbed more strongly on anatase surfaces (heat of reversible adsorption = -60 kJ/mol) than on rutile surfaces (heat of reversible adsorption = -44 kJ/mol). Further studies of IR spectroscopy of the hydroxyls in the surfaces of these materials showed substantial hydrogen bonding in the anatase hydroxyls, consistent with more hydrophilic surface and less hydrogen bonding for anatase hydroxyls than for rutile.<sup>71</sup>

Studies in CO oxidation demonstrated that water could also be a most abundant surface intermediate. Saavedra's work showed a similar trend, reaching a maximum in conversion, at 2 monolayers of water (600 Pa), and then a decrease in activity with higher water concentration.<sup>72</sup> It was suggested that weakly adsorbed water can inhibit other reaction, like CO oxidation by blocking sites at the metal-support interface that could suppress CO adsorption at the gold nanoparticle.<sup>70 66 72 67</sup> The presence of water affecting the RDS was also observed in Pt clusters<sup>70</sup> and phenol conversion over ReS<sub>2</sub>/SiO<sub>2</sub>.<sup>73</sup> The activation of H<sub>2</sub> at the metal support interface, via heterolytic cleavage could also be suppressed by water adsorption on the hydroxyls groups<sup>66</sup>

A negative effect with respect to water for Ru/anatase also suggest that water cannot play an important role in the rate determining step to reach the observed -1 order.<sup>57</sup>

### **2.6.1 Effect of phenol**

For Ru/rutile, DDO and HYD followed a first order trend at lower phenol concentration, and a negative order at higher concentration. To the other side, while reaction rates for Ru/anatase were zero order for DDO, HYD presented a fractional order with respect to phenol.

Those trends are also consistent with C-O bond cleavage being the rate-determining step and it suggest that two active sites are involved in this step. The C-O scission requires the existence of an adjacent metal site, where the phenyl group will remain adsorbed, and further hydrogenated, therefore we accounted for one interfacial and one metal site in the mechanism.

It is worth noticing that phenol can also be adsorbed at the metal nanoparticle only, leading to the HYD pathway. Therefore, phenol can be a MASI for the metal sites under certain conditions. Water may stabilize adsorbed phenol, increasing the coverage of phenolic species at high phenol concentrations and leading to the decrease in activity shown in the rutile trend at higher water concentration in in Figure 2.13. In this case, phenol could become as a site blocking agent by itself.

## **2.6.2 Derivation of the rate expression**

We propose a sequence of elementary steps as follows. This sequence accounts for the existence of two different types of active sites for DDO pathway. The first one is the interfacial site (\*) between the metal and the support, where adsorption of phenol and C-O bond cleavage takes place. The second active site is the metallic site ( $\Delta$ ) that facilitates two different types of hydrogen adsorption, and hydrogenation of the phenyl group into benzene. The existence of two active sites was also considered for the CO oxidation mechanism.<sup>66</sup> All of those assumptions are illustrated in Figure 2.16.

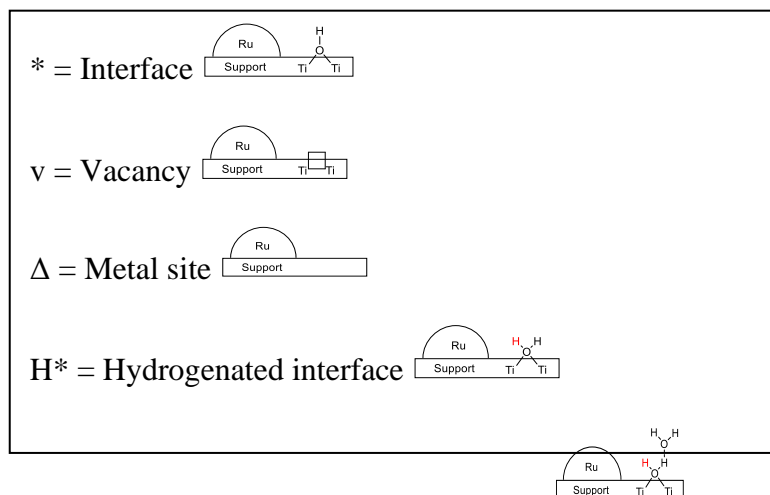
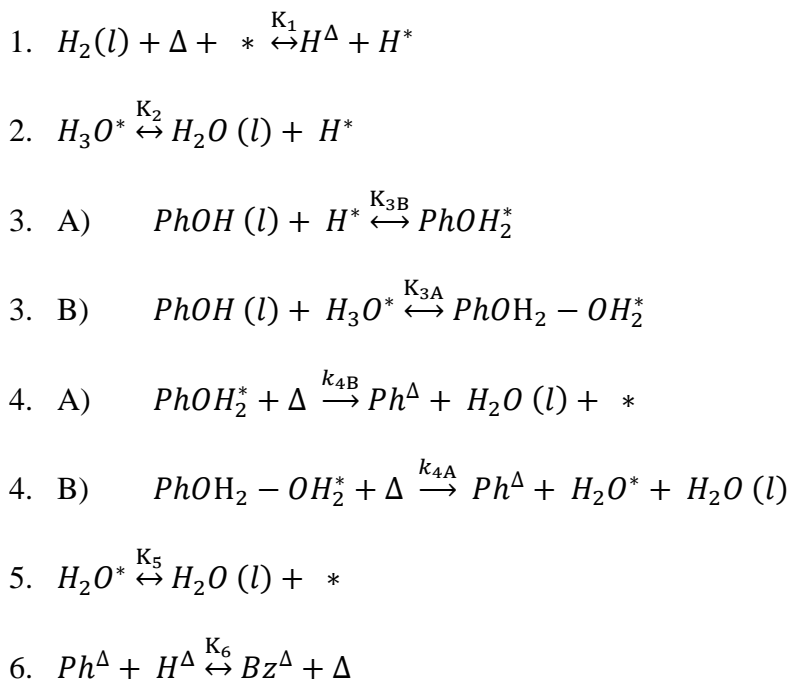
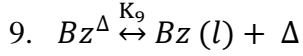
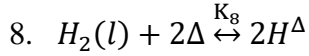
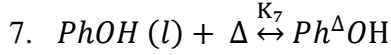


Figure 2. 16 Schematic representation of all the possible active sites used in the derivation for the rate expression. Pictures based on Figure 2.2.

We propose the following sequence of elementary steps valid for both catalysts rutile and anatase, although the RDS will be different for each case.





As mentioned earlier, the rate-determining step for DDO involves the C-O bond scission for each catalyst, although the corresponding transition state is different in each case.

For Ru/anatase, the negative order with respect to water and zero order with respect to phenol can be explained considering that step 4.A is the RDS. The derivation of the rate expression is presented as follow, and it accounts for the coverages over two different active sites; the interfacial site ( $\theta^*$ ) and the metal site ( $\sigma^{\Delta}$ ).

$$r = r_{4A} = k_{4A}\theta_{PhOH_2}\sigma^{\Delta}$$

Considering that all the other elementary steps (1-3, 5-10) are quasi-equilibrated, it is possible to express coverage as a function of the partial pressures of phenol ( $P_{PhOH}$ ), hydrogen ( $P_{H_2}$ ), benzene ( $P_{Bz}$ ), and water ( $P_{H_2O}$ ).

For the interfacial site:

$$\theta_H = \frac{K_1}{K_8^{0.5}} P_{H_2}^{0.5} \theta^*$$

$$\theta_{PhOH_2} = \frac{K_1 K_{3A}}{K_8^{0.5}} P_{H_2}^{0.5} P_{PhOH} \theta^*$$

$$\theta_{H_2O} = \frac{1}{K_5} P_{H_2O} \theta^*$$

$$\theta_{PhOH_2-OH_2} = \frac{K_1 K_2}{K_9 K_8^{0.5}} P_{H_2}^{0.5} P_{PhOH} P_{H_2O} \theta^*$$

$$\theta_{H_3O^+} = \frac{1}{K_2} P_{H_2O} \theta^*$$

and for the metal site:

$$\sigma_H = K_8^{0.5} P_{H_2}^{0.5} \sigma^\Delta$$

$$\sigma_{Ph} = \frac{1}{K_6 K_8^{0.5} K_9} P_{H_2}^{0.5} P_{Bz} \sigma^\Delta$$

$$\sigma_{PhOH} = K_7 P_{PhOH} \sigma^\Delta$$

$$\sigma_{Bz} = \frac{1}{K_9} P_{Bz} \sigma^\Delta$$

therefore,

$$r = r_{4A} = k_{4A} K_1 K_{3A} K_8^{-0.5} P_{H_2}^{0.5} P_{PhOH} \theta^* \sigma^\Delta$$

A site balance for interfacial sites led to:

$$1 = \theta^* + \theta_H + \theta_{PhOH_2} + \theta_{H_2O} + \theta_{H_3O^+}$$

therefore,

$$\theta^* = \frac{1}{1 + \frac{K_1}{K_8^{0.5}} P_{H_2}^{0.5} + \frac{K_1 K_{3A}}{K_8^{0.5}} P_{H_2}^{0.5} P_{PhOH} + \frac{1}{K_5} P_{H_2O} + \frac{1}{K_2} P_{H_2O}}$$

Correspondingly, a site balance for metal sites led to:

$$1 = \sigma^\Delta + \sigma_H + \sigma_{Ph} + \sigma_{PhOH} + \sigma_{Bz}$$

Therefore,

$$\sigma^{\Delta} = \frac{1}{1 + K_8^{0.5} P_{H_2}^{0.5} + \frac{1}{K_6 K_8^{0.5} K_9} P_{H_2}^{0.5} P_{Bz} + K_7 P_{PhOH} + \frac{1}{K_9} P_{Bz}}$$

$$r = r_{4A} = \frac{k_{4A} K_1 K_{3A} K_8^{-0.5} P_{H_2}^{0.5} P_{PhOH}}{\left(1 + \frac{K_1}{K_8^{0.5}} P_{H_2}^{0.5} + \frac{K_1 K_{3A}}{K_8^{0.5}} P_{H_2}^{0.5} P_{PhOH} + \frac{1}{K_5} P_{H_2O} + \frac{1}{K_2} P_{H_2O}\right) \left(1 + K_8^{0.5} P_{H_2}^{0.5} + \frac{1}{K_6 K_8^{0.5} K_9} P_{H_2}^{0.5} P_{Bz} + K_7 P_{PhOH} + \frac{1}{K_9} P_{Bz}\right)}$$

This expression could be further simplified, considering current experimental conditions. Since all the experiments were done at constant  $H_2$  partial pressure and at differential conditions, the partial pressure of  $H_2$  can be absorbed into the apparent rate constant and the partial pressure of benzene should be negligible, leading to the simplified expression in Equation 2.14.

$$r = r_{4A} = \frac{k' P_{PhOH}}{(K' + K_{PhOH} P_{PhOH} + K_{H_2O} P_{H_2O})(K'' + K_{HYD} P_{PhOH})} \quad (\text{Equation 2.14})$$

where,

$$k' = k_{4A} K_1 K_{3A} K_8^{-0.5} P_{H_2}^{0.5} = \text{constant}$$

$$K' = 1 + \frac{K_1}{K_8^{0.5}} P_{H_2}^{0.5} = \text{constant}$$

$$K_{PhOH} = \frac{K_1 K_{3A}}{K_8^{0.5}} P_{H_2}^{0.5} = \text{constant}$$

$$K_{H_2O} = \frac{1}{K_5} + \frac{1}{K_2} = \text{constant}$$

$$K'' = 1 + K_8^{0.5} P_{H_2}^{0.5} + \frac{1}{K_6 K_8^{0.5} K_9} P_{H_2}^{0.5} P_{Bz} + \frac{1}{K_9} P_{Bz} = \text{constant}$$

$$K_{HYD} = K_7 = \text{constant}$$

Equation 2.14 can be fitted to all the experimental trends related with Ru/anatase, considering different magnitudes of the apparent equilibrium constants and partial pressures.

Since anatase was highly hydrophilic,  $K_{H_2O}$  is expected to be a very large number. At constant phenol concentration, and assuming that water is a MASI the trend is consistent with the negative order with respect to water. Here:

$$K_{H_2O}f_{H_2O} \gg K' + K_{PhOH}f_{PhOH}$$

Neglecting the terms with lower magnitudes, the rate expression becomes as follow.

$$r = \frac{k'f_{PhOH}}{(K_{H_2O}f_{H_2O})(K'' + K_{HYD}f_{PhOH})} = k'f_{H_2O}^{-1}$$

To explain the reaction order with respect to phenol ( $n=0$ ), phenol should be a MASI in one of the two different active sites. With our data, it is not possible to elucidate which one. On the first case, phenol can be MASI on the interfacial site, therefore:

$$K''f_{PhOH} \gg K' + K_{H_2O}f_{H_2O}$$

$$K'' \gg K_{HYD}f_{PhOH}$$

Neglecting the terms with lower magnitudes, the rate expression becomes as follow, consistent with the observed zero order with respect to phenol.

$$r = \frac{k'f_{PhOH}}{(K''f_{PhOH})(K'')} = k''$$

On the other case, phenol can be a MASI on the metal site, leading to the following expression:

$$K''f_{PhOH} \ll K' + K_{H_2O}f_{H_2O}$$

$$K'' \ll K_{HYD}f_{PhOH}$$

Analogously, the rate expression becomes as follow

$$r = \frac{f_{PhOH}}{(K' + K_{H_2O}f_{H_2O})(K_{HYD}f_{PhOH})} = k''$$

For Ru/rutile the proposed sequence of elementary step is the same, but the rate determining step is different. This one accounted for the presence of the previously described weakly adsorbed water that favors the phenol adsorption and generated a proton shuttling effect as described in the CO oxidation literature. The positive order with respect to water and the volcano shape trend with respect to phenol can be explained considering that step 4.B is the RDS. The derivation of the rate expression is very similar that the one for the Ru/anatase case and also accounts for the coverages over two different active sites; the interfacial site ( $\theta^*$ ) and the metal site ( $\sigma^\Delta$ ). The rate expression is defined by:

$$r = r_{4B} = k_{4B}\theta_{PhOH_2-OH_2}\sigma^\Delta$$

$$r = r_3 = k_{4B}K_1K_2K_9^{-1}K_8^{-0.5}P_{H_2}^{0.5}P_{PhOH}P_{H_2O}\theta^*\sigma^\Delta$$

Considering that the sites coverages are the same as expressed before, the rate expression becomes as follow.

$$1 = \sigma^\Delta + \sigma_H + \sigma_{Ph} + \sigma_{PhOH} + \sigma_{BZ}$$

Therefore,

$$\sigma^{\Delta} = \frac{1}{1 + K_8^{0.5} P_{H_2}^{0.5} + \frac{1}{K_6 K_8^{0.5} K_9} P_{H_2}^{0.5} P_{Bz} + K_7 P_{PhOH} + \frac{1}{K_9} P_{Bz}}$$

$$r = r_{4B} = \frac{k_{4B} K_1 K_2 K_9^{-1} K_8^{-0.5} P_{H_2}^{0.5} P_{PhOH} P_{H_2O}}{\left(1 + \frac{K_1}{K_8^{0.5}} P_{H_2}^{0.5} + \frac{K_1 K_{3A}}{K_8^{0.5}} P_{H_2}^{0.5} P_{PhOH} + \frac{1}{K_5} P_{H_2O} + \frac{1}{K_2} P_{H_2O}\right) \left(1 + K_8^{0.5} P_{H_2}^{0.5} + \frac{1}{K_6 K_8^{0.5} K_9} P_{H_2}^{0.5} P_{Bz} + K_7 P_{PhOH} + \frac{1}{K_9} P_{Bz}\right)}$$

The same simplifications can be done, considering constant partial pressures of H<sub>2</sub> and benzene:

$$r = r_{4B} = \frac{k' P_{PhOH} P_{H_2O}}{(K' + K_{PhOH} P_{PhOH} + K_{H_2O} P_{H_2O})(K'' + K_{HYD} P_{PhOH})} \quad (\text{Equation 2.15})$$

Where

$$k' = k_{4B} K_1 K_2 K_9^{-1} K_8^{-0.5} P_{H_2}^{0.5} = \text{constant}$$

$$K' = 1 + \frac{K_1}{K_8^{0.5}} P_{H_2}^{0.5} = \text{constant}$$

$$K_{PhOH} = \frac{K_1 K_{3A}}{K_8^{0.5}} P_{H_2}^{0.5} = \text{constant}$$

$$K_{H_2O} = \frac{1}{K_5} + \frac{1}{K_2} = \text{constant}$$

$$K'' = 1 + K_8^{0.5} P_{H_2}^{0.5} + \frac{1}{K_6 K_8^{0.5} K_9} P_{H_2}^{0.5} P_{Bz} + \frac{1}{K_9} P_{Bz} = \text{constant}$$

$$K_{HYD} = K_7 = \text{constant}$$

For Ru/rutile water did not play an important role in the site-blocking effect, consistent with the positive order in Figure 2.11.a:

$$K' + K'' f_{PhOH} \gg K_{H_2O} f_{H_2O}$$

Neglecting the small terms the rate expression becomes as follow

$$r = \frac{k' f_{H_2O} f_{PhOH}}{(K' + K'' f_{PhOH})(K'' + K_{HYD} f_{PhOH})} = k^{IV} f_{H_2O}$$

For the trend in phenol at lower concentration, this was not an important site-blocking term, consistent with Figure 2.13.a:

$$K'' f_{PhOH} \ll K' + K_{H_2O} f_{H_2O}$$

$$K_{HYD} f_{PhOH} \ll K''$$

Analogously the rate expression becomes:

$$r = \frac{k' f_{PhOH} f_{H_2O}}{(K' + K_{H_2O} f_{H_2O})(K'')} = k^V f_{PhOH}$$

At higher concentration of phenol, phenol becomes an important site-blocking term, for the interfacial and the metal site, also consistent with Figure 2.13.a:

$$K'' f_{PhOH} \gg K' + K_{H_2O} f_{H_2O}$$

$$K'' \gg K_{HYD} f_{PhOH}$$

Finally, this rate expression leads to the following form:

$$r = r_3 = \frac{k' f_{PhOH} f_{H_2O}}{(K'' f_{PhOH})(f_{PhOH})} = k^{VI} f_{PhOH}^{-1}$$

## 2.7. Conclusions

Those results show significant differences for hydrodeoxygenation of phenol over Ruthenium supported on anatase and rutile. We obtained clear trends of the effect of water in reaction rates for direct deoxygenation and hydrogenation pathways. Here, water plays an enhancement effect for Ru/rutile. The increase in rates with respect to water for Ru/rutile was consistent with water molecules in close proximities to the interface, as a weakly adsorbed molecule that could act as a co-catalyst for direct C-O bond scission, lowering the activation energy for this step by playing as a proton transfer agent. We believed that water can be adsorbed at the interfacial site generating a different adsorbed phenol species than the one proposed previously by our collaborators. This water-assisted mechanism is consistent with our kinetic data, but we need more evidences to prove if this mechanism is possible and favorable.

For Ru/anatase, concentration of water plays an opposite role providing a negative trend for all our experimental conditions. We believe that under this condition the proposed water assisted mechanism is not favorable due the differences in adsorption energies between rutile and anatase, that favors the previously proposed mechanism (DDO1) because of the reduction of the energy barriers for this RDS.

To the other side, the effect of phenol in DDO rates is first order in Ru/rutile at lower phenol concentrations, while is zero order in Ru/anatase and negative order for Ru/rutile at higher phenol concentration. A similar trend is observed for the HYD pathway.

Those results are consistent with both proposed rate expression considered C-O scission as the rate determining step, and assuming that phenol can be adsorbed at the interfacial site and in the metal site leading to the HYD pathway. Under current experimental conditions is proposed that phenol is a MASI for just one of these sites over Ru/Anatase, while those effects are not significant for Ru/rutile under lower phenol concentrations. We believe also that at higher phenol concentration for Ru/phenol is a MASI in both metal and interfacial sites.

### CHAPTER 3: FUTURE WORK

The phenol HDO project can be expanded in many different ways. In first instance, it is important to point out that kinetic data is not enough to prove a mechanism but it is a very useful tool to get consistent hints that endorse one mechanism over other. Additional experiments are needed to provide more convincing evidence for what is described above.

Since current information is not enough to elucidate the reaction mechanism more reaction rates can be calculated at a wider concentration range, especially data with respect to water concentration. Here it will be possible to see if at higher water concentration the reaction order with respect to water over Ru/rutile would transition to zero order, meaning that water is also a MASI in those conditions. If at even higher reaction orders, the reaction order becomes negative for anatase, this would mean that we are in under a much more complex mechanism. If so, it would mean that water can become a site blocking agent in for two different active sites, following a similar trend than for order with respect to phenol over rutile catalysts.

Following the same thinking process it would be ideal (and also hard to reach experimentally) to run experiments at lower water concentration for Ru/Anatase to determine if at some point the reaction order here becomes positive. If at a more extended water concentration follows the same trend, it would mean that reaction mechanism is the same for these two different catalysts, as expected initially. Following isotope experiments can also be done to elucidate more information about the effect of water.

To complement this information, it would be recommended to perform a kinetic monte carlo modelling. To do that it is necessary to obtain values of enthalpy, entropy, Gibbs free energy, equilibrium constant and binding energy of all the possible intermediates for those particular catalysts.

Sometimes it is possible to obtain binding energies from literature and equilibrium constant based on current reaction conditions. If not, DFT calculations are useful tools to get those desired values. Also it is possible to get accurate values from similar components or same components over a similar catalyst. It is important to consider that in our case,  $\text{TiO}_2$  is an active support for this reaction, so another Ru catalyst would probably not have the same catalytic performance over this reaction.

Once all of this information is obtained, it is necessary to get a working kinetic model that will predict the catalytic behavior, and verify if this behavior match with current experimental data at defined reaction conditions. If not, other modifications and optimization needs to be done in order to find the best fit for the experimental data.

Also, in order to finish this work for publication, kinetics data will be compared with DFT calculations performed by our collaborators. Here it will be possible to see if the computational predictions will match with experimental data, meaning that our current conclusions are correct.

## REFERENCES

1. Bailes, M. & Stone, F. THE REACTIVITY OF OXIDES WITH WATER VAPOR. *Water* **33**, 258–272 (1989).
2. Jiang, Z. & Hu, C. Selective extraction and conversion of lignin in actual biomass to monophenols: A review. *J. Energy Chem.* **25**, 947–956 (2016).
3. Kay Lup, A. N., Abnisa, F., Wan Daud, W. M. A. & Aroua, M. K. A review on reactivity and stability of heterogeneous metal catalysts for deoxygenation of bio-oil model compounds. *J. Ind. Eng. Chem.* **56**, 1–34 (2017).
4. Furimsky, E. Selection of catalysts and reactors for hydroprocessing. *Appl. Catal. A Gen.* **171**, 177–206 (1998).
5. Bridgwater, A. V. Renewable fuels and chemicals by thermal processing of biomass. *Chem. Eng. J.* **91**, 87–102 (2003).
6. Bridgwater, A. V. & Cottam, M. L. Opportunities for Biomass Pyrolysis Liquids Production and Upgrading. *Energy and Fuels* **6**, 113–120 (1992).
7. Arun, N., Sharma, R. V. & Dalai, A. K. Green diesel synthesis by hydrodeoxygenation of bio-based feedstocks: Strategies for catalyst design and development. *Renew. Sustain. Energy Rev.* **48**, 240–255 (2015).
8. He, Z. & Wang, X. Hydrodeoxygenation of model compounds and catalytic systems for pyrolysis bio-oils upgrading. *Catal. Sustain. Energy* **1**, 28–52 (2013).
9. Saidi, M. *et al.* Upgrading of lignin-derived bio-oils by catalytic hydrodeoxygenation. *Energy Environ. Sci.* **7**, 103–129 (2014).
10. Furimsky, E. Catalytic hydrodeoxygenation. *Appl. Catal. A Gen.* **199**, 147–190 (2000).
11. Song, Q. *et al.* Lignin depolymerization (LDP) in alcohol over nickel-based catalysts via a fragmentation-hydrogenolysis process. *Energy Environ. Sci.* **6**, 994–1007 (2013).
12. Deuss, P. J. & Barta, K. From models to lignin: Transition metal catalysis for selective bond cleavage reactions. *Coord. Chem. Rev.* **306**, 510–532 (2016).
13. Yoon, Y., Rousseau, R., Weber, R. S., Mei, D. & Lercher, J. A. First-principles study of phenol hydrogenation on pt and ni catalysts in aqueous phase. *J. Am. Chem. Soc.* **136**, 10287–10298 (2014).
14. Nie, L. *et al.* Selective conversion of m-cresol to toluene over bimetallic Ni-Fe catalysts. *J. Mol. Catal. A Chem.* **388–389**, 47–55 (2014).
15. De Souza, P. M. *et al.* Role of keto intermediates in the hydrodeoxygenation of phenol over

- Pd on oxophilic supports. *ACS Catal.* **5**, 1318–1329 (2015).
16. De, S., Saha, B. & Luque, R. Hydrodeoxygenation processes: Advances on catalytic transformations of biomass-derived platform chemicals into hydrocarbon fuels. *Bioresour. Technol.* **178**, 108–118 (2015).
  17. Popov, A. *et al.* Bio-oils hydrodeoxygenation: Adsorption of phenolic molecules on oxidic catalyst supports. *J. Phys. Chem. C* **114**, 15661–15670 (2010).
  18. Espro, C., Gumina, B., Paone, E. & Mauriello, F. Upgrading Lignocellulosic Biomasses: Hydrogenolysis of Platform Derived Molecules Promoted by Heterogeneous Pd-Fe Catalysts. *Catalysts* **7**, 78 (2017).
  19. Omotoso, T. O., Baek, B., Grabow, L. C. & Crossley, S. P. Experimental and First-Principles Evidence for Interfacial Activity of Ru/TiO<sub>2</sub> for the Direct Conversion of m-Cresol to Toluene. *ChemCatChem* **9**, 2612 (2017).
  20. Zanuttini, M. S., Lago, C. D., Querini, C. A. & Peralta, M. A. Deoxygenation of m-cresol on Pt/ $\gamma$ -Al<sub>2</sub>O<sub>3</sub> catalysts. *Catal. Today* **213**, 9–17 (2013).
  21. De Souza, P. M., Nie, L., Borges, L. E. P., Noronha, F. B. & Resasco, D. E. Role of oxophilic supports in the selective hydrodeoxygenation of m-cresol on Pd catalysts. *Catal. Letters* **144**, 2005–2011 (2014).
  22. Yang, Y. *et al.* Renewable aromatic production through hydrodeoxygenation of model bio-oil over mesoporous Ni/SBA-15 and Co/SBA-15. *Microporous Mesoporous Mater.* **250**, 47–54 (2017).
  23. Ausavasukhi, A., Huang, Y., To, A. T., Sooknoi, T. & Resasco, D. E. Hydrodeoxygenation of m-cresol over gallium-modified beta zeolite catalysts. *J. Catal.* **290**, 90–100 (2012).
  24. Romero, Y., Richard, F. & Brunet, S. Hydrodeoxygenation of 2-ethylphenol as a model compound of bio-crude over sulfided Mo-based catalysts: Promoting effect and reaction mechanism. *Appl. Catal. B Environ.* **98**, 213–223 (2010).
  25. Garcia, R. *et al.* Relevance of sulfiding pretreatment on the performance of Re/ZrO<sub>2</sub> and Re/ZrO<sub>2</sub>-sulfated catalysts for the hydrodeoxygenation of guaiacol. *Appl. Catal. A Gen.* **384**, 78–83 (2010).
  26. Ruiz, P. E. *et al.* Guaiacol hydrodeoxygenation on MoS<sub>2</sub> catalysts: Influence of activated carbon supports. *Catal. Commun.* **27**, 44–48 (2012).
  27. Wang, C. *et al.* Mechanistic Study of the Direct Hydrodeoxygenation of m-Cresol over WO<sub>x</sub>-Decorated Pt/C Catalysts. *ACS Catal.* **8**, 7749–7759 (2018).

28. Wang, L. *et al.* Selective hydrogenolysis of carbon-oxygen bonds with formic acid over a Au-Pt alloy catalyst. *Chem. Commun.* **53**, 2681–2684 (2017).
29. Sepúlveda, C. *et al.* Hydrodeoxygenation of 2-methoxyphenol over Mo<sub>2</sub>N catalysts supported on activated carbons. *Catal. Today* **172**, 232–239 (2011).
30. Fang, H. *et al.* Regioselective hydrogenolysis of aryl ether C-O bonds by tungsten carbides with controlled phase compositions. *Chem. Commun.* **53**, 10295–10298 (2017).
31. Li, M., Deng, J., Lan, Y. & Wang, Y. Efficient Catalytic Hydrodeoxygenation of Aromatic Carbonyls over a Nitrogen-Doped Hierarchical Porous Carbon Supported Nickel Catalyst. *ChemistrySelect* **2**, 8486–8492 (2017).
32. Shetty, M., Zanchet, D., Green, W. H. & Román-Leshkov, Y. Cooperative Co(0)/Co(II) Sites Stabilized by a Perovskite Matrix Enable Selective C-O and C-C bond Hydrogenolysis of Oxygenated Arenes. *ChemSusChem* 1–37 (2019). doi:10.1002/cssc.201900664
33. Mendes, M. J., Santos, O. A. A., Jordão, E. & Silva, A. M. Hydrogenation of oleic acid over ruthenium catalysts. *Appl. Catal. A Gen.* **217**, 253–262 (2001).
34. Mars, P. & van Krevelen, D. W. Oxidations carried out by means of vanadium oxide catalysts. *Chem. Eng. Sci.* **3**, 41–59 (1954).
35. Tomishige, K., Nakagawa, Y. & Tamura, M. Selective hydrogenolysis and hydrogenation using metal catalysts directly modified with metal oxide species. *Green Chem.* **19**, 2876–2924 (2017).
36. van Duijne, A., Ponec, V., Koster, R. M., Pestman, R. & Pieterse, J. A. Z. Reactions of Carboxylic Acids on Oxides. *J. Catal.* **168**, 265–272 (2002).
37. Doornkamp, C. & Ponec, V. The universal character of the Mars and Van Krevelen mechanism. *J. Mol. Catal. A Chem.* **162**, 19–32 (2000).
38. Thibodeau, T. J. *et al.* Composition of tungsten oxide bronzes active for hydrodeoxygenation. *Appl. Catal. A Gen.* **388**, 86–95 (2010).
39. Moberg, D. R., Thibodeau, T. J., Amar, F. G. & Frederick, B. G. Mechanism of hydrodeoxygenation of acrolein on a cluster model of MoO<sub>3</sub>. *J. Phys. Chem. C* **114**, 13782–13795 (2010).
40. Newman, C. *et al.* Effects of support identity and metal dispersion in supported ruthenium hydrodeoxygenation catalysts. *Appl. Catal. A Gen.* **477**, 64–74 (2014).
41. Omotoso, T., Boonyasuwat, S. & Crossley, S. P. Understanding the role of TiO<sub>2</sub> crystal structure on the enhanced activity and stability of Ru/TiO<sub>2</sub> catalysts for the conversion of lignin-derived oxygenates. *Green Chem.* **16**, 645–652 (2014).

42. Nelson, R. C. *et al.* Experimental and Theoretical Insights into the Hydrogen-Efficient Direct Hydrodeoxygenation Mechanism of Phenol over Ru/TiO<sub>2</sub>. *ACS Catal.* **5**, 6509–6523 (2015).
43. Kay Lup, A. N., Abnisa, F., Daud, W. M. A. W. & Aroua, M. K. Atmospheric hydrodeoxygenation of phenol as pyrolytic-oil model compound for hydrocarbon production using Ag/TiO<sub>2</sub> catalyst. *Asia-Pacific J. Chem. Eng.* e2293 (2019). doi:10.1002/apj.2293
44. Zhang, X. *et al.* Selective Hydrodeoxygenation of Guaiacol to Phenolics by Ni/Anatase TiO<sub>2</sub> Catalyst Formed by Cross-Surface Migration of Ni and TiO<sub>2</sub>. *ACS Catal.* 3551–3563 (2019). doi:10.1021/acscatal.9b00400
45. Vriamont, C. E. J. J. *et al.* From Lignin to Chemicals: Hydrogenation of Lignin Models and Mechanistic Insights into Hydrodeoxygenation via Low Temperature C–O Bond Cleavage. *ACS Catal.* (2019). doi:10.1021/acscatal.8b04714
46. T. Dallas Swift, Christina Bagia, Vinit Choudhary, George Peklaris, V. N. and D. G. V. Kinetics of Homogeneous Brønsted Acid Catalyzed Fructose Dehydration and 5-Hydroxymethyl Furfural Rehydration: A Combined Experimental and Computational Study. *ACS Catal.* **4**, 259–267 (2014).
47. Zhao, Z. *et al.* Solvent-mediated charge separation drives alternative hydrogenation path of furanics in liquid water. *Nat. Catal.* **2**, (2019).
48. De Souza, P. M. *et al.* Role of keto intermediates in the hydrodeoxygenation of phenol over Pd on oxophilic supports. *ACS Catal.* **5**, 1318–1329 (2015).
49. Nashawi, I. S., Malallah, A. & Al-Bisharah, M. Forecasting world crude oil production using multicyclic Hubbert model. *Energy and Fuels* **24**, 1788–1800 (2010).
50. Guo, M., Song, W. & Buhain, J. Bioenergy and biofuels: History, status, and perspective. *Renew. Sustain. Energy Rev.* **42**, 712–725 (2015).
51. Daioglou, V., Doelman, J. C., Wicke, B., Faaij, A. & van Vuuren, D. P. Integrated assessment of biomass supply and demand in climate change mitigation scenarios. *Glob. Environ. Chang.* **54**, 88–101 (2019).
52. Cao, L. *et al.* Lignin valorization for the production of renewable chemicals: State-of-the-art review and future prospects. *Bioresour. Technol.* **269**, 465–475 (2018).
53. Zhang, C. & Zhang, Z. C. Essential Quality Attributes of Tangible Bio-oils from Catalytic Pyrolysis of Lignocellulosic Biomass. *Chem. Rec.* 1–15 (2019). doi:10.1002/tcr.201900001
54. Li, D., Li, X. & Gong, J. Catalytic Reforming of Oxygenates: State of the Art and Future Prospects. *Chem. Rev.* **116**, 11529–11653 (2016).

55. Mortensen, P. M., Grunwaldt, J. D., Jensen, P. A., Knudsen, K. G. & Jensen, A. D. A review of catalytic upgrading of bio-oil to engine fuels. *Appl. Catal. A Gen.* **407**, 1–19 (2011).
56. Wright, M. M., Satrio, J. a., Brown, R. C., Dugaard, D. E. & Hsu, D. D. Techno-economic analysis of biomass fast pyrolysis to transportation fuels. *Natl. Renew. Energy Lab.* **89**, S2–S10 (2010).
57. Akbar Mahdavi-Shakib, Samra Husremovic, Sohee Ki, Jessica Glynn, Lauren Babb, Janine Sempel, Ioannis Stavrinoudis, Juan Manuel Arce Ramos, Ryan Nelson, Lars C. Grabow, Thomas J. Schwartz, Brian G. Frederick, R. N. A. Titania surface chemistry and its influence on supported metal. *Polyhedron* **In Prep**, 1–19 (2019).
58. Tavana, J., Stuck, D. & Schwartz, T. J. Hydrogenolysis of C-X Bonds by Supported Metal Catalysts. **In prep.**, (2019).
59. Román-Leshkov, Y., Barrett, C. J., Liu, Z. Y. & Dumesic, J. A. Production of dimethylfuran for liquid fuels from biomass-derived carbohydrates. *Nature* **447**, 982–985 (2007).
60. Kantarci, N., Borak, F. & Ulgen, K. O. Bubble column reactors. *Process Biochem.* **40**, 2263–2283 (2005).
61. Mahdavi-Shakib, A. *et al.* Titania surface chemistry and its influence on supported metal catalysts. *Polyhedron* **170**, 41–50 (2019).
62. Smith, J. M., Van Ness, H. C., Abbott, M. M. & Swihart, M. T. *Introduction To Chemical Engineering Thermodynamics Eighth Edition.* (2018).
63. Vannice, M. A. *Kinetics of catalytic reactions. Kinetics of Catalytic Reactions* (2005). doi:10.1007/b136380
64. Mears, D. E. Tests for Transport Limitations in Experimental Catalytic Reactors. *Ind. Eng. Chem. Process Des. Dev.* **10**, 541–547 (1971).
65. Fogler, H. S. *Elements of chemical reactions engineering.* (2008).
66. Saavedra, J., Pursell, C. J. & Chandler, B. D. CO Oxidation Kinetics over Au/TiO<sub>2</sub> and Au/Al<sub>2</sub>O<sub>3</sub> Catalysts: Evidence for a Common Water-Assisted Mechanism. *J. Am. Chem. Soc.* **140**, 3712–3723 (2018).
67. Whittaker, T. *et al.* H<sub>2</sub> Oxidation over Supported Au Nanoparticle Catalysts: Evidence for Heterolytic H<sub>2</sub> Activation at the Metal-Support Interface. *J. Am. Chem. Soc.* **140**, 16469–16487 (2018).
68. Saavedra, J., Doan, H. A., Pursell, C. J., Grabow, L. C. & Chandler, B. D. The critical role of water at the gold-titania interface in catalytic CO oxidation. *Science (80-. ).* **345**, 1599–1602 (2014).

69. Schubert, M. M. *et al.* CO oxidation over supported gold catalysts -"Inert" and 'active' support materials and their role for the oxygen supply during reaction. *J. Catal.* **197**, 113–122 (2001).
70. Ojeda, M., Zhan, B. Z. & Iglesia, E. Mechanistic interpretation of CO oxidation turnover rates on supported Au clusters. *J. Catal.* **285**, 92–102 (2012).
71. Mahdavi-shakib, A. *et al.* Use of Surface Hydroxyl Frequencies to Identify the Exposed Facets of Pyrogenic TiO<sub>2</sub> Nanoparticles. *In prep.* 1–55 (2009).
72. Saavedra, J. *et al.* Controlling activity and selectivity using water in the Au-catalysed preferential oxidation of CO in H<sub>2</sub>. *Nat. Chem.* **8**, 584–589 (2016).
73. Leiva, K., Sepúlveda, C., García, R., Fierro, J. L. G. & Escalona, N. Effect of water on the conversions of 2-methoxyphenol and phenol as bio-oil model compounds over ReS<sub>2</sub>/SiO<sub>2</sub> catalyst. *Catal. Commun.* **53**, 33–37 (2014).
74. Lakshmi, G. S. *et al.* Energy Statistics. 121 (2017).
75. Román-Leshkov, Y. & Dumesic, J. A. Solvent effects on fructose dehydration to 5-hydroxymethylfurfural in biphasic systems saturated with inorganic salts. *Top. Catal.* **52**, 297–303 (2009).
76. Bloomberg. Gasoline Prices by Country. (2015). Available at: <https://www.bloomberg.com/graphics/gas-prices/#20172:Malaysia:USD:g%0Ahttp://www.bloomberg.com/visual-data/gas-prices/20144:Norway:EUR:l>.
77. Dickerson, K. & Kavkewitz, J. Biomass and Biofuels in Maine: Estimating Supplies for Expanding the Forest Products Industry. 16 (2007).
78. MGAP. Bosques plantados registrados. (2013).
79. Yang, P. *et al.* Catalytic production of 2,5-dimethylfuran from 5-hydroxymethylfurfural over Ni/Co<sub>3</sub>O<sub>4</sub> catalyst. *Catal. Commun.* **66**, 55–59 (2015).
80. Villanueva, N. I. & Marzioletti, T. G. OBTENCIÓN DE 5-HIDROXMETILFURFURAL A PARTIR DE GLUCOSA PROVENIENTE DE LICORES DE CORTEZA DE PINO Y EUCALIPTO, UTILIZANDO CATALIZADORES SÓLIDOS EN MEDIO ACUOSO. (2017).
81. Zu, Y. *et al.* Efficient production of the liquid fuel 2,5-dimethylfuran from 5-hydroxymethylfurfural over Ru/Co<sub>3</sub>O<sub>4</sub> catalyst. *Appl. Catal. B Environ.* **146**, 244–248 (2014).

82. Zu, Y. *et al.* Applied Catalysis B : Environmental Efficient production of the liquid fuel 2 , 5-dimethylfuran from 5-hydroxymethylfurfural over Ru / Co 3 O 4 catalyst. "Applied Catal. B, Environ. **146**, 244–248 (2014).
83. Yang, P. *et al.* Catalytic production of 2 , 5-dimethylfuran from 5-hydroxymethylfurfural over Ni / Co 3 O 4 catalyst Y (%) Y (%). *CATCOM* **66**, 55–59 (2015).
84. Lima, S., Chadwick, D. & Hellgardt, K. Towards sustainable hydrogenation of 5-(hydroxymethyl)furfural: A two-stage continuous process in aqueous media over RANEY® catalysts. *RSC Adv.* **7**, 31404–31407 (2017).
85. Sandoval, J. N. "PRODUCCIÓN CATALÍTICA DE 2,5-DIMETILFURANO. (University of Concepcion, 2016).
86. Liu, Y., Mellmer, M. A., Alonso, D. M. & Dumesic, J. A. Effects of Water on the Copper-Catalyzed Conversion of Hydroxymethylfurfural in Tetrahydrofuran. 3983–3986 (2015). doi:10.1002/cssc.201501122
87. Norskov, J. K., Abild-Pedersen, F., Studt, F. & Bligaard, T. Density functional theory in surface chemistry and catalysis. *Proc. Natl. Acad. Sci.* **108**, 937–943 (2011).
88. Nelson, R. C. *et al.* Experimental and Theoretical Insights into the Hydrogen-Efficient Direct Hydrodeoxygenation Mechanism of Phenol over Ru/TiO<sub>2</sub>. *ACS Catal.* **5**, 6509–6523 (2015).
89. Scientific Systems, I. *MI-Class Pump Economical Piston Pump for HPLC and High Performance Metering.*
90. Brooks Instruments. 5800 Series, Elastomer Sealed, Analog Thermal Mass Flow Meters and Controllers Data Sheet. 1–8 (2017).
91. Instruments, B. Gas and Liquid Mass Flow Secondary Electronics. (2010).
92. AutomationDirect. SOLO Temperature Controller Manual.
93. Swagelok. Pre ssure Regulators K Series. 1–59
94. Agilent Technologies. eFamiliarization for OpenLAB CDS. 90559 (2014).
95. OHAUS. Explorer Semi-Micro Balances Instruction Manual ®. (2015).
96. Weekman, V. W. Laboratory reactors and their limitations. *AIChE J.* **20**, 833–840 (1974).

## **APPENDIX A: 5-HYDROXYMETHYLFURFURAL HYDROGENOLYSIS**

### **A.1 Introduction**

The increasing global energy demand in the current years, have led to major scientific interest in the conversion of renewable resources into alternative sources of energy. This research was focused in finding alternative sources of fuels and chemicals, that were also sustainable, renewable and environmentally friendly.

Transportation sector, accounts for around 20% of the global energy consumption and is the biggest consumer of oil in the world.<sup>74</sup> In this context, production of Biofuels has reached high importance, in order to release petroleum dependency and alleviate environmental concerns.<sup>75</sup>

Countries without petroleum sources needs to import all of their oil resources from other countries being affected by political regulations, and increasing the commercial price due transportation costs, taxes and variations of the dollar price. Those variations are evidenced in Table and Figure A.1.

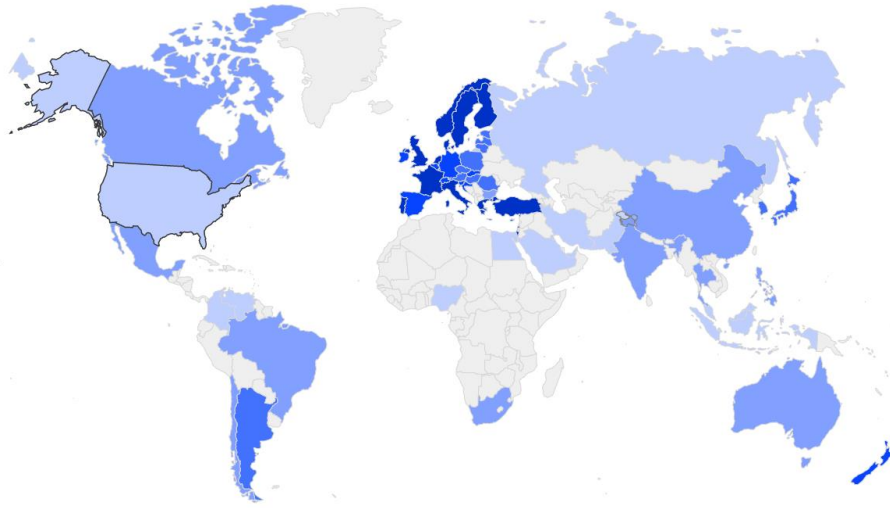


Figure A. 1 Gasoline price distribution around the world. <sup>76</sup>

Position	Country	Gasoline price (\$/gal)
1	Venezuela	0.02
3	Saudi Arabia	0.91
4	Iran	1.49
8	Russia	2.15
12	United States	2.57
14	Mexico	2.77
18	Canada	3.45
24	Chile	4.19
30	Lithuania	4.55
37	Spain	4.93
50	France	5.62
53	Sweden	5.94
60	Norway	6.53

Table A. 1 Gas price in some countries of the world in dollars per gallon. <sup>76</sup>

Biofuels are fuels produced from living organisms or from metabolic by-products with more than 80% renewable materials. Transportation fuels must have also specific physical properties for efficient distribution, storage and combustion.

Bio-ethanol is the most important 1<sup>st</sup> generation biofuel nowadays, but research have being to incorporate other generations of biofuels in the market. Round wood products and forest residues have the potential to serve as a competitive renewable feedstock for the chemical industry.<sup>75</sup>

Particularly, state of Maine and south-central Chile have the natural resources to develop a biofuels industry. Maine is the most forested state of the united states, with 89% of its land forested. If Maine's forest residues are retrieved, 2.6 million dry tons of forest residues could potentially contribute up to one-third of Maine's transportation fuel supply<sup>77</sup>. On the other hand, the BioBio region in Chile has out of 2 million forested acres has 55% available for industry use.<sup>78</sup>

## **A.2 Theoretical Background**

### **A.2.1 HMF Hydrodeoxygenation**

Production of 2,5-Dimethylfuran can be very valuable for biofuel production, because of its similar properties as gasoline. In this project, the hydrodeoxygenation (HDO) of HMF to DMF on Ni-Co<sub>3</sub>O<sub>4</sub> and Ru-Co<sub>3</sub>O<sub>4</sub> catalysts was studied in a batch Parr reactor. This part of the project included measurements of the activity and selectivity of the catalysts. The results showed the reaction pathway of HMF into DMF and its intermediate products elucidating the existence of a byproduct that was not detected. Other results were consistent with previous researches.

Similar to ethanol, 2,5-Dimethylfuran (DMF) is considered a promising new generation of alternative transportation fuels. DMF needs no major modifications to produce similar engine

performance and emission levels to gasoline. Their boiling point is in a value suitable for liquid fuels, with a comparable water solubility and a higher research octane number (RON) than gasoline; while preserving a high energy density (30 kJ/cm<sup>3</sup>). A more detailed comparison is shown in Table 3.2. The limited information available suggests that DMF is not more toxic than current fuel components.<sup>59</sup>

Properties from literature	DMF	Ethanol	1-Butanol	Gasoline
Oxygen content	16.7	34.8	21.6	100-105
Lower heat value (MJ/kg)	33.7	26.9	33.2	42.9
Boiling point (°C)	93.0	77.3	117.3	27-225
Water solubility (wt%, 20°C)	0.26	Miscible	7.7	Negligible
Kinematic viscosity (cSt, 20°C)	25.9	22.3	24.6	20.0
Research Octane Number	119	110	98	90-100

*Table A. 2 Properties from popular biofuels compared to gasoline.*<sup>79</sup>

2,5-dimethylfuran (DMF) can be obtained out of a catalytic reaction from the compound 5-Hydroxymethylfurfural (HMF). HMF is an organic molecule considered as a furan. Furans are intermediate chemicals, readily obtained from biomass<sup>46</sup> and have been identified as “key substances” because of the wide range of chemical intermediates and end-products that they can produce<sup>75</sup>. Figure A.2 shows some of the most important end-products derived from HMF: 2,5 furandicarboxylic acid (FDCA) is used to produce polyesters that could replace PET compounds. Lactic acid has great importance in the pharmaceutical industry and for food, solvents and detergent production. Formic acid is used as a preservative and antibacterial agent in livestock feed, and is also significantly used in the production of leather and cleaning products and caprolactam is the basic unit of Nylon-6.<sup>80</sup>

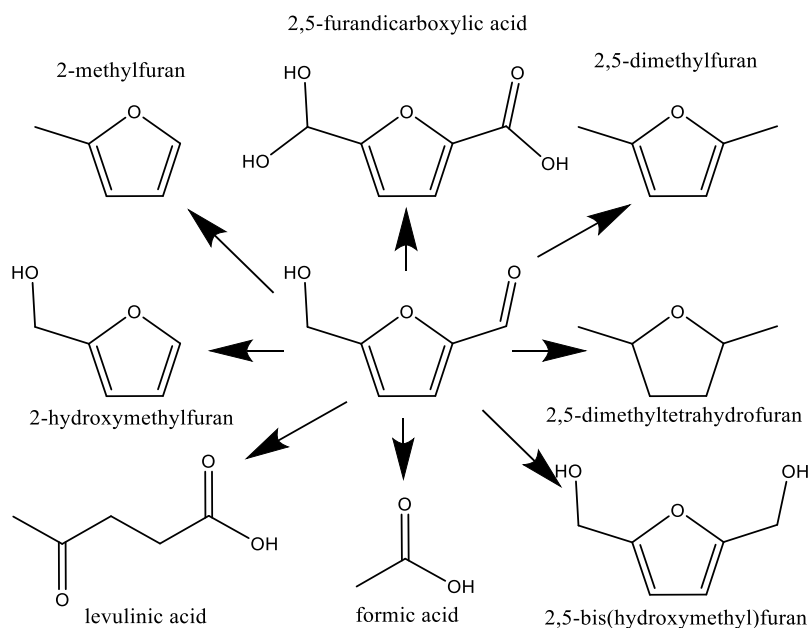


Figure A. 2 Range of end products derived from HMF. Extracted from.<sup>80</sup>

HMF can be obtained from the dehydration of fructose from lignocellulosic material, making it a renewable material. Fructose may react in solution through many different simultaneous reactions to produce HMF. The fructose dehydration is shown in Figure A.3. The first step, the dehydration of fructose to an intermediate, is considered an elementary reaction and the rate limiting step. The second step constitutes the intermediate reaction to HMF, the hydride transfer, considered irreversible and kinetically controlled.

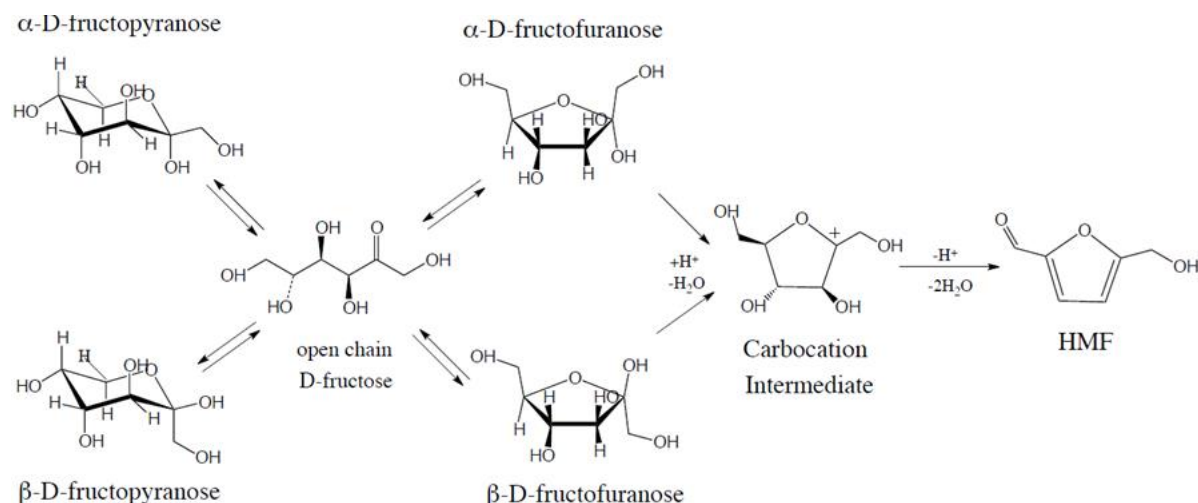


Figure A. 3 Reduced two-step fructose dehydration to HMF reaction scheme. <sup>46</sup>

Yang et al. and Zu et al. <sup>79,81</sup> investigated this reaction pathway over different cobalt supported catalysts. For their two different catalysts, they proposed a main reaction pathway for the hydrodeoxygenation of HMF into DMF, as shown in Figure A.4. HMF is first hydrogenated to bis(hydroxymethyl)furan (BHMF) and then deoxygenated to 2-hydroxymethyl-5-methylfuran (HMMF or MFA) and DMF. They also found a small amount of 5-Methylfurfural (5-MF), some of which was hydrogenated to MFA, while the rest was converted into the main by-product (1,2-ethanediy)bis [5-methylfurfural].

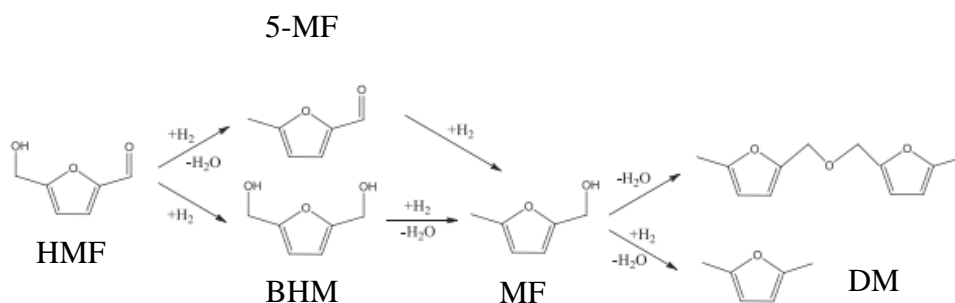


Figure A. 4 Proposed reaction pathway for HMF HDO over Ru-C  $O_3O_4$  catalyst. <sup>82</sup>

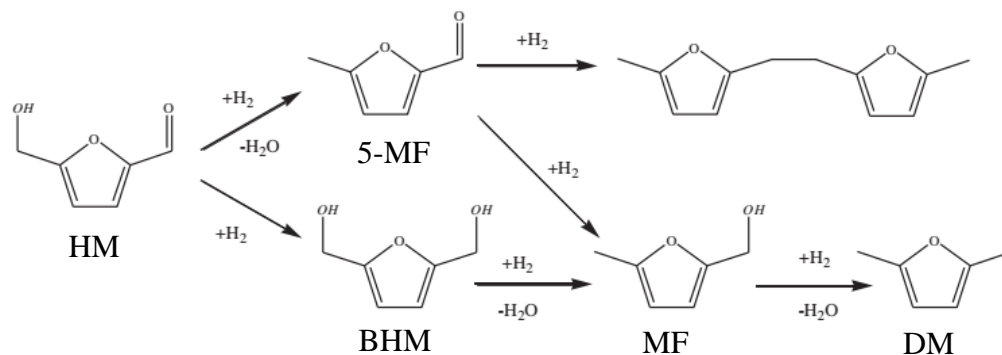


Figure A. 5 Proposed reaction pathway for HMF HDO over Ni/Co<sub>3</sub>O<sub>4</sub> catalyst<sup>83</sup>.

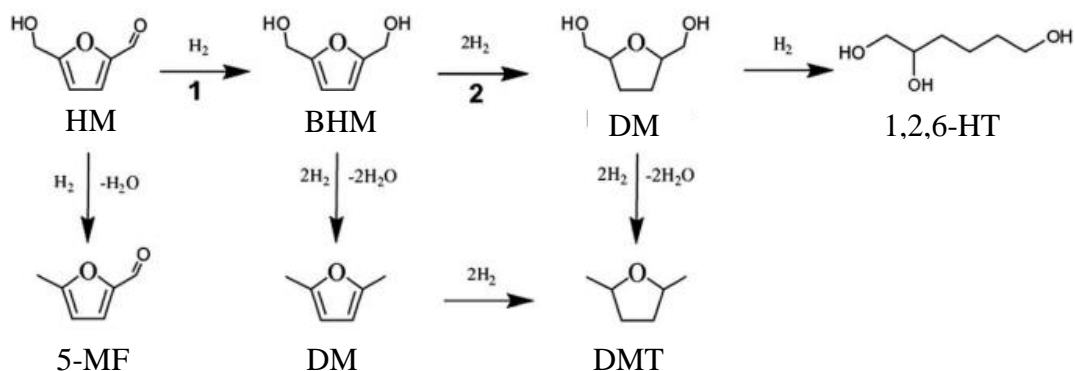


Figure A. 6 Proposed reaction pathway for further HMF hydrodeoxygenation, including hydrogenation and hydrogenolysis reactions.<sup>84</sup>

For a better understanding, most common chemical abbreviations are summarized in Table 3.3

Keyword	Definition
WHSV	Weight hourly space velocity
HMF	5-(hydroxymethyl)furfural
DMF	2,5-Dimethylfuran
BHMF	2,5-Bis(hydroxymethyl)furan
MFA	2-hydroxymethyl-5-methylfuran
5-MF	5-methylfurfural
DMTHF	2,5-Dimethyltetrahydrofuran
DHMTF	2,5-Di(hydroxymethyl)tetrahydrofuran

Table A. 3 Chemical abbreviations for HMF hydrodeoxygenation products.

This reaction could be done in a flow or batch reactor. In order to elucidate the first approximation of the reaction mechanism, a flow reactor was used.

## A.2.2 Definition of concepts

- Weight hourly space time: Employed as an indicator of similar conditions in different catalytic runs, allows comparison between catalytic runs.

$$WHST(h^{-1}) = \frac{m_{reactant}(grams)}{m_{catalyst}(grams) \cdot t (hours)} \quad (A.1)$$

- Conversion: Indicates how much of the initial reactant has converted into products.<sup>63</sup> On a constant volume reaction, with no variations of moles, conversion can be described as

$$X = \frac{C_{final}(\frac{mol}{mL})}{C_{initial}(\frac{mol}{mL}) - C_{final}(\frac{mol}{mL})} \quad (A.2)$$

- Selectivity: Indicates how much of the product of interest was obtained from the converted reactant.<sup>63</sup> Again, on a constant volume reaction, with no variations of moles, it can be described as

$$S = \frac{C_{product}(\frac{mol}{mL})}{C_{initial reactant}(\frac{mol}{mL}) - C_{final reactant}(\frac{mol}{mL})} \quad (A.3)$$

### A.2.3 Preliminary results

The following studies <sup>82,83,85</sup>, were of particular interest. Table 3.4 shows the most important results extracted from Yang et al. publication. <sup>83</sup> the catalyst evaluated was a Ni/Co<sub>3</sub>O<sub>4</sub> synthesized by a hydrothermal method. After 24h of reaction they saw complete conversion and a 76% of selectivity towards DMF.

Reduction T (°C)	t (min)	Conversion (%)	Y <sub>DMF</sub> (%)	WSHT (h <sup>-1</sup> )
550	1,440	>99	76	0.1042
-	120	-	28	1.25
-	180	-	37	0.833
-	360	-	34	0.416

Table A. 4 Reaction conditions extracted from bibliography <sup>83</sup>, with respective values of yield and conversion if reported. Reaction performed at 130°C and 1 MPa with a Ni/Co<sub>3</sub>O<sub>4</sub> synthesized by an hydrothermal method, using THF as a solvent.

Conversely, Table 3.5 shows the most important results extracted from Zu et al. publication. <sup>82</sup> the catalyst evaluated was a Ru-Co<sub>3</sub>O<sub>4</sub> synthesized by a coprecipitation method. After 24h of reaction they saw complete conversion and almost total selectivity towards DMF.

Reaction T (°C)	t (min)	Pressure (MPa)	Conversion (%)	Y <sub>DMF</sub> (%)	WSHT (h <sup>-1</sup> )
130	1,440	1	>99	94.7	0.1042
130	180	1	-	12	0.833
130	360	1	-	60	0.4165

Table A. 5 Reaction conditions extracted from bibliography <sup>82</sup>, with respective values of yield and conversion if reported. Reaction performed at 130°C and 1 MPa with a Ru-Co<sub>3</sub>O<sub>4</sub> synthesized by a co-precipitation method using THF as a solvent.

Later on, students from University of Concepcion <sup>85</sup> were working on reproduce the same Ru-Co<sub>3</sub>O<sub>4</sub> and synthesized a Ni-Co<sub>3</sub>O<sub>4</sub> catalyst by the same coprecipitation method as Zu et al. <sup>82</sup> Reaction were tested on THF and 1-butanol at an intermediate WHST. From Table 3.6 it is possible to see that catalyst performance were not comparable to the literature, and that much lower values of yield were obtained. Even though, Ru catalysts showed better performance for DMF production.

Catalyst	Solvent	T (min)	Reaction T (°C)	Pressure (MPa)	Conversion (%)	Y <sub>DMF</sub> (%)	WHST (h <sup>-1</sup> )
Ru- Co <sub>3</sub> O <sub>4</sub>	THF	240	130	1	~ 22	~ 12	0.625
Ru- Co <sub>3</sub> O <sub>4</sub>	Butanol	240	130	1	~ 99	~ 19	0.625
Ni- Co <sub>3</sub> O <sub>4</sub>	THF	240	130	1	~ 16	0	0.625
Ni- Co <sub>3</sub> O <sub>4</sub>	Butanol	240	130	1	~ 88	0	0.625

*Table A. 6 Reaction conditions extracted from bibliography<sup>82,83,85</sup>, with respective values of yield and conversion if reported. Reaction performed at 130°C and 1 MPa with a Ru-Co<sub>3</sub>O<sub>4</sub> synthesized by a co-precipitation method using THF as a solvent.*

It was also of interest seeing the effect of water over the reaction. In a study of the conversion of HMF to certain products over a Cu/g-Al<sub>2</sub>O<sub>3</sub> at 175°C, it was shown that in absence of water, HMF was converted to hydrogenolysis products 5-methylfuran and 2,5-dimethylfuran (DMF). In reactions carried out with water mixtures, (THF/H<sub>2</sub>O = 95:5 wt.) selective production of BHMF was achieved, while hydrogenolysis step was inhibited <sup>86</sup>. Since water was a common side product in biofuel production, reactions that were favored by the addition of water were of significant interest.

### **A.3 Objectives**

Understanding the hydrodeoxygenation (HDO) reaction of HMF into DMF over catalyst of Ru and Ni prepared by coprecipitation.

#### **A.3.1 Specific goals**

1. Properly quantify and determine all of the components involved the the HMF HDO reaction.
2. Learn how to use a Parr reactor.
3. Explore the steps implicated in the reaction.
4. Compare results with bibliographic and previous results <sup>82, 83</sup> and <sup>85</sup>.
5. Evaluate effect of water in the reaction.

### **A.4 Materials & Methods**

#### **A.4.1 Materials**

The chemicals bought for the reaction performance were HMF (Across Organics, 98%), DMF (TCI American, 98%), BHMF (Synquest Laboratories), MFA (Across Organics, 97%), 5-MF (Alfa Aesar, 98%). Tetrahydrofuran (Fisher, HPLC grade) and 1-butanol as a solvent (Fisher, ACS) were used as solvents and phenol (Fisher, 91%) and Formic Acid (Sigma Aldrich,  $\geq 95\%$ ) were used as internal standards.

Hydrogenation reactions were done with molecular hydrogen gas (Matheson, 99.999%). Helium (Matheson, 99.999%) and argon (Matheson, 99.999%), were used to passivate catalysts.  $\text{Co}(\text{NO}_3)_2 \cdot 6\text{H}_2\text{O}$  (Across Organics, 99%),  $\text{Ni}(\text{NO}_3)_2 \cdot 6\text{H}_2\text{O}$  (Sigma Aldrich, pure crystal) or  $\text{Ru}(\text{Cl}_3)_2 \cdot 3\text{H}_2\text{O}$  (Aldrich Chemistry, pure crystal) were the precursors for catalyst synthesis.

#### A.4.2 Principal equipment

- 25 mL Parr batch reactor model 4561.
- Parr 4857 process controller and a Parr 4875 power controller.
- Omega Thermocouple attached to SOLO temperature controller and Variac
- Acquity UPLC H-Class equipment for data acquisition
- Glass calcination cell and setup

#### A.4.3 Catalyst preparation

In previous work, expensive catalysts were used to convert HMF into DMF. Yang et al.<sup>79</sup> discovered a non-noble metal catalysts ( $\text{Ni}/\text{Co}_3\text{O}_4$ ) that was efficient and showed good stability. Also Zu et al.<sup>81</sup> presented a bulk  $\text{Ru}-\text{Co}_3\text{O}_4$  catalysts synthesized by co-precipitation. The motivation of Sandoval et al.<sup>85</sup> was to reproduce a Ni catalyst by a co-precipitation method proposed by Zu et al. switching the metal between Ni and Ru.

The  $\text{Ni}-\text{Co}_3\text{O}_4$  and  $\text{Ru}-\text{Co}_3\text{O}_4$  precursor was prepared by adding 45 mmol of  $\text{Co}(\text{NO}_3)_2 \cdot 6\text{H}_2\text{O}$  and 1mmol of  $\text{Ni}(\text{NO}_3)_2 \cdot 6\text{H}_2\text{O}$  or  $\text{Ru}(\text{Cl}_3)_2 \cdot 3\text{H}_2\text{O}$  respectively into 50mL of deionized water. The

solutions were added dropwise into deionized water at room temperature under vigorous stirring keeping the pH value between 10.7 and 11.2. Then the mixture was heated to 80°C for 24 h under magnetic stirring. After cooling down to room temperature, the solid precipitate was filtered and washed with deionized water until the pH of the filtrate was around 7. The filtrate was dried at 100°C in air for 12 h. The precursor was calcined in a Thermo Scientific muffle furnace (Lindberg/Blue M) at 500°C for 4 h with a ramp of 2°C min<sup>-1</sup> in air. After that, the calcined solution was pressed and sieved to obtain a powder between 90 and 180 µm particle size.

#### **A.4.4 Catalyst reduction**

This method consisted on reducing the recently prepared catalyst at 200°C with H<sub>2</sub> flowing through a calcination cell for 2 hours with a ramp of 2°C min<sup>-1</sup> before used as a catalyst, argon was then flown for 30 minutes to passivate the reduced catalysts.

Another reduction method evaluated was reducing the catalyst inside the reactor, following the same previous heating pattern, and then pumping the reaction solution into the reactor with an attached HPLC pump, Chromtech M1.

#### **A.4.5 Reaction procedure**

The reactor used was a batch Parr reactor. Temperature was measured by two omega thermocouples, one located inside the reactor and the over temperature thermocouple located by the outside walls of the vessel. The temperature was kept constant with a heating tape surrounded the vessel and properly isolated, attached to the temperature controller system. Samples were

agitated with a magnetic stirrer and a Parr agitator model 4848. The reactor also included a upper outlet valve, that was used as a sampling system for intermediate points during the reaction. The reactor was connected to a helium and a hydrogen tank for high pressure hydrogenation reactions.

Previously reduced and passivated catalyst (0.001g), was poured to the reactor. Then, the solvent previously measured was emptied into the reactor with 0.025 grams of HMF. If needed, also water was added to the solution. Once the reactor head is closed and adjusted, it was pressurized in helium and the proper leak check was done by pressurizing the reactor and making sure that this pressure was kept constant over time.

Under low pressure of helium, the reactor was located in the support with the thermocouple and the magnetic agitator properly located. A ramp rate of 5 °C/min was used to bring the reaction up to the reaction temperature, around 105, 120, 135 and 150°C, where it was held for 4 hours with 500 rpm stirring. Once the desired temperature was reached, the reactor was pressurized up to 500 psi with hydrogen to start the reaction time. Reaction temperatures were maintained during the reaction times ranged from 1 h to 48 hours to achieve the desired HMF conversions. Amount of catalyst, reactant and reaction time were defined in order to get a proper inverse weight hourly space time WHST.

Once the reaction time was reached, a sample was taken and filtered with a 0.45 µm syringe filter. Samples were then analyzed via high performance liquid chromatography (HPLC). Reaction products were quantified using a Waters Acquity UPLC H-Class equipment with liquid autosampler injection. Selectivity was measured based on the HPLC calibration curves, assuming

a 100% mass balance. Separation was achieved using an Acquity UPLC (BEH C18 1.7  $\mu\text{m}$ ) column.

## A.5 Results

### A.5.1 Reaction mechanism

In order to elucidate the reaction pathway between the reaction intermediates, experiments were analyzed in function of time. A mixture of equal amount of HMF and catalyst was poured into the reactor for these experiments. Experiments were carried out at 105, 120 and 135°C.

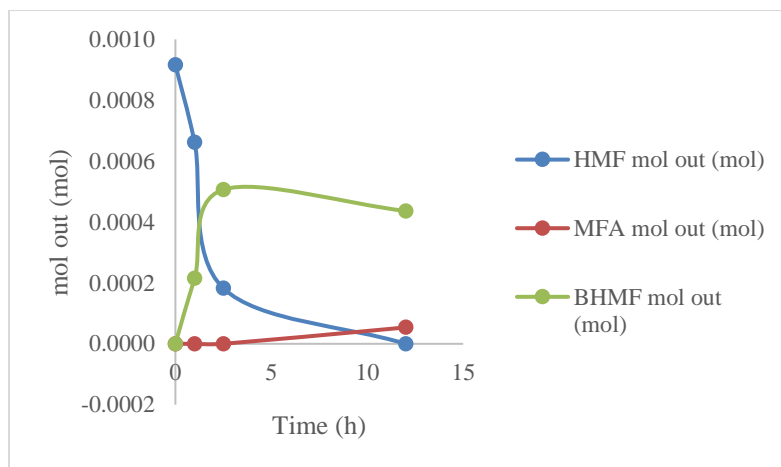


Figure A. 7 HMF hydrodeoxygenation over time. Reaction conditions: 0.04g HMF with 0.04g catalyst diluted in 10g of butanol. Reaction temperature 105°C, and 3.4 MPa.

From the experiments at lower temperatures, it was possible to determine that HMF is slowly consumed as long as BHMF is produced. At higher reaction times MFA was slowly produced while BHMF is consumed. This was consistent with reaction scheme in Figure A.4 where BHMF was converted into MFA.

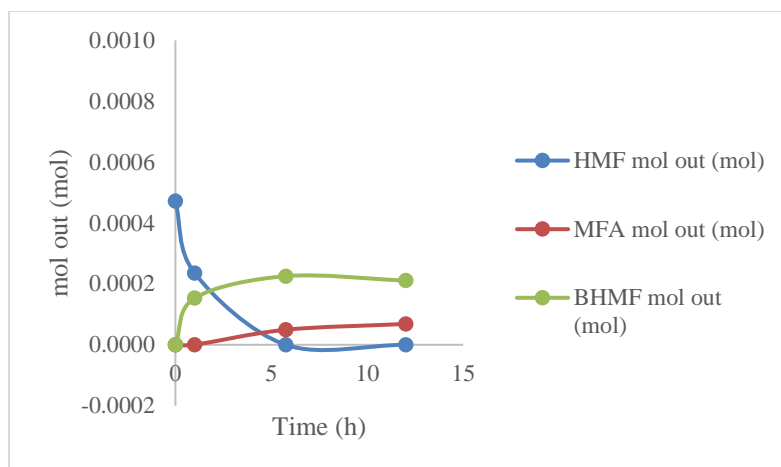


Figure A. 8 HMF hydrodeoxygenation over time. Reaction conditions: 0.04g HMF with 0.04g catalyst diluted in 10g of butanol. Reaction temperature 120°C, and 3.4 MPa.

At 120°C it was possible to see that HMF was consumed faster and more BHMF was produced. Also, a small amount of MFA is produced over time, consistent with BHMF deoxygenation.

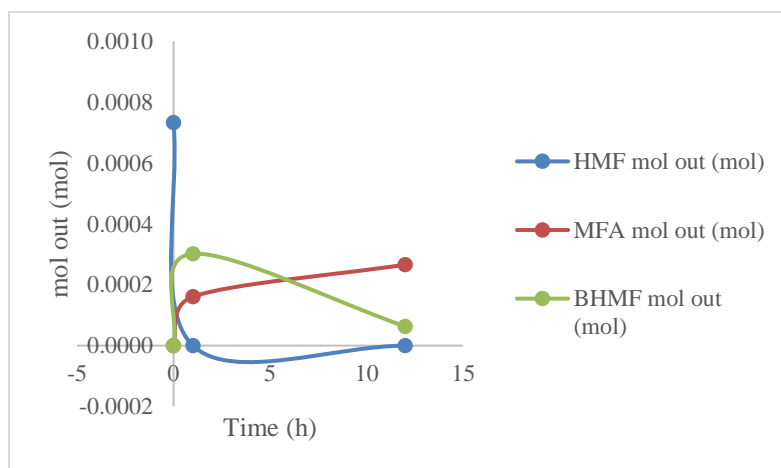


Figure A. 9 HMF hydrodeoxygenation over time. Reaction conditions: 0.04g HMF with 0.04g catalyst diluted in 10g of butanol. Reaction temperature 135°C, and 3.4 MPa.

Higher temperature led to higher reaction rates, but keeping the same reaction scheme. From last experiments it is clear that MFA was produced in more considerable amounts, while BHMF

and HMF were almost totally consumed at 12h reaction time. Interestingly, WHSH was not low enough in any condition to produce DMF.

### A.5.2 Effect of temperature

Data after 12h reaction time was showed in function of reaction temperature. Results were presented in Figure A.10.

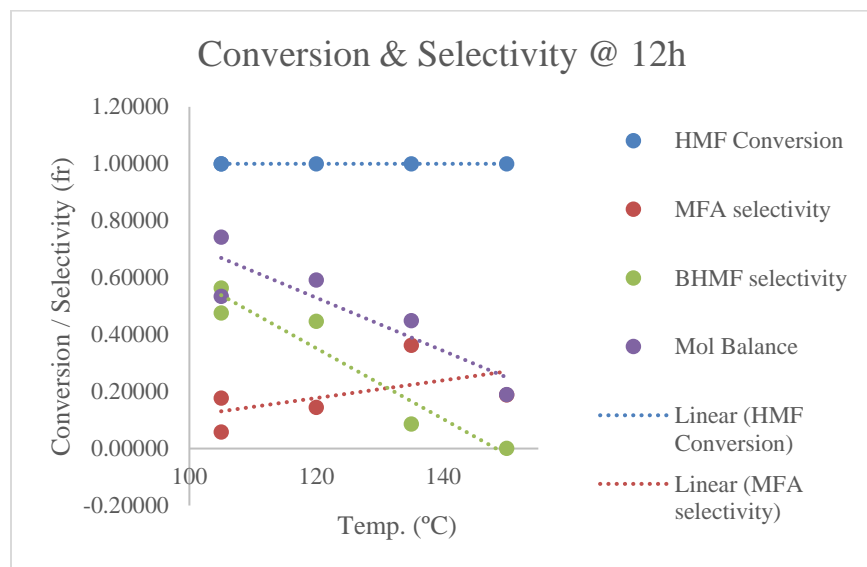


Figure A. 10 Effect of temperature in HMF hydrodeoxygenation. Reaction conditions: 3.4 MPa and  $0.08 h^{-1}$  WHST.

Trends presented in Figure A.10 were mostly consistent with previously reported. Besides the poor mole balance at higher temperatures, it was possible to see that while BHMF decreased at higher temperature more MFA was produced, consistent with reaction scheme. The poor mole balance at higher temperature was an indicator that a side product was generated not possible to quantify.

Results suggest that BHMF was transformed into another byproduct, not identified in this research. This behavior was not consistent with what was proposed for Yang et al. and Zu et al.<sup>82,83</sup> Different catalytic behaviors could exist because of reproducibility issues in making the catalyst with the co-precipitation technique.

### A.5.3 Catalysts screening

3 new catalyst were synthesized for the desired reaction:

- Ru-Co<sub>3</sub>O<sub>4</sub> (1 - first batch)
- Ru- Co<sub>3</sub>O<sub>4</sub> (2 - second batch)
- Ni- Co<sub>3</sub>O<sub>4</sub>

	WHSV (h <sup>-1</sup> )	Conversion (%)	Selectivity BHMF (%)	Selectivity MFA (%)	Selectivity DMF (%)	Exp.
Ru-Co <sub>3</sub> O <sub>4</sub> (1)	0.1193	100	69.69	13.7	0	1
Ru- Co <sub>3</sub> O <sub>4</sub> (2)	0.1154	38.26	79.04	10.7	0	2
Ru- Co <sub>3</sub> O <sub>4</sub> (2)	0.0538	100	29.32	17.70	0	3
Ru- Co <sub>3</sub> O <sub>4</sub> (2)	0.0052	100	0	0	34.27	4
Ru- Co <sub>3</sub> O <sub>4</sub> (2)	0.0026	100	0	0	14.64	5
Ni-Co <sub>3</sub> O <sub>4</sub>	0.0053	100	13.86	9.2653	41.114	6

*Table A. 7 Summary of general catalytic runs results. Reaction conditions with respective values of yield and conversion. Reaction performed at 130°C and 3.4 MPa with catalysts synthesized by a co-precipitation method using THF as a solvent.*

Regarding Ru-Co<sub>3</sub>O<sub>4</sub>(1) catalyst (exp 1), the reactions were performed in order to get similar WHSV as previous studies<sup>81</sup>, but the catalyst did not perform as expected. It was possible that the catalyst was not well synthesized, therefore another catalyst was prepared (Ru-Co<sub>3</sub>O<sub>4</sub>(2)).

The second batch of catalyst was even less active than the first one; At a similar WHST as Ru-Co<sub>3</sub>O<sub>4</sub>(1), less conversion of HMF was obtained, but a similar selectivity towards BHMF. As the WHST decreased, DMF was obtained but no other species were found. DMF was obtained for Ru-Co<sub>3</sub>O<sub>4</sub>(2) at very low WHST (exp. 4 and 5), making this catalyst a non-viable option. 5-MF was not detected in our experiments, indicating that its production is not significant or that it was a very reactive intermediate, which is further transformed into MFA or another non-detected byproduct.

#### A.5.4 Carbon balance

According to the proposed reaction pathway, carbon balance should be proportional to the furan balance. Here, those values were calculated to determine the reliability of the results. Surprisingly experiments with the second Ru catalyst presented very poor carbon balance at lower WHST.

	WHSV (h <sup>-1</sup> )	HMF in (mol/mL)	Furans out (mol/mL)	output/input (%)	Exp.
Ru-Co <sub>3</sub> O <sub>4</sub> (1)	0.1193	8.60E-06	7.13E-06	82.88	1
Ru-Co <sub>3</sub> O <sub>4</sub> (2)	0.1154	8.67E-06	8.33E-06	96.14	2
Ru-Co <sub>3</sub> O <sub>4</sub> (2)	0.0538	7.78E-06	3.68E-06	47.24	3
Ru-Co <sub>3</sub> O <sub>4</sub> (2)	0.0052	7.07E-06	2.44E-06	34.45	4
Ru-Co <sub>3</sub> O <sub>4</sub> (2)	0.0026	1.12E-05	1.64E-06	14.64	5
Ni- Co <sub>3</sub> O <sub>4</sub>	0.0053	4.84E-06	3.14E-06	64.82	6

Table A. 8 Concentrations in input and output. Reaction performed at 130°C and 3.4 MPa with catalysts synthesized by a co-precipitation method using THF as a solvent.

Assuming a proper quantification of the products, without experimental errors, it was possible that other byproducts were produced and were not detected. Especially at lower WHST, intermediate products were more likely to react, due to the increase of available active sites. According to <sup>82</sup> Zu

et al. MFA could react into (5,5-(oxybis(methylene))bis(2-methylfuran)), which was not possible to identify. Even though, previous results showed a minimal amount of this product in comparison to DMF, other possible product of MFA hydrogenation, not being consistent with current results. This implied that more side product were presented in this pathway. Since Ru and Ni catalyst shows similar behaviors, it was possible that 5-MF was also produced and rapidly converted into 2,2'-(1,2-ethanediyl)bis[5-methylfurna], which was also non possibly to quantify. Open ring product should also not be discarded, as proposed by Lup et al. <sup>3</sup>

### A.5.5 Observed reaction pathway with Ru-C<sub>03</sub>O<sub>4</sub>

It is observed that as the weight space hour time decreased conversion of HMF increased reaching 100%. BHMF decreased while MFA increased, indicating its conversion according to the reaction scheme. At lower WHST, no more BHM, nor MFA was detected but so does DMF, indicating that is was a later product in the reaction scheme, also consisted with previous research.

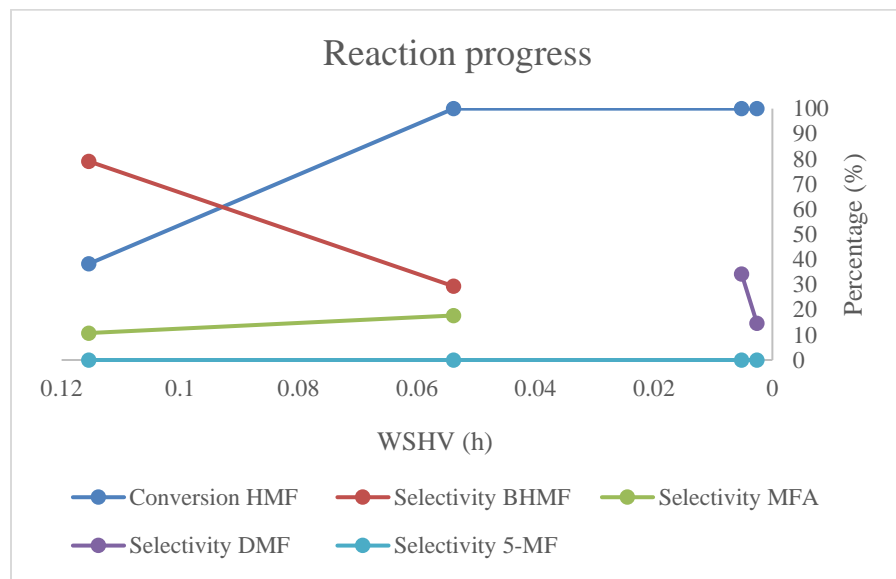
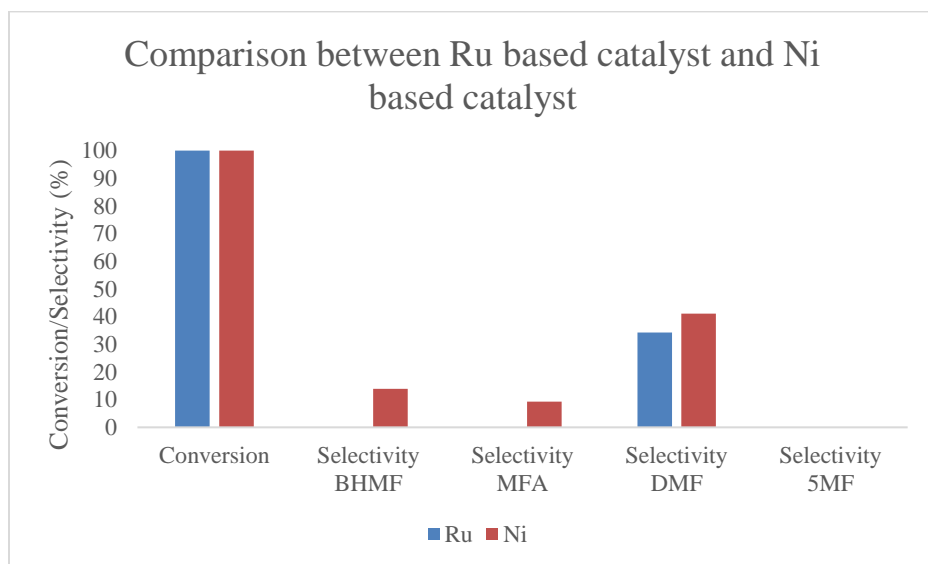


Figure A. 11 Reaction pathway with respect to WHSV for Ru-Co<sub>3</sub>O<sub>4</sub>(2) catalyst. Reaction performed at 130°C and 3.4 MPa with catalysts synthesized by a co-precipitation method using THF as a solvent.

The small decrease in DMF at the lowest WHST could be attributed to DMF further hydrogenation into DMTHF, as proposed by <sup>84</sup>. It was also expectable some variation in reaction rates because of the lower HMF concentration used in this experiment. Further analysis in GC-MS detected the presence of DMTHF in samples at lower WHST, validating that DMF was further hydrogenated.

### A.5.6 Comparison of ruthenium and nickel-based catalysts

Two catalyst were tested at the same conditions of weight hourly space time, temperature, pressure and time. Even that WHST was kept the same, amount of catalysts and concentration were different, making reaction rates determination not accurate.



*Figure A. 12 Effect of catalyst metal for HMF hydrodeoxygenation. Ru-Co<sub>3</sub>O<sub>4</sub> and Ni-Co<sub>3</sub>O<sub>4</sub> catalysts are compared. Reaction conditions: 3.4 MPa and 0.0053 h<sup>-1</sup> WHST.*

Even though experiments with Ni catalyst were done at lower HMF concentration, selectivity towards DMF was higher, therefore reaction rates were higher. It was expected that lower concentration led to lower reaction rates, assuming a first order trend with respect to HMF. This implies that Ni catalysts synthesized by co-precipitation were more active towards DMF than the Ru one. This was the opposite trend than the one observed in the literature and current results were not concise enough to make a conclusion out of those results.

## **A.6 Preliminary conclusions**

Synthesized catalysts show lower performances than the ones proposed by the literature. Unexpectedly, Ni catalysts show higher selectivity towards DMF with respect to Ru catalyst. Poor carbon balance at lower WHST was an indicator of side-products formation or experimental errors. Experimental errors could be attributed to evaporation of the sample or solvent during reaction run, affecting the concentrations of reactant and products, poor mixing inside the reactor, quantification issues, or sampling issues.

The reaction pathway for HMF hydrodeoxygenation behaves as expected with the exception of 5-MF production, which was not detected in any of the experiments. Product distribution was different than what proposed from literature. 5-MF could be an active intermediate product react

instantly to form 2,2'-(1,2-ethanediyl)bis[5-methylfurna] or MFA. Hydrogenation of the furan ring was established, due to the detection of DMTHF at lower WHST, unfortunately it was not quantified.

## **A.7 Future Work**

In order to expand the HMF project several suggestions will be given. In first instance it is important to notice that the catalyst chosen is not highly efficient, considering the fact of the very low values of WHSV that it is necessary to use in order to get complete conversion or a reasonable yield. It is recommended to update the literature review in order to find a new catalyst to test. Other efficient way to determine the proper catalyst for this reaction is referring to the Norskov <sup>87</sup> database to find the optimal combination metal-support considering calculated values of Gibbs free energy of adsorption, desorption, and reaction at normal conditions.

After chosen the right catalyst, a deeper kinetic analysis should be done to get a more detailed insight about the mechanism. Considering that HMF conversion into DMF presents many reaction intermediates it is necessary to do a deeper analysis for every step in order to determine which steps are actually kinetically relevant and requires a higher activation energy to fight with help of a catalysts. It is also recommended to do this analysis in a flow reactor to address deactivation issues and obtain kinetic data.

Knowing that Ru/TiO<sub>2</sub> is an active catalyst for C-O bond cleavage it would be interesting to see this performance for HMF HDO. If the activity is favorable it would imply that Ru/TiO<sub>2</sub> would

perform in the same interfacial mechanism than for aromatics. Also, elucidate the effect of water is desired. As mentioned before, biofuel production tends to be aqueous reactions, where avoiding the necessity of remove water is highly favorable from an operational standpoint. If the co-catalytic effect of water is also seen in furans, it is expected that all previous conclusions about the mechanism are also applicable for this reaction. If so, the same considerations can be applied to determine optimal reaction conditions.

## APPENDIX B: CATALYTIC STABILITY, SOLVENT SELECTION, AND OTHER

### PRELIMINARY WORK

#### B.1 CO Chemisorption

CO chemisorption data was performed in an Altamira Micromeritics instrument over a Ru/TiO<sub>2</sub>-P25 (UM) catalyst synthesized at the UMaine catalysis laboratory. Particle size and dispersion were calculated assuming a 1-1 coordinative adsorption on the Ru site. Adsorption isotherm was shown in Figure B.1 and calculated results were presented in Table 1.5.

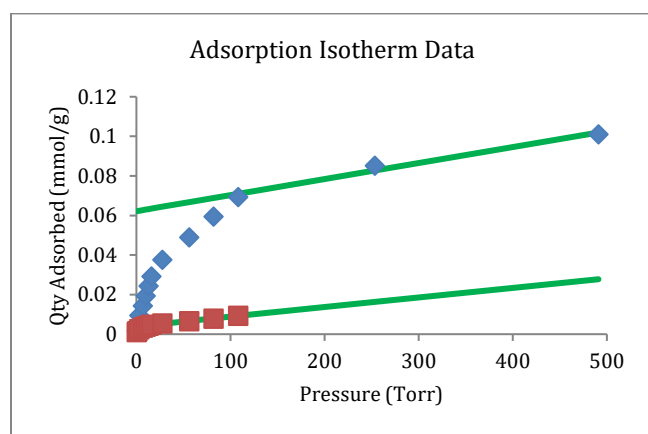


Figure B. 1 Adsorption isotherm data for Ru/TiO<sub>2</sub>-P25, UM catalyst.

Total sites (umol/g)	87.30
Dispersion (fr)	0.59
Dispersion (%)	58.82
Particle size = 1.1/D (nm)	1.87

Table B. 1 Results for the CO chemisorption analysis over Ru/TiO<sub>2</sub>-P25, UM catalyst.

## B.2 Deactivation Analysis

Thermogravimetric analysis was performed over a spent catalyst, Ru/TiO<sub>2</sub>-P90, in order to determine which deactivation mechanism was applied on our catalyst. From Figure B.2 it is possible to see that the steady state of weight loss is reached at 850K, consistent with carbon deposition calcination. At this temperature it was not possible to regenerate the catalyst without being affected by internal structure modifications.

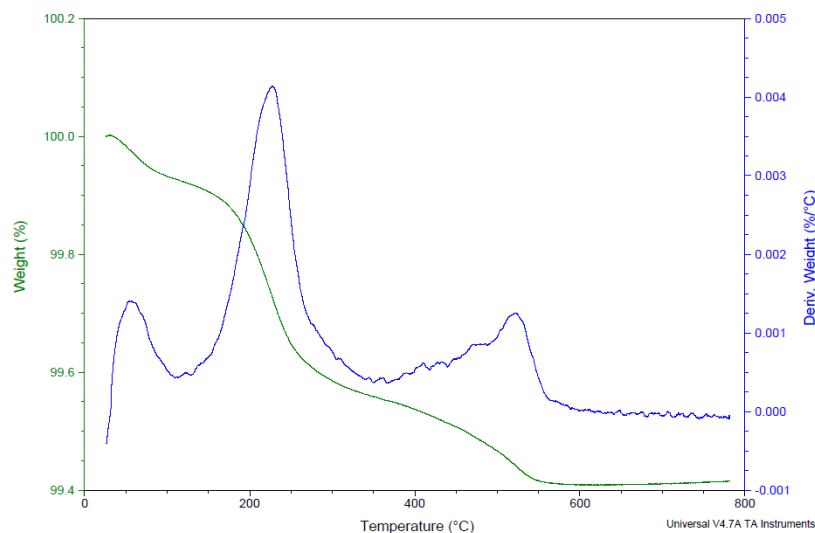


*Figure B. 2 Thermogravimetric analysis performed in 117.218 mg Ru/TiO<sub>2</sub> –P90 catalyst, after being deactivated by a phenol HDO reaction, in decalin. Instrument TGA Q500 V20. Ramp of 10K/min up to 1073K.*

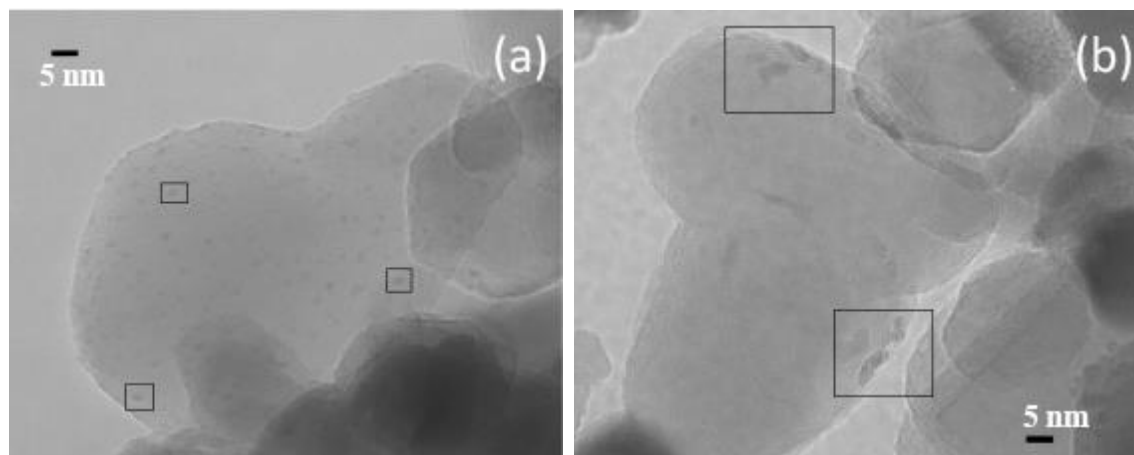


*Figure B. 3 TEM analysis performed in a Ru/TiO<sub>2</sub> catalyst, before (a) and after (b) being calcined in a phenol HDO reaction. Instrument JEOL 2010 Advanced High Performance TEM.*

Also transmission electron microscopy (TEM) pictures were taken from a uncalcined (a) and calcined (b) sample. From Figure B.3 it was possible to see that the internal structure of the catalyst was not modified after a calcination treatment, indicating that sintering is not a deactivation mechanism under our reaction condition.

High resolution TEM was carried out at the MIT Center for Material Science and Engineering (CMSE) using the JEOL 2010 Advanced High Performance TEM. The catalysts were dispersed in isopropanol, and a drop of this suspension was placed on a lacey carbon Cu grid.

### **B.3 Calibration Curves**

The calibration curves for the reactant and product involved in the phenol hydrodeoxygenation is shown in Figure B.4.

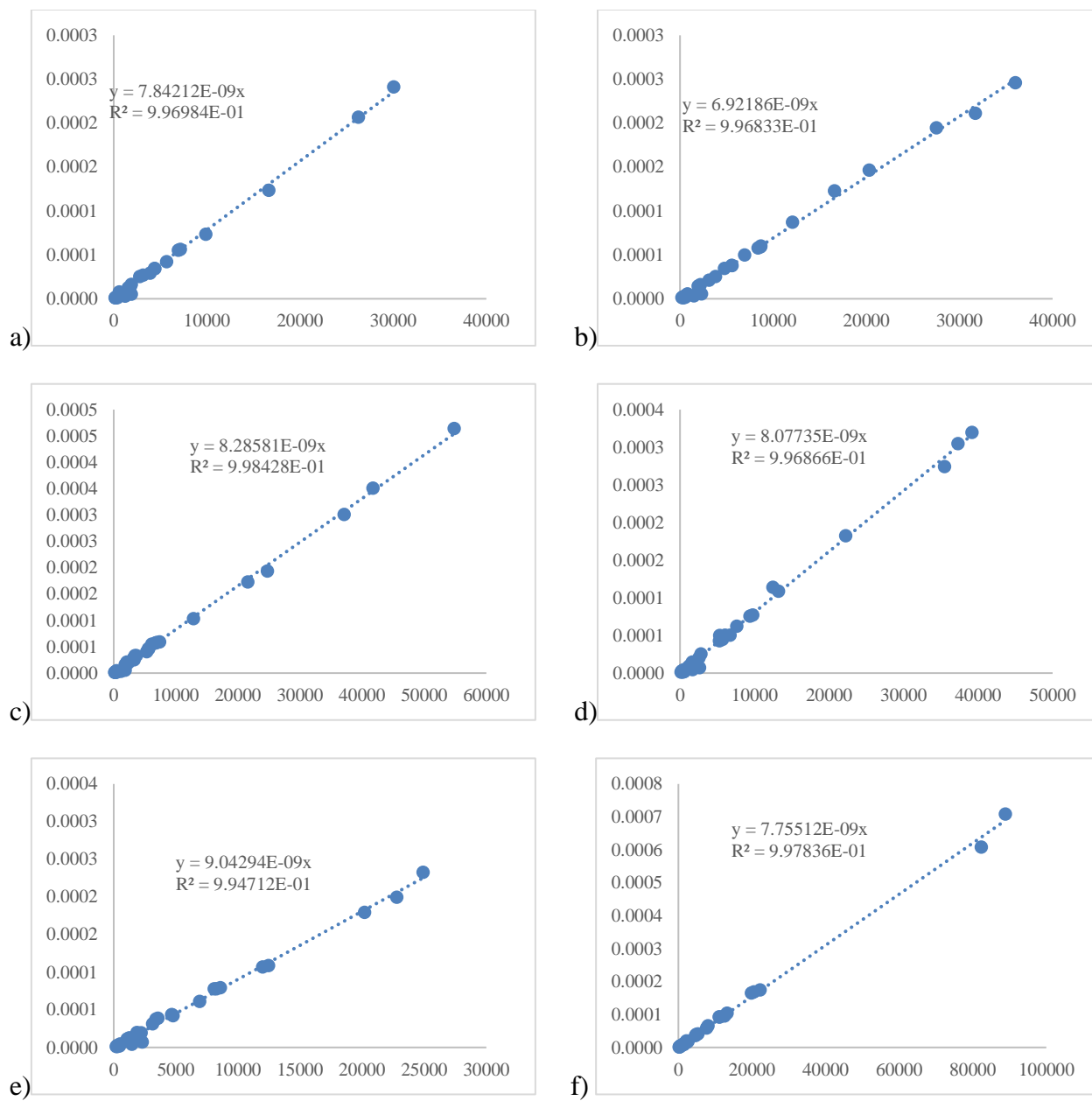


Figure B. 4 Calibration curves obtained for (a) cyclohexane at 2.3 min, (b) cyclohexene at 3.2 min (c) benzene at 5.7 min (d) cyclohexanone at 13.1 min (e) cyclohexanol at 14.7 min and (f) phenol at 21.4 min. Method DB-624 used in a Agilent DB-WAX column (30 m  $\times$  0.53 mm, 1  $\mu$ m).

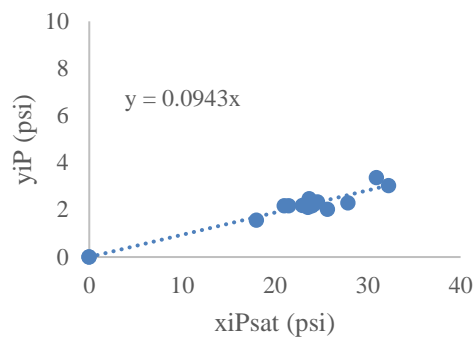
## B.4 Aspen Simulations

Table 2.5 shows the result of this reactant distribution obtaining by simulating the vapor-liquid equilibrium at a given set of reactor inlet conditions.

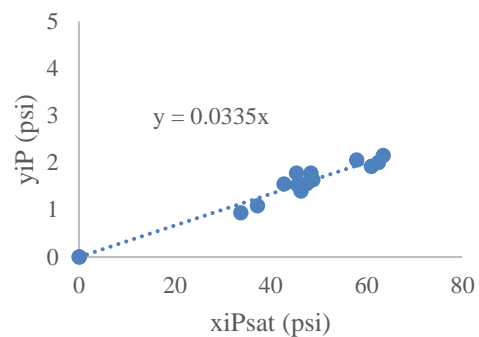
Experiments	Total mol in (mol/h)				Total mol in, liquid phase (kmol/h)				Total mol in, gas phase (kmol/h)			
	Phenol	Water	Decalin	H2	H2	Phenol	Water	Decalin	H2	Phenol	Water	Decalin
Anatase 10%	0.01053	0.00611	0.08836	0.0974	3.25E-05	5.81E-06	3.53E-07	8.30E-05	6.49E-05	4.72E-06	5.76E-06	5.39E-06
Anatase 15%	0.00630	0.00581	0.05722	0.0974	1.97E-05	2.45E-06	1.73E-07	5.11E-05	7.77E-05	3.85E-06	5.64E-06	6.10E-06
Anatase 20%	0.00621	0.00810	0.05409	0.0974	1.79E-05	2.20E-06	2.10E-07	4.74E-05	7.95E-05	4.01E-06	7.89E-06	6.65E-06
Anatase 20%	0.00419	0.00547	0.05573	0.0974	1.88E-05	1.58E-06	1.50E-07	4.97E-05	7.86E-05	2.61E-06	5.32E-06	6.07E-06
Anatase 20%	0.00476	0.00622	0.05312	0.0974	1.77E-05	1.70E-06	1.59E-07	4.68E-05	7.97E-05	3.06E-06	6.06E-06	6.29E-06
Anatase 25%	0.00457	0.00796	0.05359	0.0974	1.74E-05	1.58E-06	1.95E-07	4.69E-05	8.00E-05	2.99E-06	7.76E-06	6.67E-06
Rutile 10%	0.01044	0.00606	0.10680	0.0974	3.95E-05	6.52E-06	4.61E-07	1.02E-04	5.79E-05	3.92E-06	5.60E-06	4.87E-06
Rutile 15%	0.00466	0.00429	0.04427	0.0974	1.48E-05	1.47E-06	9.13E-08	3.82E-05	8.26E-05	3.19E-06	4.20E-06	6.10E-06
Rutile 20%	0.00464	0.00606	0.05202	0.0974	1.73E-05	1.63E-06	1.51E-07	4.57E-05	8.01E-05	3.01E-06	5.91E-06	6.28E-06
Rutile 25%	0.00338	0.00589	0.05037	0.0974	1.64E-05	1.14E-06	1.36E-07	4.40E-05	8.10E-05	2.24E-06	5.75E-06	6.33E-06
Rutile 25%	0.00446	0.00777	0.05285	0.0974	1.71E-05	1.53E-06	1.87E-07	4.62E-05	8.03E-05	2.93E-06	7.58E-06	6.65E-06
P25 5%	0.00514	0.00141	0.12099	0.0974	4.61E-05	3.62E-06	1.41E-07	1.17E-04	5.13E-05	1.52E-06	1.27E-06	3.49E-06
P25, 10%	0.01100	0.00638	0.10280	0.0974	3.79E-05	6.69E-06	4.58E-07	9.77E-05	5.95E-05	4.31E-06	5.92E-06	5.05E-06
P25 15%	0.00513	0.00473	0.04597	0.0974	1.54E-05	1.67E-06	1.06E-07	3.98E-05	8.20E-05	3.46E-06	4.62E-06	6.15E-06
P25 20%	0.00445	0.00582	0.05293	0.0974	1.77E-05	1.59E-06	1.49E-07	4.67E-05	7.97E-05	2.86E-06	5.67E-06	6.21E-06
P25 20%	0.00474	0.00619	0.05671	0.0974	1.91E-05	1.79E-06	1.73E-07	5.05E-05	7.83E-05	2.95E-06	6.02E-06	6.19E-06
P25 25%	0.00425	0.00740	0.05752	0.0974	1.89E-05	1.58E-06	2.00E-07	5.11E-05	7.85E-05	2.67E-06	7.20E-06	6.46E-06
Anatase, 0%	0.00499	0.00000	0.05486	0.0974	2.03E-05	2.09E-06	4.99E-05		7.71E-05	2.90E-06		4.93E-06
Rutile 0%	0.00507	0.00000	0.05564	0.0974	2.06E-05	2.15E-06	5.07E-05		7.68E-05	2.92E-06		4.91E-06
P25, 0%	0.00596	0.00000	0.05394	0.0974	2.00E-05	2.47E-06	4.89E-05		7.74E-05	3.49E-06		5.01E-06
P25 300 chips	0.00521	0.00000	0.05637	0.0974	2.09E-05	2.23E-06	5.15E-05		7.65E-05	2.98E-06		4.90E-06
P25 300 chips	0.00509	0.00000	0.04482	0.0974	1.61E-05	1.79E-06	3.96E-05		8.13E-05	3.30E-06		5.22E-06
P25 300 chips	0.00509	0.00000	0.05631	0.0974	2.09E-05	2.18E-06	5.14E-05		7.65E-05	2.91E-06		4.90E-06
P25 300 QW	0.00493	0.00000	0.05394	0.0974	1.99E-05	2.03E-06	4.90E-05		7.75E-05	2.90E-06		4.95E-06
P25 0% 292	0.00484	0.00000	0.05658	0.0974	2.17E-05	2.33E-06	5.26E-05		7.57E-05	2.51E-06		3.96E-06
Rutile 0% 292	0.00491	0.00000	0.05626	0.0974	2.16E-05	2.36E-06	5.23E-05		7.58E-05	2.55E-06		3.97E-06
Anat. 0% 292	0.00486	0.00000	0.05535	0.0974	2.12E-05	2.31E-06	5.14E-05		7.62E-05	2.55E-06		3.99E-06
Anat. 0% 284	0.00480	0.00000	0.05292	0.0974	2.08E-05	2.46E-06	4.96E-05		7.66E-05	2.34E-06		3.29E-06
Rutile 0% 284	0.00504	0.00000	0.05731	0.0974	2.27E-05	2.72E-06	5.41E-05		7.47E-05	2.32E-06		3.21E-06
P25 0% 284	0.00486	0.00000	0.05510	0.0974	2.18E-05	2.56E-06	5.19E-05		7.56E-05	2.30E-06		3.25E-06

Table B. 2 List of all the experiments analyzed by Aspen Plus™, given the input of total moles (mol/h) in, the output of the simulation is the distribution of all the reactants flowrates in the gas and liquid phase in kmol/h going through the reactor column.

Figure B.5 is another way to represent the data from Table 2.6. The slope of each graphic corresponds to the activity coefficient for water and phenol respectively, according to Equation 2.7. It is possible to see that both values were very different than one, showing the big deviation to ideality.



a)



b)

*Figure B. 5 Partial pressure of (a) water and (b) phenol with respect to their respective liquid phase composition, times their saturation pressure. The slope represents the activity coefficient for each case.*

## B.5 Preliminary Work

In 2017, different experiments were done to elucidate the performance of the Ruthenium Nitrosyl Nitrate Catalyst supported on TiO<sub>2</sub>-P25 over a flow reactor in comparison with the already analyzed batch reactor. In first instance, experiments with diluted phenol were done. Here, the amount of phenol was kept at 5% wt. in three different water concentrations (5 – 10 – 20% wt.) and the corresponding amount of tetrahydrofuran (THF) as a solvent. The purpose of this experiment (Experiment 1) was to elucidate the effect of water in favoring the direct deoxygenation (DDO) pathway into benzene.

The first set of results led to the conclusion that increasing water concentration favored the DDO pathway in first instance until a peak was reached and after that, higher amount of water led

to an activity and selectivity decrease. Those results suggest that previous publications <sup>88</sup>, based on computational modelling over Ru/TiO<sub>2</sub>-Rutile were not consistent with experimental data.

To determine the cause of catalyst deactivation, different experiments were done. A second reduction treatment after fully deactivation did not show any reactivation sign, indicating that adsorbed water or oxygen were not responsible for deactivation of the sites. A further recalcination of the packed catalyst at 300 and 400°C did not show reactivation either, meaning that the deactivation was not caused by carbon deposition. Finally, some TEM images of the spent catalyst were taken, but those images were not enough information to determine sintering of the catalyst.

In compliment to previous results, more experiments were done to determine values of reaction rates in terms of turnover frequencies (TOF). For that, the weight hourly space velocity (WHSV) used was increased by 10 times to obtains conversion closest to 20%. Those ranges allowed to model the reactor as a differential reactor and obtained values of reaction rates (Experiment 2).

Five different concentration of water were tested, increasing the range of water concentration. For these experiments, water concentrations of 0 – 5 – 10 – 15 and 20% wt. were tested. Values of initial TOF, initial selectivity and deactivation constants in function of water concentration does not show any clear influence of water, in discrepancies with previous results. Still confused with previous data, new efforts were added to determine the effect of the temperature over the reaction and try to elucidate activation barriers.

Newer sets of experiments were done under the same water concentration values at 350 and 400°C. those results led to a very low activity of the catalyst, turned out to be because of a phenomenon called strong metal support interaction (SMSI effect).

To obtain accurate values of TOF, the active sites presented in the catalysts must be known. For that, characterization of the catalyst was done by CO chemisorption (Experiment 4), where the isotherm of adsorption data led to a 59% dispersion. This catalyst was made in the University of Maine facilities, by incipient wetness impregnation.

### **B.5.1 Experiment 1: Effect of water at high conversion (80 – 40%)**

Reaction Conditions:

- Temperature: 300°C
- Liquid Feed
- 0.05 mL/min
  - 5% wt. phenol
  - 5 – 10 – 20% wt. H<sub>2</sub>O
  - 90 – 85 – 75% wt. THF
- Gas Flow: 60 sccm hydrogen, 420 psi
- $WHSV = 4.770 \text{ h}^{-1}$
- 25 mg Ru/TiO<sub>2</sub>-P25
- Ruthenium Nitrosyl Nitrate/TiO<sub>2</sub>-P25 by Incipient Wetness Impregnation
- Reduction under 60 sccm flowing H<sub>2</sub>: 420 psi, 300°C for 1h

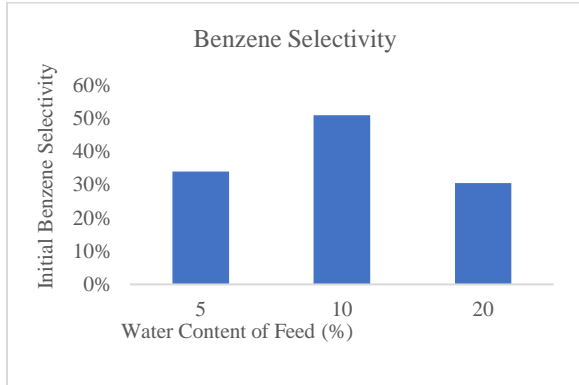


*Figure B. 6 Initial Benzene selectivity for phenol hydrodeoxygenation at different water concentrations.*

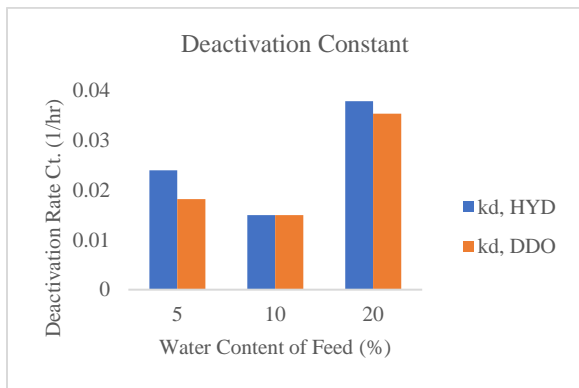


*Figure B. 7 Deactivation constant for phenol hydrodeoxygenation at different water concentrations.*

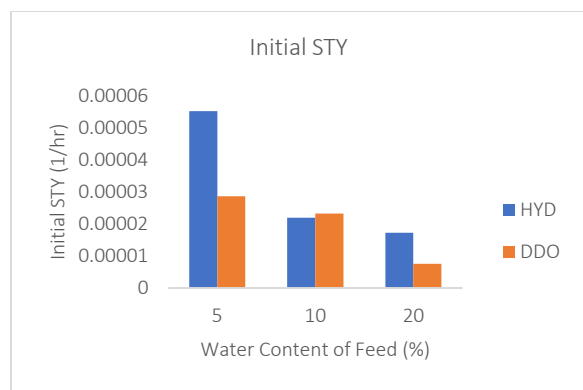


Figure B. 8 Initial Site time yield (STY) for phenol hydrodeoxygenation at different water concentrations.

## B.5.2 Experiment 2: Low Conversion, TOF, and Reproducibility

### Reaction Conditions

- Liquid flow: 0.15 mL/min
  - 5% wt. Phenol
  - 0 – 20% wt. Water
  - 95 – 75% wt. THF
- Gas Flow: 60 sccm hydrogen, 420 psi
- WHSV: 35.8 h<sup>-1</sup>
- Reaction Temperature: 300°C
- Heating ramp of 1.5°C/min
- 10 mg Ru/TiO<sub>2</sub>-P25 Catalyst
- Ruthenium Nitrosyl Nitrate/TiO<sub>2</sub>-P25 by Incipient Wetness Impregnation

- Reduction under 60 sccm flowing H<sub>2</sub>: 420 psi, 300°C for 1h

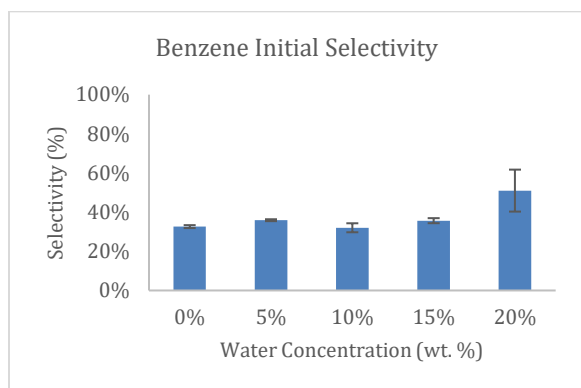


*Figure B. 9 Initial Benzene selectivity for phenol hydrodeoxygenation at different water concentrations.*

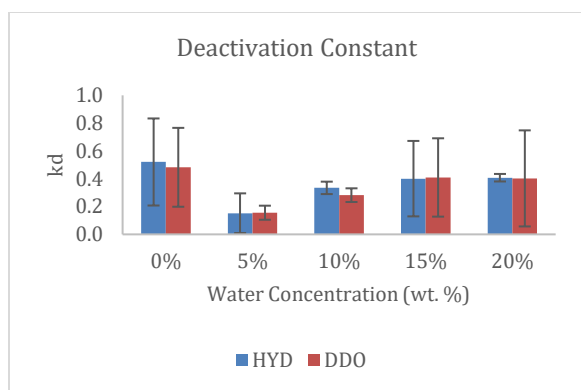


*Figure B. 10 Deactivation constants for phenol hydrodeoxygenation at different water concentrations.*

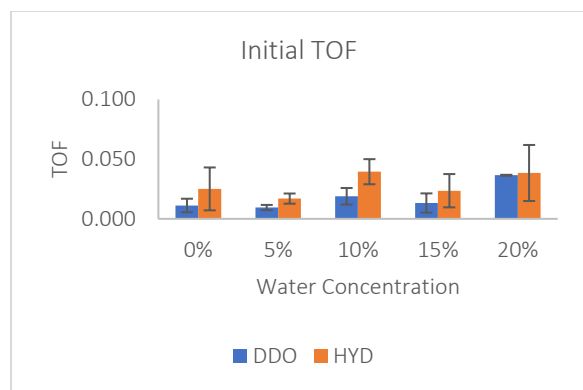


Figure B. 11 Estimated initial TOF for phenol hydrodeoxygenation at different water concentrations.

### B.5.3 Experiment 3: New Temperature Test

#### Reaction Conditions

- Liquid flow: 0.15 mL/min
  - 5% wt. Phenol
  - 0 – 5 – 10 – 15 – 20% wt. Water
  - 95 – 90 – 85 – 80 – 75% wt. THF
- Gas Flow: 60 sccm Hydrogen, 420 psi
- WHSV: 35.8 h<sup>-1</sup>
- Reaction Temperatures: 350°C
- Heating ramp of 1.5°C/min
- 10 mg Ru/TiO<sub>2</sub>-P25 Catalyst
- Ruthenium Nitrosyl Nitrate/TiO<sub>2</sub>-P25 by Incipient Wetness Impregnation

- Reduction under flowing H<sub>2</sub>: 420 psi, 300°C for 1h

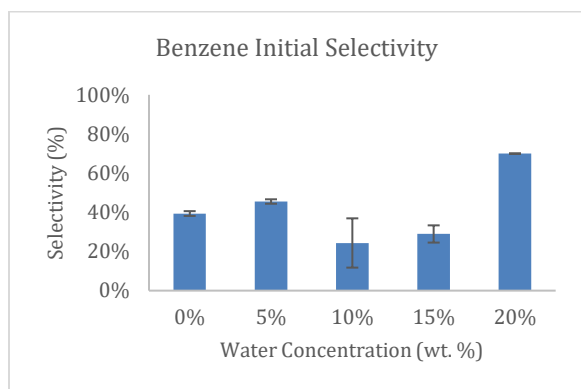


*Figure B. 12 Initial Benzene selectivity for phenol hydrodeoxygenation at different water concentrations at 350°C.*

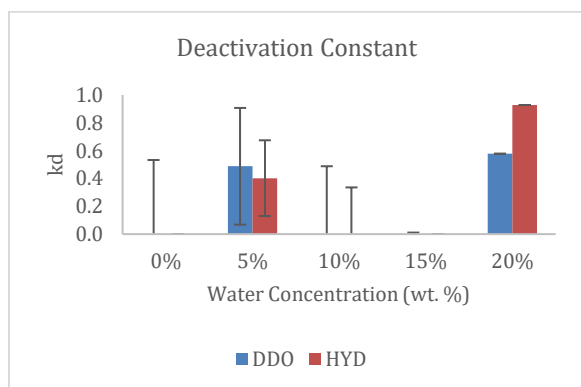


*Figure B. 13 Deactivation constants for phenol hydrodeoxygenation at different water concentrations at 350°C.*

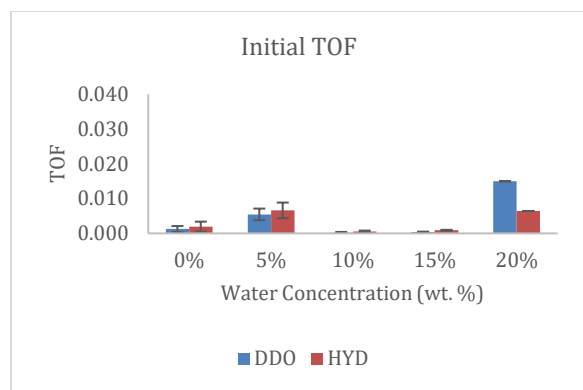


*Figure B. 14 Estimated initial TOF for phenol hydrodeoxygenation at different water concentrations at 350°C.*

#### Reaction Conditions

- Liquid flow: 0.15 mL/min
  - 5% wt. Phenol
  - 0 – 5 – 10 – 15 – 20% wt. Water
  - 95 – 90 – 85 – 80 – 75% wt. THF
- Gas Flow: 60 sccm Hydrogen, 420 psi
- WHSV: 35.8 h<sup>-1</sup>
- Reaction Temperature: 400°C
- Heating ramp of 1.5°C/min
- 10 mg Ru/TiO<sub>2</sub>-P25 Catalyst
- Ruthenium Nitrosyl Nitrate/TiO<sub>2</sub>-P25 by Incipient Wetness Impregnation
- Reduction under flowing H<sub>2</sub>: 420 psi, 300°C for 1h

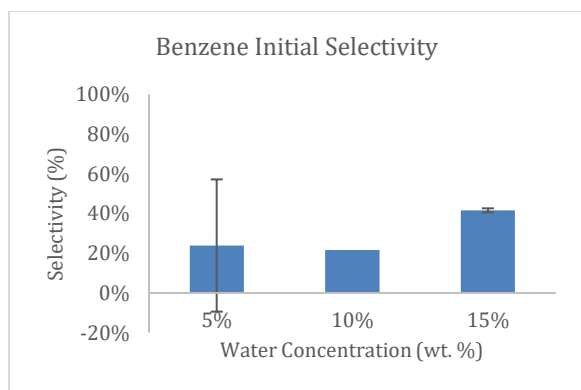


Figure B. 15 Initial Benzene selectivity for phenol hydrodeoxygenation at different water concentrations at 400°C.

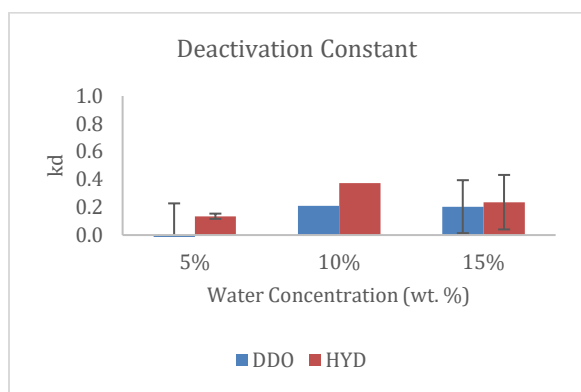
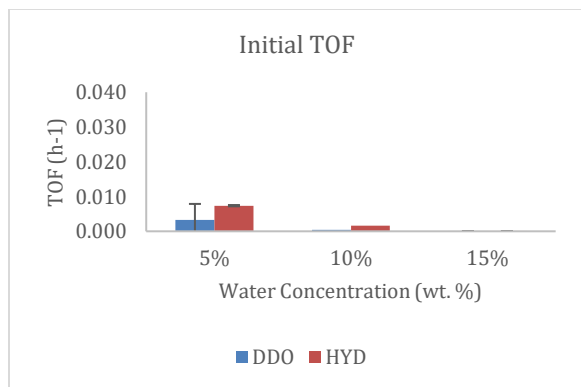


Figure B. 16 Deactivation constants for phenol hydrodeoxygenation at different water concentrations at 400°C.



*Figure B. 17 Estimated initial TOF for phenol hydrodeoxygenation at different water concentrations at 400°C.*

## APPENDIX C: TROUBLESHOOTING GUIDE

This guide is made to troubleshooting liquid-phase flow reactors, based on the flow reactor located in lab 203, Jenness Hall, University of Maine 2017-2019. Problems are organized by principal equipment and then some recommendations are given for proper reaction condition determination will be given.

### C.1. HPLC Pump <sup>89</sup>

#### C.1.1 Start-up procedure

- Once the pump is properly connected, prime the outlet of the seal wash (upper part) with a syringe to fill the whole line with solvent mixture (IPA/water mixture)
- Then, connect the outlet of the pump to an open line and use this opening to prime some fluid through the pump, start with a safe solvent, with similar properties to the solvent that you will be further flow in this pump
- Make sure that the pump is pumping, do not worry about the flowrate yet
- Use the liquid back-pressure regulator to condition the pump for about 30 min
- Connect the outlet of the pump to a line that can be isolated and has a pressure gauge in it
- Flush some liquid to the outlet of the system
- Pump the liquid to the closed line and watch the pressure build up
- If the system is smoothly building pressure, even at very low flowrates, and hold it once the pump stops, then the pump is working correctly

- Chromtech guys are really helpful and nice, try to call them if you need further assistance

### **C.1.2 Reasons for not building pressure**

- The fittings might be leaking, make sure that there is no liquid coming out of the unions
- It could be an air bubble in the line; air can be compressed, affecting the measurement of the pressure. To fix that, open the line in the most upper part (sometimes the gauge itself needs to be disconnected) and let the liquid flush the line
- The seals could not be properly set, try to condition the pump for a longer time

Make sure you are using the right seal for your mixture: aqueous is yellow and organic is black, check the Chromtech manual to see how to replace the seals

### **C.1.3 Reasons for not pumping**

- Check if the inlet is full with liquid and that the inlet tube is actually submerged in fluid
- Make sure that there is no bubbles in the line, if so, prime the liquid again and try to restart.  
If that does not work try to recondition the pump

## **C.2. Mass flow controller <sup>90</sup>**

### **C.2.1 Reasons for having none or different flowrate out of the MFC**

- Check the pressure of the gas cylinders, if the pressure is lower or the same as the system you are flowing to, gas is not going to flow through
- Check that the mass flow transmitter <sup>91</sup> is properly set
- Always check your lines to avoid risk of overflowing, if the valve underneath the reactor column is closed while the pump is flowing through the system, the liquid is going to start flowing upstream the reactor and can go into the mass flow controller (the check valve is not capable to hold high pressures of liquid back)
- If the liquid gets into the mass flow controller, it will damage the sensors and the MFC will stop controlling properly, it is possible to clean it up if there is not much liquid in it
- Remove MFC out of the line and remove the outlet fittings connections to see how much liquid can come out of it, if liquid is something that can solidify (like phenol) once dry, immediate actions need to be taken. Try to flush this solid out with solvent, usually acetone or IPA works fine
- Flush as much as possible making sure to not wet even more the system. Then let it sit for a long time (overnight is a good idea), before trying to reinstall it and see if it works
- If that doesn't work try to set the MFC to 100% (higher possible flowrate) and let it there for a while
- Afterwards try to see if it is controlling properly, by setting up a lower flowrate in the mass flow transmitter. Sometimes increasing or decreasing the pressure upstream and downstream the MFC helps, try many times
- If you feel confident it is a good idea to open this equipment and try to clean up all the parts that look dirty or damaged, if the material allows it (check compatibility online) sink it in solvent (IPA or acetone) and let it sonicate for a while. Always refer to the proper

manual to do that and take picture of every step so you know how to reassemble it properly.

Be always very careful and ask for help to someone that has done that before

### **C.2.1 Reasons for not seeing gas coming out of the bubble meter**

- Not seeing gas coming out is not always because the MFC is not working
- Check that the line is actually going to the bubble meter, check that the proper valves are open/closed
- Check that the reactor outlet is connected to the panel board and that the panel board is connected properly to the bubble meter
- Check that the outlet of the bubble meter is properly connected to the vent, and that the vent is not over suction
- It is expectable to see differences in flowrates before and during reaction. This is because you could be either consuming or producing more gas products
- If you need to extract only liquid samples, make sure you cover your separator with ice packs to condense all your product, larger flowrates will make it more difficult to cool the solution out
- You can also check what gases are coming out the reactor by sending the outlet to a gas phase GC-FID

## **C.3. Temperature controller <sup>92</sup>**

### **C.3.1 Operation suggestions**

- Set up the proper ramp/soak patterns, instruction are available in the SOLO manual, or through the SOLO software installed to our computers
- Always use two (2) thermocouple attached to the temperature controller, one is the over temperature controller and the other one is the temperature controller
- Temperature controller will be set to follow the ramp/soak pattern, and should be as close as possible to the catalyst
- Over temperature controller is set for safety reasons, and should stay so, It will make the system to shut off if the temperature is higher than the alarm limit (usually 500C)
- check that the alarms are properly set, alarm level should remain higher than operation temperature, if not the temperature controller would stop heating
- Check that the thermocouple type is the right one: K type, is a y type in the screen
- Check that the TC is connected to the VARIAC and this is connected to the heating tape

### **C.3.2 Reasons for not seeing temperature rise**

- Thermocouple might not be properly connected or broken. Put the thermocouple in a hot surface (even your hands are at 36C) and see if temperature rise
- Heating tape might not be working. Connect the heating tape to a regular plug and check if it is warming up. Watch out because it gets really hot quickly

- Variac might be too low, check the value of the VARIAC and increase it if it is too low, usually we operate them at 80%
- Variac fuses might be blown out, connect a lamp to it and see if the lamp is lighting. If not, check and change the fuses if needed
- TC might not be sending the right signal, connect a lamp direct to the TC outlet, while the ramp/soak pattern is running and check if the lamp is lighting. If not, check the ramp/soak patterns, alarms and make sure that the TC is “ON” and “Enable”
- If nothing works check with Amos Cline if something electrical is wrong with the TC

## **C.4. Back pressure regulator <sup>93</sup>**

### **C.4.1 Operation suggestions**

- Always check your lines to avoid risk of overflowing, if valve underneath the reactor is closed, liquid is going to start flowing upstream the reactor and can go into the back pressure regulator
- If liquid get into the BPR, it will damage the diaphragm, and it will not control the pressure properly. It is possible to clean it up if there is not much liquid in it
- Remove BPR out of the line and open the bottom part to see how much liquid can come out of it, if liquid is something that can solidifies (like phenol) once dry, immediate actions needs to be taken, try to flush this solid out with solvent, usually acetone works fine.
- Flush as much solvent as possible through it, making sure to not wet even more the system

- Then, let it sit for a long time (overnight is a good idea), before trying to reinstall it and see if it works
- If that doesn't work try to set the BPR to 100% open valve (lower possible pressure) and let it flow for a while
- Afterwards try to see if it is controlling flow, by setting up a lower flowrate. Sometimes increasing or decreasing the pressure upstream and downstream helps, try many times
- If you feel confident it is a good idea to open this equipment and try to clean up parts that looks dirty or damaged, if the material allows it (check compatibility online) sink it in solvent (IPA or acetone) and let it sonicate for a while. Always refer to the proper manual to do that and take picture of every step so you know how to reassembly properly. Be always very careful and ask for help to someone that has done that before

## **C.5. GC-FID <sup>94</sup>**

### **C.5.1 Operation tips**

- Check proper use of vials, if they are the reduce volume ones, make sure that the bottom of the vials doesn't contain bubbles
- Check that all the needed gas cylinders are open and with enough pressure. GC-FID only needs about 10 psi to work
- Check the hydrogen lines to make sure that they are not leaking
- If hydrogen comes from a hydrogen generator far away from it, the pressure drop along the lines in the lab could be huge

- Redo your standard every two month to double check that your sensitivity hasn't change
- Always double check the retention time of your standards, sometimes you might not be seen the component you think you are
- If you are collecting samples over time, and catalyst deactivates, it is expectable to see smaller concentrations over time. If concentrations are not decreasing consistently, then the peak is not the right one
- Always dilute your experimental samples in THF or other solvent before injecting. Recommended peaks areas are between 100 – 1000. Too low is not reproducible, and too high might damage the column

## **C.6. Balance <sup>95</sup>**

### **C.6.1 Operation suggestions**

- Do not weight solutions lower that 0.002 g in the balance, if you need less material consider dilute a larger amount and then weight out the diluted material
- Always check if the balance is properly centered
- Be aware of static problems, especially in dry seasons like winter. Do not leave material in the balance for a longer period of time, you will see that the weigh will start changing progressively
- Use a working static gun to avoid this problem, in only require one shot and the handle needs to be moved very slow

- Use a starting weighing vial with cap, weigh it until you get here time the same value to assure reproducibility. Then, add the materials one by one and weigh the vial with the material again three times. Calculate the difference.
- Always use caps to avoid evaporation of components, while preparing solutions
- Make sure that all your glassware is clean and free of contamination

### **C.7. Packing the column**

- Reactions can have reproducibility problems for bad practices in packing the column
- Dilute the catalyst in crushed fused silica, in a 1/9 or 1/99 ratio, that will avoid hot spots inside the bed
- Try to get a bed length of at least 1 mm
- Use always diluted solutions, so the heat of reaction will be small and avoid heat transfer limitation problems
- Crush and sieve it to get an homogeneous particle diameter, try to get a size close to mesh 50 and 70
- Make sure that you dump all the catalyst inside the column, weigh the weighing vial afterwards to double check that the initial value match
- Use a funnel for dumping the catalyst and make sure that catalyst doesn't stay in it
- Be consistent in the way to pack the column, try to apply the same pressure every time and to locate the catalyst in the same position every time, channeling problems are real
- Put a mark with a sharpie of the actual position of the catalyst in the column so you can then match the position of the thermocouple to it later

## **C.8. Reactor operation**

- Safety: Make sure that reactor is free of hydrogen and depressurized before open it. Flush some inert gas to the system for at least 30 min before open
- Before connecting a new column, drain the reactor out as much as you can, be careful, and open all the possible drain valves. You can also flush it out with some inert gas but be aware of not vaporizing chemicals to the environment
- Once connected the column, make sure to do a proper leak test by pressurizing the system and watch for any pressure drop after at least 30 min
- Also wet the connections with soapy water and watch for any bubbles that indicates a leak
- Run some blank tests with just the solvent and the catalyst, or solvent and crushed fused silica, to make sure that all the innerts actually are
- Repeat two experiments with the same conditions in a row to address reproducibility problems. Be as consistent as you can and **DO NOT CHANGE** anything
- If the first reproducibility test works, repeat the same experiment a week and a month later, to calibrate yourself and look for differences

## **C.9. Damaged Catalysts**

- It doesn't get reduced under hydrogen, check is hydrogen was flowing upwards trough the catalyst overnight, if upper valve remained opened, then catalyst is damaged

- Check if temperature ramp is smooth enough to not sintering the catalyst. At least keep a heating ramp of 2K/min or slower
- Make sure that the temperature of the catalyst is actually properly measured, check position of thermocouples

### **C.10. Reaction Condition <sup>96</sup>**

- Get a proper weight hourly space velocity (WHSV) by defining concentration, mass of catalyst and flowrates; consider the trade-off of modifying each of them
- You will need small conversions to get differential conditions
- Reaction rates are independent of WHSV but conversion is dependent of it
- As a rule of thumbs, higher WHSV leads to lower conversion
- More catalyst leads to lower WHSV and therefore higher conversion, no influence in TOF
- Higher flowrate leads to higher WHSV, and therefore lower conversion. Be aware that if you are co-feeding gas, your sample can be vaporized so your concentration is affected by the gas/liquid ratio. If you increase the liquid flowrate, increase the gas flowrate proportional to it
- Also higher flowrates are harder to control and samples needs to be taken more frequently, they are also harder to cool it down in the separator
- Reactant concentration will modify reaction rates according to the rate expression (except the ones that are zero order). Most likely lower concentration will lead to lower reaction rates

- Lower concentrations will lead to lower WHSV if keeping the same flowrates, and therefore a higher conversion is reached, if rates doesn't change
- Lower concentrations and lower conversions will make it very difficult to see products in the GC-FID

If nothing works cry, take a break, and start over at the next day ☺

...

Lab work can be hard but it will give you results as some point, do not give up!

## **BIOGRAPHY OF THE AUTHOR**

Daniela Stück was born in Concepción, Chile on January 6<sup>th</sup>, 1992. She was raised in Concepción and graduated from the German School of Concepción (DSC) in 2010. She attended the University of Concepción and graduated in 2016 with a Bachelor's degree in Chemical Engineer. She came to Maine and entered the Chemical Engineering graduate program at The University of Maine in the fall of 2017. After receiving her degree, Daniela will be joining the National Renewable Energy Laboratory in Golden, Colorado to begin her career in the field of heterogeneous catalysis. Daniela is a candidate for the Master of Science degree in Chemical Engineering from the University of Maine in August 2019.